5

Optical Imaging Based on Intrinsic Signals

Nader Pouratian and Arthur W. Toga

Laboratory of Neuro Imaging, UCLA Department of Neurology, Los Angeles, California 90095-1769

I. Introduction

Several functional brain mapping techniques have been developed over the past 3 decades which have revolutionized our ability to map activity in the living brain, including positron emission tomography (PET), functional magnetic resonance imaging (*f*MRI), optical imaging, and, more recently, near-infrared spectroscopy (NIRS) and transcranial magnetic stimulation (all are discussed in other chapters of this book). Each modality of fers distinct information about functional brain activity and has certain advantages and limitations. In choosing a functional imaging modality for experiments, one should consider a modality 's spatial and temporal resolution, the etiology of its brain mapping signal, the practicality of the imaging methodology , as well as the cost of implementation. In this chapter , the methodological details of optical imaging of intrinsic signals are explored, with special attention to the considerations listed above.

Optical imaging of intrinsic signals maps the brain by measuring intrinsic activity-related changes in tissue reflect ance. Functional physiological changes, such as increases in blood volume, hemoglobin oxymetry changes, and light scattering changes, result in intrinsic tissue reflectanc

changes that are exploited to map functional brain activity . This of fers a distinct advantage over extrinsic signal imaging, such as dye imaging, which may cause phototoxicity, especially in *in vivo* preparations, and thereby alter the normal physiology of the sample. It is unclear how normal physiology may be af fected by the addition of dyes and radioisotopes or electrode insertion. By not requiring any contact with the tissue of interest whatsoever , optical imaging of intrinsic signals is ideally suited to studying chronic preparations, in which an investigator may wish to image a sample over a period of days, weeks, or months, and for intraoperative mapping of the human cortex during neurosurgery (Mazziotta *et al.,* 2000).

Although activity-related intrinsic optical changes in tissue reflectance associated with electrical activity o metabolism were first observed over 50 years ago (Hill an Keynes, 1949), it was not until the 1980s that these intrinsic optical changes were used to map cortical activity *in vivo* (Grinvald *et al.,* 1986). Since this initial report, intrinsic optical changes have been reported in rodents (Masino *et al.,* 1993; Narayan *et al.,* 1994), cats (Frostig *et al.,* 1990; Bonhoeffer and Grinvald, 1991), monkeys (T s'o *et al.,* 1990; Grinvald *et al.,* 1991), and humans (Haglund *et al.,* 1992; T oga *et al.,* 1995a). The increasing popularity of optical imaging of intrinsic signals is lar gely because this technique offers both high spatial and high temporal resolution simultaneously . The spatial resolution of intrinsic imaging is unparalleled among *in vivo* imaging techniques (on the order of micrometers), making it ideal for studying the fine functional o ganization of sensory cortices as well as the physiology of neurovascular coupling at the level of the arteriole, venule, and even capillaries. Although the temporal resolution of optical imaging is not as great as with electrophysiological techniques, imaging is commonly performed at video frame rates (30 Hz). This is more than sufficient for imaging the slowly evolving perfusion-relate responses, which peak 3 to 4 s after stimulus onset.

Because of these advantages, the number of studies using optical imaging of intrinsic signals has been growing rapidly (especially now that optical imaging systems are commercially available). This chapter provides a detailed methodology for investigators to design their own imaging system, with special attention to the limitations of certain approaches and dif ferent strategies that have been devised by various groups to overcome them. Understanding the various limitations and strategies will give investigators greater versatility in designing their systems and experiments and avoid making the commercially available optical imaging systems "black boxes" that merely produce functional maps.

This chapter surveys a wide array of optical imaging techniques and applications, including discussions of how optical spectroscopy has significantly advanced our under standing of intrinsic signal etiology , advantages and disadvantages of the dif ferent species used for optical imaging, different approaches to cortical immobilization, advances in detector technology, recent advances in both single-wavelength and spectroscopic analysis, baseline vasomotion and how it complicates data analysis, recent advances in optical imaging in humans, and integrating optical imaging with other functional imaging techniques to better understand the etiology of functional brain mapping signals.

II. Sources of Intrinsic Signals and Wavelength Dependency

Although investigators regularly draw conclusions about neuronal activity from functional imaging studies, most modern functional imaging techniques, including optical imaging of intrinsic signals, do not directly measure neuronal activity (V illringer and Dirnagl, 1995). Instead, they detect activity-related changes in perfusion and metabolism, such as increases in cerebral blood flow and changes i hemoglobin oxygenation. An understanding of the hemodynamic response and its relationship to electrophysiology and metabolism is therefore required to attach the appropriate significance to the results being reported. Moreove , it is critical to understand which aspects of the hemodynamic response underlie intrinsic signals.

It has been known for well over a century that neuronal activity causes local perfusion-related and metabolic changes (Roy and Sherrington, 1890). While electrophysiological changes occur on the order of milliseconds, perfusion-related changes occur on the order of seconds. The increase in blood flow supplies nutrients such as oxygen and glucose to meta bolically active neuronal areas. The cascade of events includes regional vasodilatation (Ngai *et al.,* 1988), blood flow changes (Co *et al.,* 1993; Lindauer *et al.,* 1993), blood volume increases (Frostig *et al.,* 1990; Belliveau *et al.,* 1991; Narayan *et al.,* 1995), and changes in relative hemoglobin concentrations (LeManna *et al.,* 1987; Kwong *et al.,* 1992; Malonek and Grinvald, 1996; Mayhew *et al.,* 1999; Nemoto *et al.,* 1999). Metabolic changes include increases in local oxygen consumption (Frostig *et al.,* 1990; Malonek and Grinvald, 1996; Vanzetta and Grinvald, 1999) and glucose utilization (Sokolof f *et al.,* 1977; Fox *et al.,* 1988). All of these electrophysiological and metabolic changes may contribute to intrinsic optical changes.

Several studies have demonstrated close spatial coupling of neuronal activity and perfusion-related mapping signals (see Villinger and Dirnagl, 1995, for review). Intrinsic signals, specificall , have been shown to be in good spatial agreement with electrophysiological activity in rodents (Masino *et al.,* 1993; Narayan *et al.,* 1994), cats (Grinvald *et al.,* 1986; Frostig *et al.,* 1990), nonhuman primates (Grinvald *et al.,* 1986; Frostig *et al.,* 1990), and humans (Haglund *et al.,* 1992; Toga *et al.,* 1995a; Pouratian *et al.,* 2000a). Interestingly, in most cases, optical signals seem to

overspill regions of electrophysiological activity . This phenomenon of "spread" mostly has been observed in the rodent somatosensory cortex in response to whisker stimulation (Godde *et al.,* 1995; Chen-Bee and Frostig, 1996; Masino and Frostig, 1996). Narayan *et al*. (1995) reported that intrinsic optical and intravascular fluorescent dye map overspilled regions of electrophysiologic activity (using single-unit recordings) by about 20%. Optical maps encompass not only the principal barrel but also adjacent barrels. This may be due to low-level neuronal activity which occurs in adjacent barrels in response to stimulation of adjacent, nonprincipal whiskers.

Three major components of optical signals have been identified: blood volume changes, hemoglobin oxymetr changes, and light scattering (Frostig *et al.,* 1990; Malonek and Grinvald, 1996; Mayhew *et al.,* 1999; Nemoto *et al.,* 1999).

A. The Blood Volume Component

The first component of the intrinsic signal originate from functional changes in blood volume related to either dilation of local vasculature or local capillary recruitment or both in cortically active areas. To determine the contribution of blood volume changes to intrinsic signals, Frostig and colleagues (1990) injected and imaged a fluorescent dy (Texas red dextran, MW 70,000; Molecular Probes) that was restricted to the intravascular compartment and compared the fluorescence signal with the intrinsic signal changes at hemoglobin isobestic point (point of equal absorption of oxy- and deoxyhemoglobin), 570 nm. The signals were essentially identical (both showing increased absorption due to increased blood volume), leading the authors to conclude that the major component of the intrinsic signals measured at 570 nm originates primarily from blood volume changes. Narayan and colleagues (1995) subsequently compared functional intravascular fluorescent dye maps (once agai using Texas red dextran) with intrinsic optical reflectanc decreases at 610 and 850 nm, finding similar timing an localization of intrinsic signals and blood volume changes. Both studies found that the blood volume changes, however, extend beyond the electrophysiologically active cortex, suggesting that the majority of activity-dependent blood volume changes and related intrinsic signal changes are not specific to or finely regulated at the level of individual fun tional domains.

B. The Oxymetry Component

The second component of intrinsic signals arises from activity-dependent changes in hemoglobin oxygen saturation. Current theory holds that the first change to occur fol lowing neuronal activation is likely a brief burst of oxidative metabolism at the site of neuronal activity (Fox and Raichle, 1986; Frostig *et al.,* 1990; Vanzetta and Grinvald, 1999). This burst of oxidative metabolism is believed to produce a local increase in deoxyhemoglobin concentrations which is very tightly spatially coupled with electrophysiologically active neurons. Consistent with this theory , studies using oxygen-dependent phosphorescence quenching dyes demonstrated that oxygen tensions briefly decrease follow ing functional activation (V anzetta and Grinvald, 1999). These initial increases in oxidative metabolism and deoxyhemoglobin concentrations remain controversial since not all groups have observed them (V anzetta and Grinvald, 1999; Kohl *et al.,* 2000; Lindauer *et al.,* 2001). W ithin seconds of activation, cerebral blood flow increases i excess of cerebral metabolic rate of oxygen (~6:1 according to Fox and Raichle 1986), causing a *decrease* in capillary and venous deoxyhemoglobin due to an "overperfusion" of blood rich in oxyhemoglobin (Ngai *et al.,* 1988; Frostig *et al.,* 1990; Narayan *et al.,* 1995). Intrinsic signals in the 600 to 630 nm range have a biphasic time course reminiscent of the changes expected in deoxyhemoglobin concentrations: an initial increase in absorption followed by a phase reversal and more prolonged decrease (Fig. 1). This is attributed to the fact that in this wavelength range, the absorption of light by oxyhemoglobin is negligible compared to that of deoxyhemoglobin. Although it is clear that other optically active processes, such as light scattering and changes in total hemoglobin, still contribute to the intrinsic signals at these wavelengths, it is commonly held that the major contributor to intrinsic signals in this wavelength range is the change in deoxyhemoglobin concentration (Frostig *et al.,* 1990; Nemoto *et al.,* 1999).

Imaging at wavelengths that are sensitive to oxygen extraction (i.e., 600–630 nm) may produce maps that are more spatially correlated with underlying neuronal activity than wavelengths that are influenced by blood volum changes (i.e., 550 nm) (Frostig *et al.,* 1990; Grinvald *et al.,* 1991; Hodge *et al.,* 1997; Vanzetta and Grinvald, 1999). This may be because fast changes in oxidative metabolism are more tightly coupled to electrical activity than the more delayed perfusion-related responses (Vanzetta and Grinvald, 1999). Imaging at 600–630 nm also of fers the greatest signal-to-noise ratio and, when focused 2.0 mm beneath the cortical surface (using an imaging apparatus with a shallow depth of field), least emphasizes blood vessel artifact (Hodge *et al.,* 1997).

C. Light Scattering Component

Light scattering changes that accompany cortical activation, which contribute to intrinsic signals, arise from ion and water flux; morphological changes (i.e., expansion o contraction) in vascular , cellular , and extracellular conformations (which may be intimately related to ion and water movement); and blood volume changes (Lou *et al.,* 1987;

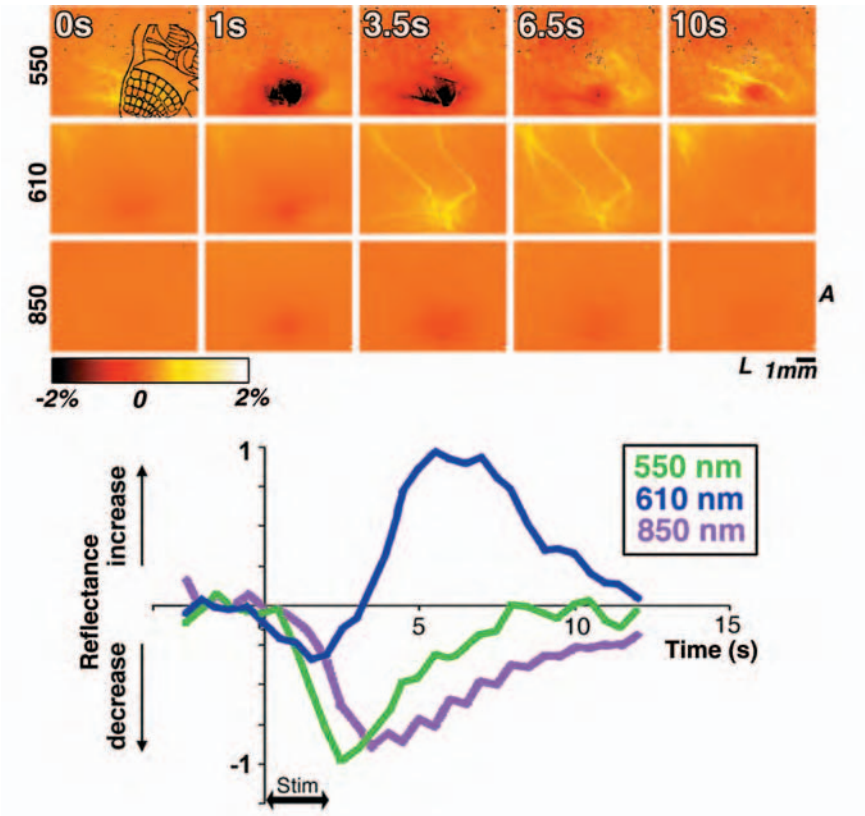

Figure 1 Distinct spatial/temporal patterns of functional intrinsic signals depending on wavelength. Optical responses to 2-s C1 whisker stimulation over the rodent somatosensory cortex are displayed at 550, 610, and 850 nm. 550 nm: The response at 550 nm is believed to represent changes in total hemoglobin (see Fig. 2) and is typically high intensity and monophasic. The monophasic time course is shown in the graph at the bottom. Overlaid on the 0 s image is a schematic representation of the rodent somatosensory barrel cortex for comparison. 610 nm: Responses at 610 nm are believed to emphasize changes in deoxyhemoglobin (see Fig. 2). Following stimulation, there is initially a focal increase in absorption (at 1 s, interpreted as an increase in deoxyhemoglobin and oxygen extraction) followed by a more widespread decrease in absorption (3.5–6.5 s, interpreted as a decrease in deoxyhemoglobin concentration). The second phase is related to the BOLD *f*MRI signal. The biphasic time course of optical responses at 610 nm is shown in the graph at the bottom. 850 nm: At 850 nm, neither isoform of hemoglobin absorbs much light. Instead, the signal is believed to originate from light scattering changes. This signal, like at 550 nm, is monophasic (see time course depicted on bottom graph) but is significantly less intense than the 550-nm response. Time courses were calculated by determining the average reflectance change within a statistically defined region of interest, using methods described by Blood *et al.* (1995). Time courses were normalized for comparison across wavelengths. The height of the graphs, therefore, does not reflect the magnitude of the reflectance changes. The optical signals and time courses were derived from averaging 12 trials in a single animal. A, anterior; L, lateral.

Narayan *et al.,* 1995). The light scattering component exists at all wavelengths but becomes a significant source of intrinsic signals at wavelengths with very small hemoglobin absorption (i.e., above 630 nm, see Fig. 2). In fact, in the near-infra red range (>750 nm), the light scattering component dominates the intrinsic signal.Although the specific etiology of light scattering changes cannot necessarily be defined in *in vivo* preparations, Narayan and colleagues (1995) demonstrated that functional light scattering changes at 850 nm correlated well, both spatially and temporally, with blood volume changes (as measured using intravascular fluorescent dyes). This is consistent with the fact that erythrocytes are the primary scatterers in whole blood; light scattering changes can be induced either by functional changes in the number of erythrocytes or by functional erythrocytic distortions (Zdrojkowski and Pisharoty, 1970). It should not, however, be assumed that all light scattering changes at 850 nm represent blood volume changes. For example, O'Farrell and colleagues (2000) showed that only the latter two of three phases of the triphasic 850-nm optical response to cortical spreading depression represented blood volume changes. The first phase may represent changes in the extracellular compartment or dendritic beading, which both may potentially change the light scattering properties of the tissue (O'Farrell *et al.,* 2000).

The light scattering signal introduces a potential confound to intrinsic signal mapping studies. Light scattering both blurs images and expands the apparent area of activity. In the cortex, however, the estimated error due to light scattering is smaller than 200 μm (Orbach and Cohen, 1983).

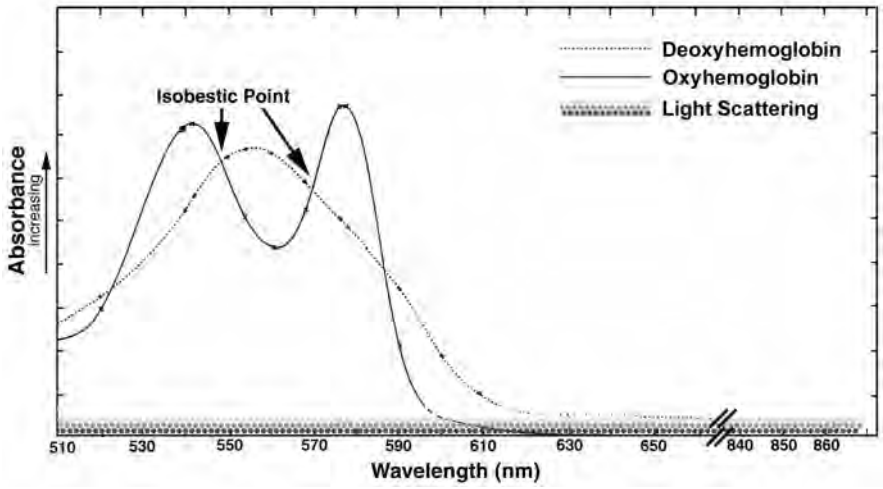

Figure 2 Hemoglobin absorption curves. The absorption curves for oxy- and deoxyhemoglobin are displayed to demonstrate the differential absorption of light by the primary moieties of hemoglobin at different wavelengths. This makes it possible to emphasize different physiological processes by imaging at specific wavelengths (see Section II.D.1). For example, imaging at 550 and 570 nm (the isobestic points) emphasizes changes in total hemoglobin because at these wavelengths the two major moieties of hemoglobin absorb equally. When imaging in the 600 to 630 nm range, on the other hand, oxyhemoglobin absorption is negligible so most of the intrinsic signal response is believed to represent changes in deoxyhemoglobin concentrations. At longer wavelengths both hemoglobin moieties have negligible absorbance and light scattering effects predominate. Light scattering is believed due to cellular swelling and changes in blood volume and blood flow, as well as many other unaccounted-for phenomena. Circles at the bottom of the graph represent light scattering occurring at all wavelengths, but its impact on the optical signal becomes significant only at longer wavelengths. The differential absorption of the major hemoglobin moieties is also essential for spectroscopic analysis of intrinsic signals (see Section II.D.2).

Recently, Nomura and colleagues introduced a new protocol for mapping light scattering changes *in vivo* without any contribution from hemoglobin absorption (Nomura *et al.,* 2000). This was accomplished by exchange transfusion with fluorocarbon (Green Cross, Osaka, Japan). Fluorocarbon is artificial blood with adequate oxygen-carrying capacity to maintain life for a number of days but without any absorption in the visible and near-infrared range. Although this approach allows imaging isolated light scattering changes *in vivo,* results using this model may not be extensible to intrinsic signals measured with whole blood intact since the oxygen-carrying capacity and solubility of fluorocarbon are significantly different from those of hemoglobin. These differences result in a doubling of cerebral blood flow and preferential flow increases to the cortex and cerebellum (Le *et al.,* 1988).

Similarly, the light scattering signal has emerged as an extremely useful mapping signal in slices (Stepnoski *et al.,* 1991) and the isolated brain. The light scattering signals obtained in these *in vitro* preparations are, in a way, simpler to interpret than *in vivo* signals because they are not superimposed on signals arising from hemoglobin-related changes. However, the difficulty of ascribing a specific signal etiology to the light scattering signal still remains.

D. How Can the Different Components of the Intrinsic Signal Be Resolved?

The major chromophores that influence intrinsic signal changes are oxyhemoglobin and deoxyhemoglobin, each of which has a unique absorption spectrum (Fig. 2). Based on the differential absorption of light by these two chromophores, two approaches have been developed to determine the etiology of intrinsic signals. The first approach herein referred to as "single-wavelength imaging," is to emphasize different physiological processes by imaging at specific wavelengths of light which either accentuate the differences between the chromophores (e.g., at 610 nm, deoxyhemoglobin absorbs significantly more than oxyhemoglobin) or minimize the difference between the chromophores (e.g., 570 nm is an isobestic point at which oxy- and deoxyhemoglobin absorb equally) (Fig. 2). The second approach, herein referred to as "spectroscopic imaging," is to image multiple wavelengths simultaneously and use post hoc spectroscopic analysis to determine the contribution of the different intrinsic signal components.

1. Single-Wavelength Imaging

The selection of wavelengths for single-wavelength imaging is primarily based on the absorption spectra of oxy- and deoxyhemoglobin. As would be expected, the time course and spatial involvement of optical responses at different wavelengths are unique (Fig. 2) (Hodge *et al.,* 1997; Nemoto *et al.,* 1999). For example, at 610 nm, the absorbance of oxyhemoglobin is negligible compared to that of deoxyhemoglobin (Fig. 2). Therefore, imaging at 610 nm is believed to emphasize changes in deoxyhemoglobin (Frostig *et al.,* 1990, Nemoto *et al.,* 1999). Consistent with blood oxygen level-dependent (BOLD) *f*MRI studies (Hu

et al., 1997; Logothetis *et al.,* 1999; Yacoub *et al.,* 1999) and oxygen-dependent phosphorescence-quenching dye studies (Vanzetta and Grinvald, 1999), optical imaging at 610 nm indicates an initial focal increase in deoxyhemoglobin (analogous to the "initial dip") followed by a more global decrease in deoxyhemoglobin (Fig. 1). In contrast, imaging at 550 or 570 nm, which are isobestic points, should emphasize changes in total hemoglobin, since deoxyhemoglobin and oxyhemoglobin absorb equally at these wavelengths. Accordingly, the time course and spatial extent of the response at these wavelengths is significantly di ferent from that observed at 610 nm. Finally, imaging at 850 nm, which is near infrared and at which the absorption of both hemoglobin moieties drops dramatically , is dominated by light scattering changes. Studies comparing intrinsic and intravascular dye signals suggest that these light scattering changes correlate well with changes in cerebral blood volume and may not be directly influenced by hemoglobi levels and oxygenation (Fig. 2) (Narayan *et al.,* 1995; Cannestra *et al.,* 1998a; O'Farrell *et al.,* 2000).

The signal at any particular wavelength is multifactorial; it can only be said that certain components are *emphasized* at a particular wavelength. They cannot and should not be assumed to represent just those components described here. Also, different wavelengths of light penetrate the cortex to different degrees (longer wavelengths penetrate deeper into the cortex) and therefore one should be cautious about interpreting results across wavelengths since dif ferent cortical volumes may be sampled at different wavelengths (Mayhew *et al.,* 1999).

Although intrinsic signals at various wavelengths originate from dif ferent sources, they can all be used for functional mapping. These differences in intrinsic signals across wavelengths may be exploited depending on the scientifi question at hand. To characterize the functional architecture of, or "map," the brain, it may be more appropriate to image at 610 nm. However, to characterize blood volume changes, it would be better to image at 550 or 570 nm.

2. Spectroscopic Analysis of Intrinsic Signals

Spectroscopic analysis of intrinsic signals has become increasingly popular because it allows a more specific deter mination of the etiology of intrinsic signals.Two approaches have been suggested. The first approach is to acquire simul taneous spectral information from many locations in the form of a spatiospectral image. In order to gain the spectral dimension, a spectrophotometer is used to spectrally decompose the image and at least one spatial dimension must be sacrificed. Still, under most circumstances, signals originat ing from cortex, draining veins, and feeding arterioles can be separated. In order to retain at least one spatial dimension from the imaged area, the optical imaging apparatus must be modified to have two image planes, instead of the one plan used in the conventional apparatus (see Section IV.C). In the first image plane, a narrow slit isolates a selected line acros the cortical surface. This cortical slit (Fig. 3) is then projected onto a dispersing grating (in the spectrophotometer), whose grooves are aligned parallel to the slit, so that the image of the selected cortical band is dispersed into its spectral components along the orthogonal axis. Thus, in the second image plane, a two-dimensional image is produced, with one spatial dimension and one spectral dimension, showing the spectral information about multiple cortical points simultaneously (Fig. 3). The detector is placed in the second image plane to capture this spatiospectral image.

Alternatively, in order to retain two dimensions, a filte wheel can be used to acquire multiwavelength data *near* simultaneously. By interleaving images at dif ferent wavelengths throughout a single trial and by imaging at dif ferent wavelengths at the same time point across dif ferent trials, a four-dimensional volume set can be acquired (two spatial dimensions, time, and wavelengths), which can be used for subsequent spectroscopic analysis. The limitation of this approach is that the multiwavelength/spectral data being collected are not simultaneous, and it is well known that intrinsic signal responses can vary greatly across trials (Chen-Bee and Frostig, 1996; Masino and Frostig, 1996).

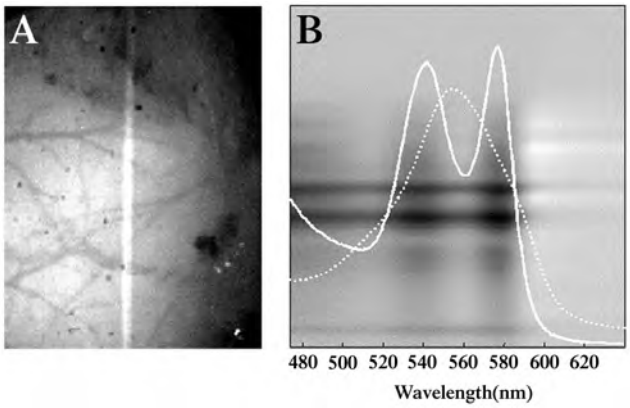

Figure 3 The "cortical band" and optical spectroscopy . (**A**) Image of the cortical surface with the position of the cortical slit from which spectroscopic data are collected. White light is transmitted through only the indicated portion of the image and directed into a spectrophotometer to create a spatiospectral image as shown on the right. (**B**) Image of the spatiospectral pattern obtained after the gratings in the spectrophotometer disperse the light transmitted through the cortical slit. This image is obtained in the second image plane where the camera detector is positioned. The image was obtained by subtracting the peak (~3.5 s after stimulus onset) of the averaged response (30 trials) following electrical whisker stimulation from the mean baseline (8 s) before stimulation. The *y* axis corresponds to the position down the slit, shown in (A). The *x* axis in the spatiospectral image corresponds to the wavelength. The "textbook" absorption spectra of oxy- and deoxyhemoglobin are superimposed on the image (oxy—solid line, deoxy—dotted line). The increases in absorption (darker vertical regions) are primarily due to an increase in the proportion of oxyhemoglobin. The predominant dark horizontal bands reflect the changes in bloo volume in the middle cerebral artery . Adapted, with permission, from Mayhew *et al.* (2000).

This limitation can be statistically overcome by acquiring a large number of trials (i.e., high *N*) so that the variability of the response is accounted for.

Once spectral data have been obtained, a modifie Beer–Lambert Law is used to extract the contribution of the different chromophores to the intrinsic signal. The spectral changes are fitted by the known spectra of oxyhemoglobi and deoxyhemoglobin as well as cytochromes and light-scattering components. The first such study applied a linea component analysis to extract the etiology of the intrinsic signals (Malonek and Grinvald, 1996), but this approach has been called into question recently. More sophisticated analyses are now available which incorporate terms such as wavelength-dependent path-length factors (Mayhew *et al.,* 1999; Nemoto *et al.,* 1999). (Details on methodology are provided in Section VI.B.)

E. The Time Course of Intrinsic Signals

As alluded to earlier, intrinsic signal changes at different wavelengths have dif ferent time courses. There are two major patterns of intrinsic signal time courses: monophasic (decreased reflectance) and biphasic (initially decrease reflectance followed by increased reflectance). In t visible spectrum up to ~590 nm, functional intrinsic signal changes monophasically decrease reflectance. Between 60 and 760 nm, a biphasic pattern is observed. Finally , at wavelengths greater than 760 nm, a monophasic pattern reminiscent of wavelengths less than 590 nm is observed.

For monophasic responses, responses generally appear approximately 1 s after stimulus onset, peak between 3 and 4 s after stimulus onset, and return to baseline by approximately 8 s (Nemoto *et al.,* 1999) (Fig. 1, bottom). For the biphasic responses, the initial response to stimulation is usually a little more rapid, appearing within 500 ms, peaking between 1.5 and 2 s after stimulus onset, reversing phases at about 3 s, peaking in the opposite polarity approximately 5 s after stimulus onset, and returning to baseline by approximately 10 s (Fig. 1, bottom). This time course is generally consistent with the time course of the "initial dip" in deoxyhemoglobin concentrations (Menon *et al.,* 1995; Malonek and Grinvald, 1996; Mayhew *et al.,* 1999; Nemoto *et al.,* 1999; Cannestra *et al.,* 2001).

Based on spectroscopic studies published, time courses of the individual components that contribute to intrinsic signal changes have also been characterized. Deoxyhemoglobin concentrations are believed to rise immediately following stimulus onset, peak between 1 and 2 s after stimulus onset, return to baseline 2–3 s after stimulus onset, decrease and peak between 4 and 6 s after stimulus onset, and finally retur to baseline concentrations. Oxyhemoglobin concentrations on the other hand are slower to respond to stimulation, increasing approximately 1 s after stimulus onset, peaking at approximately 4 s after stimulus onset, and returning to baseline (monophasic) (Malonek and Grinvald, 1996; Mayhew *et al.,* 1999; Nemoto *et al.,* 1999).

III. Preparation of an Animal for Optical Imaging

A. Species

Optical imaging of intrinsic signals is done in a variety of species, including rodent (Narayan *et al.,* 1994; Masino and Frostig, 1996), cats (Grinvald *et al.,* 1986; Frostig *et al.,* 1990), nonhuman primates (Bonhoef fer and Grinvald, 1991), and humans (Haglund *et al.,* 1992; T oga *et al.,* 1995a). Each offers distinct advantages and drawbacks.

1. Rodents

The rodent somatosensory cortex is or ganized somatotopically as a ratunculus (Chapin and Lin, 1984), analogous to the homunculus. The posteromedial barrel subfiel (PMBSF) of the rodent somatosensory cortex (W oolsey and Van der Loos, 1970) has cytoarchitecturally and functionally discrete groups of cells called "barrels," each representing one contralateral whisker (Woolsey and Van der Loos, 1970; Simons, 1978) (Fig. 4C). Anterior and medial to the PMBSF, there are sensory cortices representing the hindlimb and forelimb of the rodent. Electrophysiology (Chapin and Lin, 1984) and 2-deoxyglucose autoradiography (Durham and Woolsey, 1977; Kossut, 1988) confirm that functional somatotopy i tightly coupled with cytoarchitecture, making this system ideal for investigating the coupling of neuronal activity and perfusion-related and metabolic responses. Another advantage of the rodent model is the small intersubject anatomic variability in rodent (Toga *et al.,* 1995b). The rodent brain is also lissencephalic, thereby eliminating much of the geometric registration issues that complicate gyrencephalic studies. Because of the small size of rodents, imaging in these subjects is also amenable to a thin bone preparation and avoids the need for implantation of an imaging chamber , significantly simplifying imaging procedures (see Sectio III.C.2). Finally , and perhaps most importantly , the rodent model allows investigators to conduct population-based studies instead of basing measurements on a small number of subjects, as is often the case in studies involving cats, primates, or humans. This may be a critical point, considering that representations across populations may vary greatly (Chen-Bee and Frostig, 1996). Chen-Bee and Frostig (1996) have shown that functional whisker representations in rodents may be between 54.6% smaller and 50.6% lar ger than the average areal extent across the population. The major drawback to using the rodent model is that the extensibility of results to human subjects is unclear . If the goal of the research is to characterize neurophysiology to better understand the human condition, it is clearly preferable to use

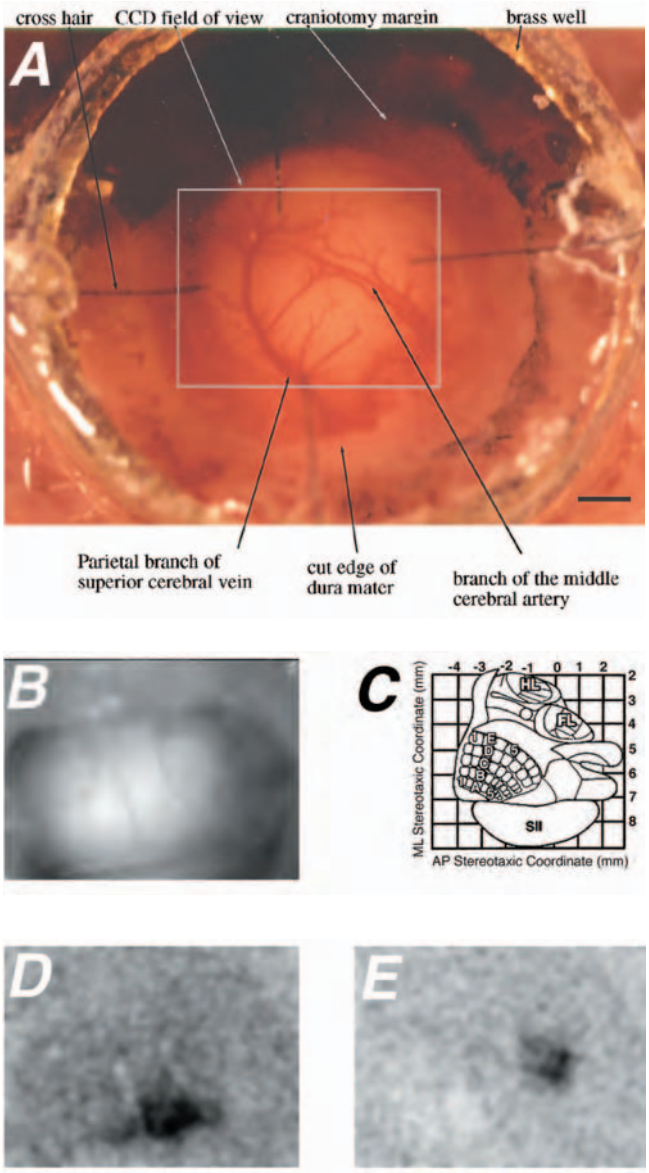

Figure 4 Cranial window for optical imaging. (**A**) Photograph of closed cranial window over the rodent somatosensory cortex, demonstrating a clear view of major cerebral vessels as labeled. Note that the closed cranial window design can be adapted to different species. Although a rodent model is portrayed here, similar systems are used in cats and primates. (**B**) Image of another cranial window overlying rodent somatosensory cortex as observed through a 610-nm filter. Once again, prominent venous vessels are observed at this wavelength, which emphasizes deoxyhemoglobin absorption. The image is slightly blurred because the imaging plane is focused below the cortical surface. (**C**) Stereotactic coordinates of the rodent somatosensory cortex. FL, forelimb; HL, hindlimb; SII, secondary somatosensory cortex. Other labels indicate the corresponding whiskers for each barrel found in the rodent somatosensory cortex. Notice that the area of somatosensory cortex responding to hindlimb stimulation is anterior and medial to the area that responds to whisker stimulation. (**D** and **E**) Activations observed at 610 nm corresponding to whisker and hindlimb stimulation of the rodent, respectively, using the cranial window preparation displayed in (B).Activations appear in appropriate locations and are consistent with the schematic stereotactic map displayed in (C).

subjects that are phylogenetically closer to humans, such as nonhuman primates.

2. Cats

Intrinsic imaging studies in cats have significantly furthered our understanding of both neurophysiology (Grinvald *et al.,* 1986; Frostig *et al.,* 1990; Malonek and Grinvald, 1996) and the organization of the visual cortex (Bonhoeffer and Grinvald, 1991, 1993a). The larger size of the brain relative to the rodent and its greater complexity are both significant advantages of using this subject over rodents. For example, rodents have very poorly developed visual cortices, which would have prohibited all of the major advances in visual cortex characterization achieved using intrinsic imaging (Bonhoeffer and Grinvald, 1991, 1993a,b; Grinvald *et al.,* 1991; Grinvald, 1992; Victor *et al.,* 1994; Shmuel and Grinvald, 2000). The higher complexity of the cat brain makes it more likely that results can be extrapolated to humans. Furthermore, the larger size of the brain has made it easier to isolate and characterize functional perfusion-related changes in different brain compartments (for example, see Malonek and Grinvald, 1996).

3. Nonhuman Primates

Primates offer the best opportunity to conduct studies that are extensible to human subjects without actually facing the challenges of intraoperative brain mapping. However, this very significant advantage comes at a cost. The care of primates is much more expensive and time consuming than that of rodents and cats. Because of the investment required in each subject, population studies of more than a few subjects are not practical. Furthermore, because of the thickness and density of the cranium and dura, imaging in primates requires craniotomy and removal of the dura. In many respects, these are small costs to pay to obtain physiological data that can be directly applied to humans.

4. Humans

Intraoperative mapping provides an unparalleled opportunity to examine the basic physiology and the organization of the functioning human brain. The opportunity exists to study questions that are impossible in other species, such as language organization and higher cognitive functions (Cannestra *et al.,* 2000; Pouratian *et al.,* 2000a). At the same time, intraoperative mapping poses unique challenges for the acquisition, analysis, and interpretation that are over and above those issues that are part of any other intact *in vivo* brain mapping. These include the operating room environment, time constraints, spatial resolution, status of the brain under anesthesia or performance during awake protocols, a dynamic cortical geometry, and other considerations. Imaging must be compatible with the intraoperative environment, most important of which are sterility and mobility. Another challenge faced by intraoperative imaging is that

the site of imaging must be determined by clinical indications since subjects are primarily being admitted for treatment of intracranial pathologies. This may result in suboptimal imaging in many cases. Also, as anesthesia is dictated by clinical standards, the investigator cannot control anesthetic type or depth. It should be noted, also, that human experimentation requires institutional approval of human subjects research.

B. Anesthesia

Anesthesia has a strong effect on the coupling between cerebral blood flow and neuronal activity (see, for example Buchweitz and Weiss, 1986). Therefore, anesthesia must be chosen with great care and levels must be monitored very closely. The level of anesthesia is especially important since a major component of intrinsic signals is related to hemoglobin oxymetry changes. Excessive anesthesia may adversely alter the ventilation and therefore relative hemoglobin concentrations of the subject. Shtoyerman and colleagues (2000) demonstrated that if anesthesia is well controlled, intrinsic signals under general anesthesia will have time courses similar to those observed in awake, behaving animals, although smaller in magnitude. Under most circumstances, experiments are conducted under general anesthesia. Barbiturates and gas anesthetics (e.g., isoflurane) are both popular and work well for optical imaging. This does not preclude the possibility that other anesthetics may be suitable for experiments. However, one should remember that the effect of anesthetics on neurovascular coupling may be species and/or strain dependent.

Anesthetic depth should be monitored continuously throughout experiments (especially those in which the effect of a certain manipulation is being ascertained) since anesthetic depth may affect the magnitude of the intrinsic signals. In general, anesthetic depth can be determined in all species by determining the response to a noxious stimulus. For example, in rodents, one can monitor depth by testing the toe-pinch reflex. The goal should always be to maintain a constant anesthetic depth for the duration of imaging.

There is increased interest in measuring intrinsic signals in awake, behaving subjects. As mentioned earlier, intrinsic signals in awake, behaving monkeys have been shown to have temporal profiles similar to those in general-anesthetized subjects, although with a larger magnitude (Shtoyerman *et al.,* 2000). Imaging responses in awake subjects offers the exciting opportunity to characterize neurophysiology without any possible pharmacological side effects. Conversely, such studies may help elucidate the pharmacological effects of certain drugs on cerebral perfusion. However, these experiments come at the expense of decreased investigator control of the subject. The most significant complication is the introduction of increased cortical movement and noise to the imaging procedure. However, the benefits of imaging awake, behaving subjects may far outweigh the costs since it affords the opportunity to image language and cognitive functions in humans, which may otherwise be impossible using intrinsic signal imaging (Cannestra *et al.,* 2000; Pouratian *et al.,* 2000a).

Optical intrinsic signals arise primarily from changes in cerebral blood flow, cerebral blood volume, hemoglobin oxygenation, and light scattering. It is therefore critical to monitor physiological parameters that may alter cerebral perfusion and metabolism independent of functional activity to ensure that any observed changes are not due to changes in systemic variables.

1. Ventilation and End-Tidal CO2

The ventilation rate and end-tidal CO_2 of the subject can and will have a direct impact on the hemoglobin oxygenation (see Section III.B). Under most circumstances, intubation or tracheotomy should be performed so that the investigator has complete control over respiration. Monitoring these parameters is also critical when a craniotomy has been performed since hypoventilation can result in cerebral edema and alter the normal neurophysiology of the brain.

2. Blood gases

In some cases, it may be appropriate to monitor arterial blood gases to ensure that the subject is adequately ventilated. Blood gas analysis provides measures of not only the oxygen and carbon dioxide content of the blood, but also its pH, all of which may affect cerebral perfusion. Blood gas analysis is particularly important in cases in which normal homeostatic mechanisms and reflexes may be severel impaired (e.g., deep anesthetic states and seizures).

3. Pulse Oxymetry

A pulse oxymeter allows noninvasive monitoring of the oxygen saturation and heart rate of the subject. Monitoring the heart rate is critical since a drop in heart rate will result in a decreased cardiac output (cardiac output = heart rate $\times$ stroke volume of left ventricle) and may affect cerebral perfusion.

4. Blood Pressure Monitoring

Similar to monitoring heart rate, it is important to ensure that blood pressures do not change since this may also impact cerebral blood flow and volume (Ferrar *et al.,* 1992).

5. Core Body Temperature

Finally, it is critical to monitor core body temperature since thermoregulation is one of the first homeostatic mechanisms to be compromised during anesthesia. Changes in core body temperature can significantly alter peripheral vascular resistance and systemic perfusion (because of the body's attempt to retain heat). Animals that are not adequately thermoregulated will frequently fail to produce any optical

signal changes. A self-regulating heating blanket, which monitors the subject's core body temperature (usually rectal) and adjusts the temperature of the blanket appropriately, is highly recommended.

C Immobilization of Cortex

To take advantage of the superior spatial resolution of optical imaging, it is critical that images acquired before and during activation be in identical locations, since the former will be subtracted from the latter during analysis.The movement of the brain due to respiration and heartbeat presents a major obstacle. Five different strategies have been devised to overcome this challenge: the cranial window, the thin-skull preparation, stabilization using glass plates, synchronization with respiration and heartbeat, and postacquisition image registration. These approaches are not mutually exclusive and under several circumstances, more than one strategy can be used in a single experiment (e.g., cranial window and synchronization with respiration and heartbeat, Grinvald *et al.,* 1991; glass plate and postacquisition image registration, Haglund *et al.,* 1992).

1. The Cranial Window

The first method to stabilize the cortex employs an elaborate chamber system (a "cranial window") (adapted from Bonhoeffer and Grinvald, 1996). The chamber, composed of a circular, stainless steel ring, with an inlet and outlet valve to which tubing can be attached, is mounted on the skull with dental cement before the skull is opened (Fig. 4). The normal procedure is to make the trephination of the skull and to mount the chamber with dental cement before taking the piece of bone out of the skull. If trephination is carried out with a high-speed drill, heat can accumulate and may be particularly dangerous and harmful to the cortex. Excessive heat should be controlled for with constant irrigation during drilling. To perfect the seal between the chamber and the skull, dental wax is melted (with a microcauterizer) into the remaining gaps between the inside of the chamber and the skull. After the chamber is mounted, the bone and dura can be removed. Prior to excising the dura, large dural blood vessels should be occluded with thread or forceps to avoid contact between the exposed cortical surface and blood. Alternatively, the superficial dural vessels can be occluded prior to resection of deeper dural layers. Finally, the remaining cerebrospinal fluid or saline is removed from the cortex using small triangles made from cellulose fibers (Sugi Escheburg, Germany).

The chamber is then sealed with a round coverslip and filled with silicon oil (e.g., Dow Corning 200, 50 cSt) or artificial cerebral spinal fluid via the inlet valve. It is critical that excessive pressure not be applied to the cortex. This is best achieved by having the fluid flow into the chamber from an upright syringe without the piston and adjusting the level of the syringe with respect to the chamber for precise regulation of the pressure of the fluid in the chamber. If the chamber is filled perfectly, i.e., without any air bubbles or cerebrospinal fluid droplets, this arrangement provides a ideal optical interface and, at the same time, stabilizes the brain.

In long-term experiments the stainless steel chamber just described has to be modified in several important ways. For chronic recordings, the inlets of the chamber can be closed with screws. Moreover, if the window of the chamber is large, it is important to have a metal lid that can be screwed into the chamber instead of the breakable cover glass. Finally, the chamber should be produced from titanium instead of stainless steel because titanium, although difficult to machine, is strong, light, and, above all, highly inert to bodily fluids. Even with implantation times over many months, no difficulties have been observed with a chamber made from this material (Shtoyerman *et al.,* 2000). In long-term experiments it is also of great importance that the chamber is mounted on the skull such that there is no danger of the chamber detaching even after long survival times. This is particularly problematic in young animals in which the bone is often still relatively soft. It has proven useful to clean and degrease the skull with ether and to place screws in the bone next to the chamber. These screws are then covered with the dental cement for mounting the chamber and thus help anchor the chamber firmly onto the skull

Cortical edema, or herniations, due to hypoventilation or other reasons may be extremely traumatic when using a cranial window (especially when the exposed cortical area represents a large fraction of the brain surface area, such as in rodent preparations). There are several ways to deal with this problem, including injecting high-molecular-weight sugars (e.g., mannitol), lowering the position of the body, hyperventilation, applying 10–20 cm of hydrostatic pressures in a closed chamber for a limited period of time, or puncturing the cisterna magna.

2. Thin Skull Preparation

The thin skull preparation is a strategy used in rodents that takes advantage of the fact that the rodent skull is not very thick to begin with. Masino and colleagues (1993) demonstrated that if the rodent skull is uniformly thinned using either a scraping instrument or a dental drill over the cortical area of interest, intrinsic signal could be imaged through the intact skull. If a dental drill is used to thin the skull, care should be taken to thin slowly in order to (1) prevent cortical damage from excessive heat due to friction and (2) ensure that the skull is thinned uniformly throughout the area of interest. Heat damage can also be prevented by constant irrigation with saline during drilling. In order to increase the translucency of the skull for the duration of the imaging period, silicon oil should be applied to the skull. If the bone has been thinned adequately, arterioles and venules

should be easily visualized in the field of view of the detec tor. The one difficulty with this preparation is that during th thinning procedure, epidural and subdural hematomas, which will interfere with signal detection, can be induced. If hematomas are observed, subjects should be excluded from studies. The utility of this approach has been confirmed b other studies as well (Cannestra *et al.,* 1998a; Polley *et al.,* 1999a,b; O'Farrell *et al.,* 2000).

3. Glass Plate

The use of a sterile glass plate atop the cortex immobilizes the cortex by applying pressure to the cortical surface to prevent its movement (Haglund *et al.,* 1992). This approach has been used only in human subjects. While this method may achieve immobilization, it is not considered ideal because it physically interferes with the cortex and therefore may alter normal functional blood volume and cellular swelling patterns.

4. Synchronization with Heartbeat and Respiration

Synchronization of image acquisition with respiration and heartbeat in subjects who are being ventilated is achieved by halting respiration after exhalation for a short time (less than 1 s). The respiration is then reinitiated when an appropriate trigger circuit detects the next heartbeat. If data acquisition is synchronized this way, the images will always be collected in the same phase of heartbeat and respiration, enabling cancellation of physiologically induced motion artifacts during data analysis. Synchronization between heartbeat, respiration, and data acquisition reduces the noise, even in a well-sealed chamber, by a factor of approximately 1.5 (Grinvald *et al.,* 1991; Toga *et al.,* 1995a).

In awake subjects or those not being ventilated, synchronizing image acquisition with respiration and heart rate requires monitoring of pneumographic and electrocardiographic waveforms. All trials (control and experimental) should begin at the same point in time during the respiration cycle, after which acquisition is synchronized to the cardiac cycle (500 ms post-R-wave). Experimental and control trials should be collected alternately on sequential respiratory expirations. Each experimental image will have a separate control image taken from either the preceding or subsequent expiration cycle. Since data acquisition occurs at similar time points during every respiration cycle, all images are collected with the brain in a similar position, minimizing the effect of periodic brain motion.

5. Postacquisition Image Registration

Under certain circumstances (e.g., intraoperatively), the investigator may be restricted from employing the previously described strategies for cortical immobilization. This is particularly true in the intraoperative environment, in which imaging time needs to be minimized and additional physical procedures for research purposes may not be authorized. Postacquisition image registration utilizes automated image registration (AIR) algorithms (W oods *et al.,* 1992). When acquiring images independent of pneumographic or electrocardiographic waveforms, the precise location of the cortex within the field of view varies from image to image. AIR can be used to realign all images in a series to a reference image either at the beginning or in the middle of the acquisition series. The realignment of images is intensity-based, using the extremely lar ge difference in light intensities emanating from sulci and gyri to place the images into correspondence. Higher order warps may be necessary to achieve proper realignment if there is significant motion in the z direction (i.e., toward and away from the detector). Functional changes in cortical reflectance do not interfere with this realignmen algorithm since functional reflectance changes, which ar <1% in magnitude, are minimal compared to the dif ference in reflectance from sulci and gyri (gyral light intensity level can be up to 2000 times that of sulci). Postacquisition image registration effectively compensates for movement between images and minimizes the need to interface with operating room monitors (Cannestra *et al.,* 2000, 2001; Pouratian *et al.,* 2000a).

IV. The Apparatus

A. The Camera

1. Photodiode Arrays

The first functional maps based on intrinsic signals wer created using a 12 × 12 photodiode array (Grinvald *et al.,* 1986). Photodiode arrays generally of fer a lar ger dynamic range (>17 bits) than other types of detectors and the capability for much higher temporal resolution (on the order of milliseconds). It is clear , however, that the low number of pixels in standard diode arrays limits their usefulness for high spatial resolution intrinsic imaging. While some may argue that these fast cameras with their millisecond time resolution may be of value for studying the time course of intrinsic signals (for example, with the imaging spectroscopy approach discussed earlier), the temporal resolution gained by using a photodiode array is not necessarily required (depending on the experiment) since the time course of perfusion-related signals is on the order of seconds. These devices may be particularly useful for optical imaging of voltage-sensitive dyes (as opposed to intrinsic signals) for monitoring extremely fast electrophysiological changes that occur within 100–200 ms.

2. Video Cameras

The first attempt to use video cameras to image cortica activity was made in 1974 by Schuette and collaborators (1974). More than 10 years later, Gross and colleagues digitally intensified video imaging with voltage-sensitive dye

to image voltage changes across single cell membranes (Gross *et al.,* 1986). Shortly afterward, Blasdel and Salama (1986) used a similar technology with an *in vivo* preparation to obtain spectacular images of the functional architecture of the macaque visual cortex. Compared to photodiode arrays, the increased spatial resolution of video cameras is at the expense of temporal resolution (Kauer , 1988). However , for intrinsic signal imaging, the extremely high temporal resolution of photodiode arrays is not a critical parameter . A more important limitation is the signal-to-noise ratio (SNR) of standard video cameras of approximately 100:1 to 1000:1.

3. Slow-Scan CCD Cameras

Slow-scan digital CCD (char ge-coupled device) cameras offer very good SNR while retaining the advantages of high spatial resolution and moderate cost. Like video devices, CCDs have lower temporal resolution than photodiode arrays. However, as mentioned earlier , this is lar gely of no consequence since intrinsic signal time courses are on the order of seconds. Ts'o and colleagues (1990) were the first to use CC cameras for intrinsic signal imaging to image the functional architecture of the visual cortex in the living brain.

Several important parameters which may influenc image quality, SNR, and acquisition capabilities should be considered when comparing CCD cameras. They are discussed in detail below.

a. Shot noise. The magnitude of intrinsic signal changes is exceedingly small, on the order of 0.1%. In order to be able to ascribe statistical and biological significance to such meas urements, one must be able to dif ferentiate these intrinsic signal changes from stochastic fluctuations in photon emis sions. That is, one has to ensure that small changes in reflectance are physiological in origin and not caused by th statistical fluctuations of the light-emitting process. The number of photons that can be attributed to statistical fluctua tions equals the square root of the total number of photons emitted. Consequently , the number of photons needed to detect a signal change of 0.1% with a SNR of 10 is 100,000,000 (signal = 100,000, noise = 10,000, therefore SNR = 10). These calculations highlight the fact that light intensity and the well capacity of the CCD have to be chosen appropriately such that an adequate number of photons is accumulated during the experiment. Note that it is not necessary to accumulate this number of photons in a single frame (in fact, this would be impossible considering that the well capacity of most CCDs is on the order of 300,000 to 700,000). Rather, this number represents the total number of photons that should be collected over all trials; multiple trials can also be averaged to increase the SNR (by the square root of the number of trials).

b. Well capacity. The well capacity of a CCD denotes the total number of photons that can be accumulated on 1 pixel before there is char ge overflow or saturation Because of the previously mentioned considerations (see Shot noise above), it is important that well capacities be as large as possible. Well capacities generally range from 300,000 to 700,000; smaller well capacities can also be used but will require a greater number of trials to be able to detect similar small intrinsic signal changes. One way to increase the ef fective well capacity in existing chips is to combine the char ge from several adjacent pixels using "on-chip binning." (This, however, results in a loss of spatial resolving power so the advantage of binning relative to increased spatial resolution must be considered.) Normally , on-chip binning is limited to 2×2 or 3×3.

c. Analog-to-digital converters. Although purchasing a CCD with a greater well capacity will theoretically allow an investigator to increase SNR (as explained above), this advantage is lost if the high-quality camera output is digitized using only an 8-bit analog-to-digital (AD) converter . Eight-bit AD converters have become an industry standard because they of fer an economical means to digitize video signals. Although image enhancement strategies have been developed to allow continued use of such converters (i.e., differential video imaging, see section below), under most circumstances it is essential to incorporate a frame grabber with sufficient resolution to preserve the quality of the dat obtained by the camera. To illustrate, imagine a CCD chip with a 500,000-electron-well capacity . Using an 8-bit AD converter would result in the equivalent of approximately 2000 electrons per level (256 levels total). Assuming baseline images are acquired in the middle of the dynamic range of the camera (~250,000), this would mean that each gray level of digitization would be approximately equal to a 0.7% intensity change. If the goal of intrinsic signal imaging is to detect signals as small as 0.1%, this is clearly insufficient. I contrast, if a 14-bit frame grabber were to be used, this would be equivalent to 30 electrons per level (16,384 levels total) or a 0.01% intensity change per level. Although the increased resolution comes at a price, it is a worthwhile investment since it would otherwise negate the significan investments made in the camera.

d. Advances in sensitivity and signal to noise. Recent advances in CCD camera technology have significantl increased the sensitivity and SNR of CCD chips. In general, back-thinned CCD chips are associated with greater sensitivity and quantal efficiency and have become standard i almost all CCD cameras. Intensified CCDs and electron bombardment CCDs (EB-CCDs) have also recently been introduced into the market. In both types of cameras, a photocathode between the image and the CCD converts photons to electrons, acting to intensify the image and increase the quantal efficiency of the CCD. In EB-CCDs, the photo cathode releases electrons (with variable gain) to be subse-

quently accelerated across a gap (via a high-voltage gradient) and "bombard" the CCD chip. The advantages of these new devices over a traditional slow-scan CCD are the additional gain and accompanying speed, allowing exposure times of as little as 1 ms while maintaining very good spatial resolution. These advantages are at a cost of diminished dynamic range. The increased gain, sensitivity, and SNR may be critical in certain applications, such as intraoperative imaging of human cortex in which image exposure needs to be minimized to reduce intraimage cortical movements.

e. Frame transfer. CCD cameras require that that during readout of the acquired image, illumination of the area containing the image information be avoided by all means. Some cameras use a mechanical shutter during the readout time to accomplish this. The mechanical shutter approach is problematic for optical imaging applications since the fastest readout times are on the order of 50 ms and therefore would require the shutter to be closed (and therefore not acquiring data for that period of time). Additionally, the large number of exposures in a single experiment and lifetime of a CCD would be incompatible with the limited lifetime of a mechanical shutter. Alternatively, many CCD cameras offer a "frame transfer mode." In frame transfer mode, half of the light-sensitive area of the CCD chip is covered with an opaque coating. After each exposure the accumulated charges from the illuminated area are shifted to the opacified area within approximately 1 ms. While the "transferred frame" is read out from the opacified portion of the CCD, the light-sensitive region of the CCD can begin to accumulate charges from the next exposure. Since this mode of operation allows acquisition of "back-to-back" images and avoids complications of a mechanical shutter with a limited lifetime, the frame transfer mode of operation is the recommended mode of operation.

4. Differential Video Imaging

As explained earlier, when a high-quality camera output is digitized using only 8 bits, the advantages of the camera are lost. Consequently, several image enhancement approaches have been developed to allow the use of an 8-bit frame grabber while retaining the details of the data offered from a higher resolution imaging device. Most of these techniques, however, use procedures that enhance the image only after its initial 8-bit digitization. These approaches in fact cannot detect intensity changes that are smaller than 1 part in 256 (~0.4%) since these intensity values would have been reduced to the same gray-scale value on initial digitization. Another common approach to image enhancement is to subtract a DC level from the data and amplify the resulting signal prior to its digitization. This approach is, however, applicable only to flat images with very low contrast

An alternative approach for image enhancement is to process (i.e., subtract) images prior to digitization so that the difference images are digitized instead of original images. This approach uses analog differential subtraction of a stored "reference image" from the incoming video images. An apparatus which uses this alternative approach is commercially available (Optical Imaging, Inc., Germantown, NY). It uses analog circuitry to subtract a selected reference image from incoming camera images and then performs a preset analog amplification of the differential video signal before digitizing it using an 8-bit analog-to-digital converter. Although this approach is not as precise as using a higher resolution analog-to-digital converter and storing the original images for subsequent calculations, it offers exquisite sensitivity, is less expensive, requires less storage space, and has been used successfully by numerous groups. The noise can be further reduced, as with any approach, by trial averaging. The digital image of a given reference image and the corresponding enhanced sequence of images can later be combined.

Another significant advantage of the commercially available system is that an enhanced image is displayed in real time (video rate) on a monitor, thus providing important online feedback to the investigator. This feedback allows problems to be corrected at the earliest stages of the experiment rather than waiting until data have been analyzed offline. Because of the strongly amplified picture, minor optical changes that would later result in large artifacts are immediately noticed. These include moving bubbles of air or cerebrospinal fluid in the closed chamber, excessive noise due to imperfect stabilization of the cortex, or minute bleeding.

A major limitation of differential video imaging is that the original raw optical images are not stored and may therefore limit the versatility of the optical imaging apparatus. This prevents post hoc offline analysis of data using methods other than the subtraction–ratio approach. Such special analyses may be necessary if the investigator does not know *a priori* which image is to be used as the reference or control image (see Section VI.A.1) or if the investigator wishes to compare activations relative to a different control after the experiment has already been conducted. Although the original raw images can theoretically be back-calculated, the resulting images would be of low resolution (8-bit). For a review of different analytic approaches, see Section VI of this chapter.

B. Illumination

Illumination parameters are clearly critical for intrinsic optical imaging since it is the reflectance changes in this illumination pattern which determine the intrinsic signal changes. The wavelengths of the illuminating light depend on the components of the intrinsic signals that the investigator is attempting to emphasize (see discussion above). Apart from this consideration it is also important that the wavelength used provides sufficient penetration into the tissue and, when using a thin bone preparation, through the skull. Shorter wavelengths (e.g., 500 to low 600 nm range) do not

penetrate tissue as well as longer wavelengths, especially in the near-infrared range (e.g., 700 and 800 nm range).

In order to relate the obtained activity maps to the anatomical landmarks, it is also useful to record pictures of the blood vessel patterns. These are best obtained with the brain illuminated by green light, which will highlight both arterial and venous vessels. A band-pass filter between 550 and 590 n with a narrow range (+5 nm, e.g., 550 + 5 nm) is therefore very useful for obtaining the blood vessel picture. Moreover , it may be useful to increase the depth of field of the image b reducing the lens aperture in order to eliminate the blurring of cortical vasculature due to a curved cortical surface.

1. Lamps

A standard 100- or 150-W tungsten halogen lamp housing [e.g., Newport (Irvine, CA), Oriel (Stratford, CT)] with a focusing lens is suitable for illumination. The lamp should be powered by a high-quality regulated, voltage-stabilized power supply in order to achieve strong and stable illumination. It should provide adjustable DC output up to 15 V and 10 A (this can be controlled via serial port in many light sources allowing automated control of incident light levels). Ripple and slow fluctuations should be smaller than 1:1000 An excessive ripple can be improved by adding lar ge capacitors in parallel with the output.The uniformity of the emission spectra is yet another important consideration in selecting an appropriate lamp. For example, arc lamps, which have characteristic distinct lines in their emission spectra, would be inappropriate for optical imaging since uniform lighting across wavelengths would be ideal.

2. Filters and Filter Wheels

Filters and filter wheels should be placed between th lamp housing and the light guides (Fig. 5). An adapter which can hold at least two filters should be fitted so that it connec to the lamp housing on one side and a dual- or triple-port light guide on the other . Alternatively, a high-speed filte wheel can be placed in this position. Most standard filte wheels (e.g., Sutter Instruments, Novato, CA) hold 10 filter and are computer controlled. Using a filter wheel allow acquisition of intrinsic signals at multiple wavelengths interleaved within the same trial. Incorporation of a filter whee into the optical imaging apparatus will prevent the acquisition of truly back-to-back images since time must be allocated between successive images for the filter wheel to mov (usually approximately 50 ms between adjacent filter posi tions). This, however, may not be an issue due to the relatively slow time course of perfusion-related responses being imaged by intrinsic signal imaging. Band-pass filters tha would be useful for single wavelength imaging include: (1)

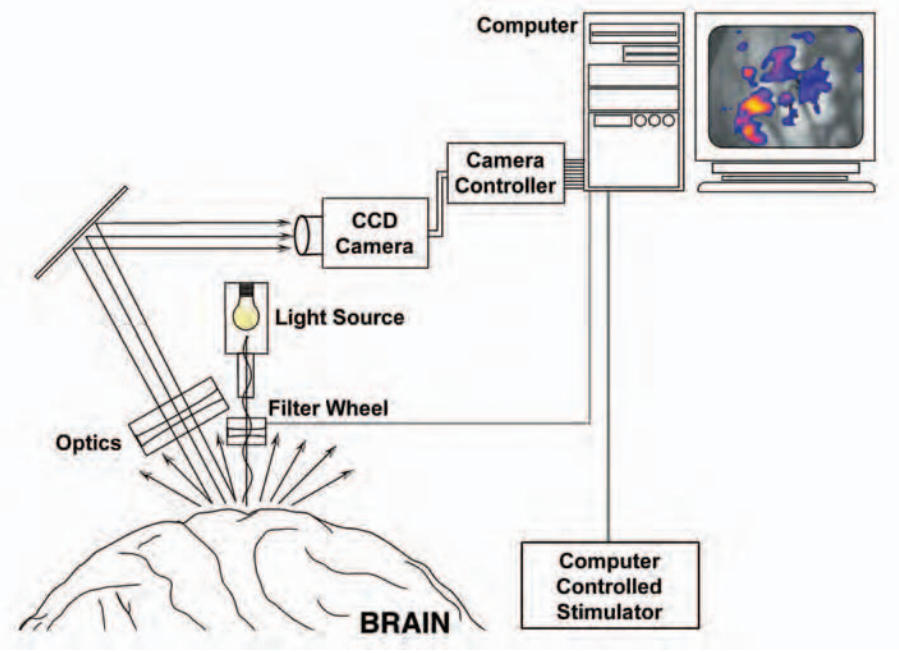

Figure 5 Schematic diagram of the optical imaging of intrinsic signals setup.A light source provides white light which is filtered by a compute -controlled filter wheel before illuminating the cortex. The reflected light is directed through appropriate optics and captured by a CCD camera (or other detector) which is synchronized with stimulation and the filter wheel by a compute -controlled camera controller. The camera controller contains an analog-to-digital converter that digitizes the image before sending the data to the computer to be stored on hard disk. Images are captured during rest and during stimulation. The two sets of images are then compared to detect at which pixels there are significant changes i reflectance. These changes in reflectance correlate with underlying electrophysiological changes

green filte , 505, 550, or 570 nm—for blood vessel pictures and imaging total hemoglobin; (2) orange/red filte , 600, 605, 610, or 630 nm—for imaging hemoglobin oxymetry changes (the difference between oxy- and deoxyhemoglobin is maximized at 600 nm); (3) near -infrared filters, 730, 750 790, 850 nm—for imaging functional light scattering changes; (4) heat filter KG2; (5) long-wavelength heat filt RG9. In general, it is best to use filters with a narrow ban pass so that the investigator knows precisely what wavelengths are being imaged. However , using excessively narrow band-pass filters (i.e., ~1 nm) may limit the amoun of light that reaches the imaging device and therefore limit the resolving power of the imaging setup. In general, investigators should attempt to use filters with a full width half maximum of 10 nm. A 3 OD attenuator (×1000 attenuation) is also often useful in order to artificially produce a signal o 1000 to test the apparatus (see below).

3. Light Guides

Although theoretically epi-illumination *through the lens* should be ideal to achieve a uniform illumination, this mode of illumination does not work well for imaging the live brain because the brain is a curved surface and some parts of the brain absorb more light than others. Therefore, for *in vivo* imaging, using two or three flexible light guides has prove by far the most useful tool in providing evenly illuminated images of the cortex. It is important to confirm even illumi nation of the brain by looking at an online image from the imaging device. This is especially critical when imaging using near-infrared light that is not visible to the human eye. Liquid light guides provide a more uniform illumination than fiber optic guides. Adjustable lenses can be used at the front end of the light guides to focus the incident light on the cortex. Schott (Mainz, Germany) of fers suitable light guides and small, adjustable lenses that attach at the preparation side.

4. Shutter

Some groups have found it advantageous, particularly when experimenting with higher light intensities, to have a shutter on the light source so that the cortex is illuminated only during data acquisition. Note that this shutter is not used during imaging since it would introduce vibration into the imaging experiment and would have a limited lifetime due to the excessive number of image exposures used during any given optical experiment. It is important to ensure that if a shutter is used, it introduces minimal vibration into the system. Good shutters can be obtained from a variety of sources [e.g., Uniblitz (Rochester, New York), Prontor (Germany)].

C. The Macroscope (Adapted from Bonhoeffer and Grinvald, 1996)

Photographic macrolenses have a lar ge depth of field resulting in large blood vessel artifacts in the functional maps. These artifacts often hampered the observation of subtle features in the recorded maps. To alleviate this problem, Ratzlaff and Grinvald (1991) constructed a "macroscope" tandem-lens arrangement with an exceedingly shallow depth of field

This device is essentially a microscope, with a low magnification (around 0.5–1 ×), composed of two "front-to-front" high-numerical-aperture photographic lenses. By doing this, the macroscope provides an unusually high numerical aperture compared to commercial, low-magnification microscop objectives, resulting in a very shallow depth of field (e.g., 50 μm, nominal for two coupled 50-mm lenses with f = 1:1.2). Therefore, when focused 300–500 μm below the cortical surface, the surface vasculature is sufficiently blurred an artifacts from it virtually disappear (Ratzlaf f and Grinvald, 1991).

1. Lenses

The macroscope can easily be built by connecting two camera lenses front to front. The magnification of thi tandem-lens combination is given by $f1/f2$, where $f1$ is the focal length of the lens close to the camera and $f2$ is that of the lens close to the brain. To build a macroscope from conventional 35-mm camera lenses, items (1) and (2) listed below are needed, plus one or more of the combinations of lenses that are listed.

(1) C-mount to camera adapter (e.g., "Pentax" if Pentax lenses are used).

(2) Adapter for the tandem-lens arrangement. A solid ring with proper threads to connect the front part of each of the camera lenses. (This lens thread is usually used for standard camera filters.) To minimize vibration and to protect the lenses it is advantageous to add support.

(3) For a magnification of × (covering approximately 9×6 mm^2 with a standard camera), use two 50-mm Pentax lenses with $1/f$ of at least 1.2. Alternatively, a video lens with a shorter working distance (3 cm) but an even higher numerical aperture (0.9) can be used.

(4) For a magnification of 2. × (covering approximately 3.3×2.2 mm^2), use one 50-mm and one 135-mm lens. Pentax offers a 135-mm lens with a numerical aperture of 1.8. If the 50- and 135-mm lenses are installed in the reverse order, then the tandem lens will cover a very lage portion of the cortex (approximately 22×14 mm^2).

(5) A 2× standard camera extender provides flexibility fo additional magnification or for demagnificatio

(6) A zoom lens covering the range of 25–180 or 16–160 mm can be used as the top lens. A zoom lens has the advantage of allowing adjustment of the magnificatio without the replacement of lenses. This flexibility is however, achieved at the cost of a lower aperture that causes a larger depth of field

(7) For imaging human cortex during neurosur gery, a zoom lens with a larger working distance starting at approximately 10 cm is preferable to a tandem-lens combination.

In the tandem-lens combination, commercial home video CCD lenses may also be used as the lens next to the camera. Their use as the lens next to the cortex may be problematic whenever the working distance is important. The advantage of using the home video lenses is that the numerical aperture of home video CCD lenses is often lar ger than that of 35-mm camera lenses.

The camera can also be mounted on a conventional microscope or on an operative microscope, preferably one that of fers a high numerical aperture and, consequently , a short working distance (5–7 cm). The final working dis tance, or distance from the first lens to the specimen, shoul be at least 3 cm in order to manipulate the specimen, including proper alignment of light guides and electrode placement. Numerical aperture, illumination, working distance, and precise mechanical stability should all be considered in the final design

2. Camera Mount

The video camera should be rigidly mounted to a vibration-free support. The ideal arrangement is to mount the camera to an immobile support system so that the camera has no means of moving. This is especially important because many modern imaging devices have built in cooling devices that may vibrate the camera. By placing the camera on a firm support, this source of vibration can be eliminated In such a system, the subject would be placed on an *xyz* translator so that it would be moved into the appropriate field of view of the camera and translated in the *z* direction to focus. The next best approach would be to allow the macroscope one direction of movement, the *z* direction, to enable it to focus. Still the subject would have to be placed on an *xy* translator to move it into the appropriate location relative to the field of view of the camera for imaging Finally, the camera can be mounted onto an *xyz* translator, but this arrangement gives the camera the most means of inadvertent movements. For all arrangements, the *z* direction of movement should preferably have a coarse, lar ge travel distance control as well as a fine focus control Furthermore, it is advantageous to construct the camera holder such that it allows rotation of the camera around its optical axis as well as tilting it at any desired angle.

D. The Spectrophotometer

For spectroscopic analysis of optical intrinsic signals, it is necessary to include a spectrophotometer in the optical imaging apparatus. The details of how the spectrophotometer is integrated into the apparatus have been described earlier (Section II.D.2). Briefl , a modified macroscop setup which has two image planes is used, instead of the one plane used in the conventional apparatus. In the first imag plane, a narrow slit isolates a selected line across the cortical surface which is projected onto a dispersing grating (in the spectrophotometer). The spectrally decomposed image is then projected onto the second image plane, where it is captured by the CCD. Spectrophotometers are commercially available (e.g., Roper Scientific, Trenton, NJ). Gratings should be appropriately chosen to disperse the reflected ligh in the visible spectrum.

V. Data Acquisition

A. Basic Experimental Setup

The basic experimental setup for intrinsic optical imaging experiments is shown in Fig. 5. First, the subject's head must be stabilized either by a stereotaxic frame (in animal subjects) or by a Mayfield apparatus (in humans) Once the cortical area of interest has been exposed, the brain is illuminated with filtered light using light guides The camera should be positioned over the cortical exposure such that the area of interest is centered within the field o view of the camera. Images are taken of the cortex at rest and during activation. The camera controller digitizes the images and forwards the data to the data acquisition computer.

B. Timing and Duration of a Single Data Acquisition

As mentioned earlier, optical imaging of intrinsic signals offers the best combination of both spatial and temporal resolution compared to other brain mapping methods. It is advisable therefore to design experiments such that a time course can be reconstructed from the data. Since the time course of intrinsic signals are on the order of seconds, it is often sufficient for frames to be collected every 250–500 m in order to capture the temporal profile of the response

When should imaging begin relative to stimulus onset? Although blood volume changes do not occur until approximately 1 s after stimulus onset, hemoglobin oxymetry changes may begin within a few hundred milliseconds of neuronal activation (Malonek and Grinvald, 1996; Mayhew *et al.,* 1999; Nemoto *et al.,* 1999). It is therefore essential that image acquisition begin, at the very latest, simultaneous with stimulus onset. Analysis of optical images, however , often requires at least one baseline image (i.e., prior to stimulus onset) in order to determine percentage change in signal from baseline. Some methodological approaches require an even greater number of baseline frames (see for example Zheng *et al.,* 2001) in order to be able to estimate and "subtract out" baseline vascular oscillatory signals. Therefore, ideally it is advisable to collect approximately 8 s of baseline images prior to stimulus onset.

How long should images be collected after stimulus onset? Most of the components that contribute to intrinsic

signals return to baseline between 8 and 12 s after stimulus onset. Therefore, in order to capture the entire temporal profile of the intrinsic signal response, one should image fo approximately 15 s after stimulus onset. The intrinsic signal response, however, generally peaks within 5 s after stimulus onset so many groups image for only 5 s after stimulus onset. If the investigator is interested in only the peak mapping signal and not in response time course, this approach suffices and is actually advantageous because i reduces the volume of data. For experiments that aim to investigate physiology, the "return to baseline" phase of the intrinsic signal may be an important component that should be imaged. For example, Berwick *et al.* (2000) found that inhibiting neuronal nitric oxide synthase did not af fect the early increase in deoxyhemoglobin, but significantly damp ened the late functional increases in total hemoglobin and oxyhemoglobin. These later changes would not have been identified if imaging did not last longer than 5 s

C. Interstimulus Interval

Intrinsic signals decay back to baseline in 12–15 s for a stimulus lasting 2 s. The interstimulus interval, or the time between successive stimuli, should therefore not be too short in order to avoid systematic errors in the resulting functional maps. It is also important to avoid short inter-stimulus intervals because of reports of "hemodynamic refractory periods," or reduced vascular response capacities with temporally close stimuli (Cannestra *et al.,* 1998b; Ances *et al.,* 2000). The magnitude of the optical response to a stimulus presented immediately after another temporally close stimulus is significantly reduced. Howeve , choosing excessively long stimulus intervals in practice also results in lower quality maps since fewer images can be averaged in the same amount of time. Moreover, systematic errors can at least partly be avoided by randomizing the sequence of stimuli.

D. The Amount of Data

It is important to collect and average a sufficient numbe of trials to increase the signal-to-noise ratio of the imaging experiment. SNR increases with the square root of the number of trials. The number of trials used by dif ferent groups varies between 8 and 128. In most cases, however , 32 trials seems sufficient to achieve acceptable SNR. For more precise methodology of determining the correct number of trials, see Section IV.A.3.

High-resolution optical imaging produces vast amounts of data. Ideally , to maximize map quality during offlin analysis, one should store every single frame acquired. Normally, this is impractical. The amount of storage space needed for a typical experiment lasting 1 h with a data acquisition time of 23 s (8 s prestimulus, 15 s poststimulus) and an interstimulus interval of 37 s could amount to 30 Gbyte [23 s × 30 video frames/s × (768 × 576) pixels × 60 trials × 2 bytes/pixel ~ 40 Gbyte]. Twenty hours of data collection (which is not exceptional) would require ~1 Tbyte. Beyond the problem of storage space, one obviously would be faced with enormous amounts of time for data transfer and image analysis. These considerations necessitate a massive reduction of the amount of data. The first reductio of data occurs on the CCD chip itself with on-chip binning (e.g., 2 × 2 or 3 × 3 binning). Next, video frames can be accumulated into a single image for data analysis purposes, effectively reducing the temporal resolution of data acquisition. Moreover, data accumulated under identical stimulus conditions (i.e., same time relative to identical stimulus) are normally averaged 8–32 times, which again reduces the amount of data by this number. For those investigators who focus on data analysis techniques, preserving data from each trial may still be important.

E. Testing the Apparatus (Adapted from Bonhoeffer and Grinvald, 1996)

Two tests have proven particularly useful in testing the optical imaging apparatus before using it for experiments: (1) testing SNR and (2) testing whether data acquisition and stimulus presentation are properly timed.

(1) The following procedure is used to generate an artificial test signal that is comparable to a typical intrinsi signal as recorded from the living brain. A LED display of the number "8" (with seven individual LEDs) is connected to the data acquisition system such that for the dif ferent stimulus conditions the dif ferent segments of the LED display are switched on. The brightness of this LED is set to use the full dynamic range of the camera. This brightness is then attenuated by a factor of 1000 with a 3 OD filte . If, finall , this whole arrangement is then illuminated with red light so that its brightness is again almost at the saturation level of the camera, one has a device that produces modulation of 1 in 1000 on a relatively high absolute light intensity The optical imaging apparatus can then be tested by acquiring data under these conditions and seeing whether this very weak modulation can be picked up by the system with the proper SNR.

(2) In order to test the consistency of data acquisition, data analysis, and stimulation, it is useful to run a test experiment in which a visual stimulator produces patterns that can easily be distinguished from each other . If the stimulator is controlled by the data acquisition program in the same manner as in a real experiment and if the camera is pointed directly onto the stimulator screen, one has a very simple testing procedure: data analysis of the pattern that the camera imaged from the screen will immediately reveal any inconsistencies in the stimulation, data acquisition, and data analysis procedures.

VI. Data Analysis for Mapping Functional Architecture

Intrinsic signal data can be collected in two ways: (1) single wavelength or (2) multiple wavelengths simultaneously using a spectrophotometer. The analysis of these different types of data is quite distinct and so is discussed separately in this section. One should keep in mind that intrinsic signal maps can and will dif fer depending on the method of analysis used. Therefore, it is critical to understand the assumptions and limitations of each approach, both when *selecting* a particular approach and when *interpreting* results. The methodology, assumptions, and limitations of dif ferent analytic methods are discussed in this section.

A. Analysis of Single-Wavelength Data

1. Ratio Analysis

In order to obtain activity maps from the cortex, images have to be acquired both while the cortex is stimulated and while the cortex is at rest. A "reference image" is then subtracted from and divided into all subsequent images on a pixel-by-pixel basis in order to determine the percentage change in reflectance at each pixel at each time point.The reference image is divided into the difference images in order to normalize for uneven illumination. The selection of the reference image is not trivial, has important implications, and can influence the appearance of maps. Three different approaches have been employed: (a) prestimulus cortical image, (b) cocktail blanks, and (c) poststimulus cortical image.

a. Prestimulus cortical image. Using a cortical image prior to stimulus onset as a reference image makes the fewest assumptions about the functional architecture and physiology of the brain (Fig. 6). The advantage of a picture of the inactive cortex is that no assumption is made about the complete set of stimuli that are required to activate the cortex uniformly (as is the case with cocktail blanks, see below). The disadvantage of using the blank picture is that it can cause very strong, activity-related blood vessel artifacts in the maps (Fig. 6). These vascular artifacts often overwhelm the fin mapping details that emerge when a cocktail blank is used for analysis instead. Other strategies than the cocktail blank approach have been developed to reduce these vascular artifacts, including using a poststimulus cortical image as a reference image [Chen-Bee *et al.,* 1996; see (c) below], using a macroscope (Ratzlaff and Grinvald, 1991; see Section IV .C), and focusing below the blood vessels so that they do not contribute significantly to the intrinsic signal maps (Hodg *et al.,* 1997). Alternatively, Chen-Bee and colleagues (2000) have recommended averaging only the first 1.5 s after stimulu onset when imaging in the low 600 nm range, which coincides with the period of fast oxygen consumption of active neurons but precedes the activation of lar ge surface vessels, thereby minimizing the contribution of vascular artifacts to the final map (Chen-Be *et al.,* 2000).

b. Cocktail blank. The cocktail blank is the sum of multiple individual cortical images under different stimulus conditions. It is intended to represent the uniformly activated cortex. The only dif ference between the single-activity map and the cocktail blank hypothetically is the orientation of the stimulus; it is ar gued that the picture is not confounded with an additional dif ference in overall activity (i.e., functional vascular activity). The disadvantage, however , is that assumptions are made about the functional architecture and neuronal interactions within the cortex of interest, resulting

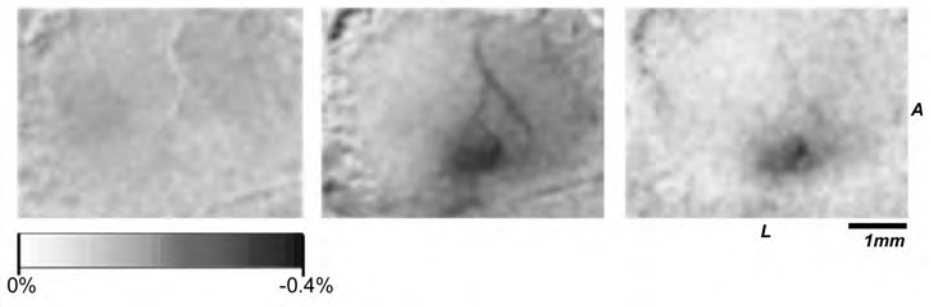

Figure 6 The effect of using different reference images (prestimulus vs poststimulus cortical image) on optical map. Optical reflectance changes over the right somatosensory cortex of rodent were imaged in response to left C1 whiske deflection at 610 nm. **Left:** This image shows no significant optical changes in a control frame prior to stimulus onset **Middle:** Using a prestimulus cortical image as a reference image for ratio analysis can result in significant activity-relate vascular artifacts in the optical map. Specificall , decreases in reflectance in draining veins are seen medial to the focu of optical activity overlying the location of the stimulated barrel. **Right:** When an average of a prestimulus (0.5 s prestimulus) and poststimulus (2.5 s poststimulus) cortical image is used as the reference image for ratio analysis, vascular artifacts can be minimized (Chen-Bee, *et al.*, 1996). This method of data analysis exploits the dif ferent time courses of stimulus-dependent *cortical* activity and stimulus-dependent *vessel* activity. The significant vascular artifacts seen in th middle image are greatly reduced by using this alternative approach, providing a much more focal representation of cortical activation. A, anterior; L, lateral.

in a circular argument. If the goal of intrinsic signal mapping is to characterize the functional or ganization of the cortex, then how can one create a cocktail blank, which requires assumptions about the underlying functional cortical architecture? When recording iso-orientation maps from the primary visual cortex of the cat, for instance, it is normally assumed that a complete set of all orientations activates the cortex evenly and therefore the stimulus set is used to calculate the cocktail blank. In some cases, when a cocktail blank composed of all the different presupposed stimuli for a given cortical area is divided by the unstimulated blank, an underlying structure emerges in the resulting map, suggesting that some characteristic of the stimuli used disproportionately activates some regions of the cortex. In fact, it was speculated by Bonhoeffer and Grinvald (1993a) that a clear pattern obtained when a cocktail blank was divided by a prestimulus reference might hint that spatial frequency maps may exist in cat area 18. Indeed such spatial frequency maps have been demonstrated using optical imaging. This example shows that a cocktail blank under some circumstances can be inadequate since it imposes a structure onto activity maps. It is therefore important to divide the cocktail blank by a prestimulus image to ensure that it does not contain any structural information within itself. Conversely, this procedure may be beneficial because it can give hints to the existence of addi tional stimulus attributes that are represented on the cortex in a clustered fashion.

c. Poststimulus cortical image. This method of data analysis exploits the dif ferent time courses of stimulus-dependent *cortical* activity and stimulus-dependent *vessel* activity in order to minimize the contribution of vascular artifacts to intrinsic signal maps (Chen-Bee *et al.,* 1996) (Fig. 6). Intrinsic signals from blood vessels tend to persist longer than those arising from the cortex. Therefore, cortical images greater than 2–3 s after stimulus onset provide a "map" of the vascular signal. If this vascular signal is used as part of the reference image, the intrinsic signals from the vessels can be minimized. To do this, the reference image used is an average of a prestimulus cortical image and an image after stimulus-dependent cortical activity has subsided but intrinsic vascular activity persists (usually 2–3 s after stimulus onset). Chen-Bee and colleagues (1996) have shown the success of this approach in reducing vascular components in intrinsic signal maps. This approach, however, assumes that the vascular and cortical intrinsic signals can be well separated in time, which is not always the case. Furthermore, this approach tends to underestimate intrinsic signal magnitude since the poststimulus image will inevitably contain intrinsic signals emanating from the area of interest even after the majority of the cortical signal has subsided.

Single-condition maps. Single-condition maps are calculated by taking the activity map obtained with one particular stimulus and dividing this image by the reference image. The resulting map then shows the activation that this particular stimulus causes.

e. Differential maps. In dif ferential maps, to maximize the contrast, one activity map is divided by (or subtracted from) the activity map that is *likely* to give the complementary activation pattern. This approach makes further assumptions about the underlying cortical architecture (which may or may not be true) and therefore must be carefully considered. One example of a problem using differential maps is that a gray region in such maps (e.g., pixel value of ~128) can correspond to cortical regions that were not activated by either stimulus or alternatively to regions that were strongly activated by the two stimuli but with equal magnitude. Single-condition maps using the cocktail blank are free of these problems. These considerations are similar to those encountered when choosing between unipolar and bipolar electrodes for electrophysiological recordings, in that single-condition maps are analogous to unipolar electrodes and dif ferential maps are analogous to bipolar electrodes.

Two different methods can be used to calculate dif ferential maps. One possibility is to calculate the ratio between the maps A and B. The other possibility is to subtract the two maps and then divide the result by a general illumination function like the cocktail blank: $(A - B)$/blank. Whereas the first calculation provides information about the relativ activity at each pixel in A vs B, the second calculation highlights the *difference* between the maps as the important entity. Although these two calculations may seem very different, they are equivalent under the assumption that the reflectance changes are exceedingly small relative to base line (Bonhoeffer, 1995).

The assertion is that

$$\frac{V-H}{B} \cong \frac{V}{H} \tag{1}$$

where V is the image obtained with a vertical grating, H is the image obtained with a horizontal grating, and B is the blank image.

Since the changes of reflected light intensity are smal compared to the absolute values of the reflected light inten sity, one can write

$V = I_0(1 + \Delta V)$ and $H = I_0 + \Delta H)$, with $\Delta V, \Delta H \quad 10^{-3}$.

Since $B \quad I_0$, the left-hand side of the first equation can b rewritten as

$$\frac{I_0(1+\Delta V) - I_0(1+\Delta H)}{I_0} = \Delta V - \Delta H \tag{2}$$

and the right-hand side of the same equation can be written as

$$\frac{V}{H} = \frac{I_0(1+\Delta V)}{I_0(1+\Delta H)} = \frac{(1+\Delta V)}{(1+\Delta H)} . \tag{3}$$

Since $1/(1 + x)$ $1 - x$ for $x < 1$ and since $\Delta H < 1$, one can further write

$$\frac{(1+\Delta V)}{(1+\Delta H)} \approx (1+\Delta V)(1-\Delta H). \quad (4)$$

Thus, the original equation can be rewritten as

$$\Delta V - \Delta H \quad 1 + \Delta V - \Delta H - \Delta V \Delta H.$$

For intrinsic signals, ΔV and ΔH are in the range of 10^{-3}. Therefore, $\Delta V \Delta H$ is approximately 10^{-6}, which is 1/1000 of the intrinsic signal change that is normally observed and therefore negligible, so it can be disregarded. Moreover , since the scaling of the activity maps is done with an arbitrary offset, the 1 on the right side of the equation can be disregarded. Consequently, under these circumstances, dividing images and subtracting images yield the same result.

2. Principal Component Analyses

Because of the exceedingly small magnitude of the intrinsic mapping signals in the background of relatively lar ge magnitude global signals (e.g., blood volume changes, which are generally not specific to the activation paradigm), othe analytic paradigms than the "ratio analysis" presented above have been implemented to extract the significant mappin components of intrinsic optical signals. In particular, several groups have focused on variations of principal component analyses to exclude the so-called global signals and noise from the final intrinsic signal map (Cannestr *et al.,* 1996; Gabbay *et al.,* 2000; Stetter *et al.,* 2000; Zheng *et al.,* 2001). Principal component analysis (PCA) assumes that the data are made up of a linear sum of signals, which can be decorrelated based on dif ferences in variance. The mathematical procedure for PCA has been outlined in detail (Geladi *et al.,* 1989; Yap *et al.,* 1994). Briefl , given a set of images [X_t = 0 to N] from time points 0 to N, a single matrix [X_S] is constructed such that the columns represent a pixel intensity of a specific image and the rows represent the intensity tim course of a single pixel from the image set. Matrix [X_S]^T is transposed, and the covariance matrix [C] determined from the relation: [C] = [X_S] [X_S]^T. The eigenvalues (? ^{i}) and eigenvectors (V?^{i}) are determined by the Jacobi transformations technique.

With high SNR (as is often the case in intrinsic signal imaging in rodents), the first principal component can b used as an accurate measure of the time course of the intrinsic signal response (Cannestra *et al.,* 1996) (Fig. 7). The eigenvector corresponding to the first principal componen can then be used to reconstruct the data set without noise. In cases of low SNR, however , more complex approaches to

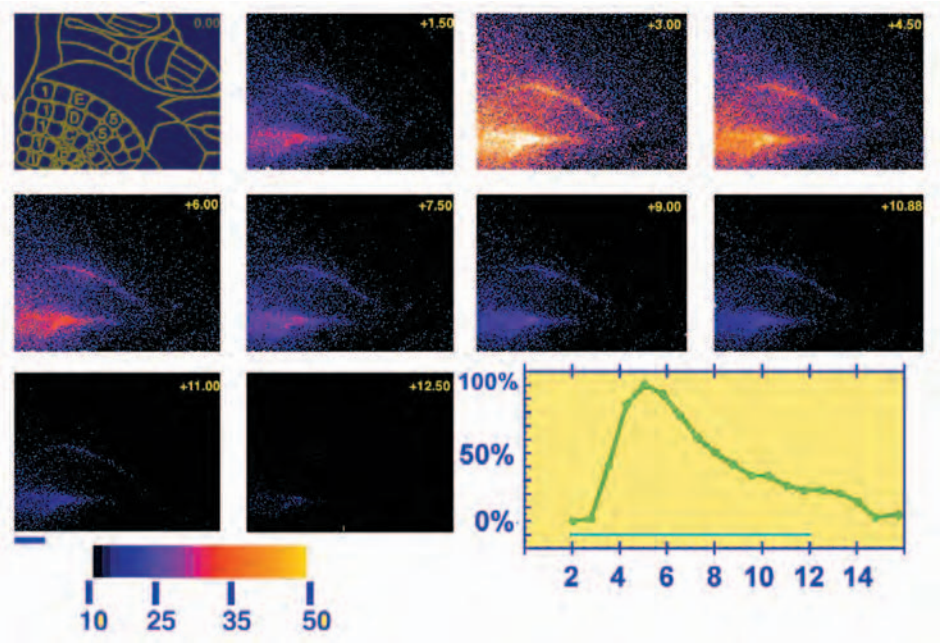

Figure 7 Principal component reconstruction of intrinsic signal responses at 850 nm over rodent somatosensory cortex. Whisker C1 on the contralateral face was stimulated through a 30° angle at 10 Hz for 10 s. With high SNR, the first principal component can be used as an accurate measure of the time course o the intrinsic signal response (Cannestra *et al.,* 1996). The images displayed here are a reconstruction of the data set using the eigenvector corresponding to the first principal component. Using principal componen analysis can significantly reduce the contribution of noise to the final data reconstruction **Bottom right:** Calculated time course of the first eigenvecto, showing an initial peak intrinsic signal response approximately 4–5 s after stimulus onset and a return to baseline after stimulus termination. Scale bar is 1 mm. Color bar represents reflectance decrease $\times 10^{-4}$. Adapted, with permission, from Cannestra *et al.* (1996).

PCA of intrinsic signal maps must be used. Gabbay and colleagues (2000) recommended that only those principal components whose time course correlates with the stimulus presentation sequence be used for the reconstruction of the final intrinsic signal map. Specifically, a contiguous range of principal components is chosen whose probability of being genuinely related to the stimulus is high. This range typically excludes the higher power principal components, which they ascribe to "vegetative processes," including circulation and respiration, and the lower power components, which are ascribed to background noise (Gabbay *et al.,* 2000).

PCA is limited by the fact that the only means of separating out signals is variance. If mapping signals and background noise have similar variances, PCA cannot separate these signals. Blind signal separation (BSS) builds upon PCA, attempting to separate out the underlying signal sources by making assumptions about the statistical structure of the underlying signal sources. One example of BSS is by extended spatial decorrelation (ESD) (Stetter *et al.,* 2000). ESD assumes that each signal component varies smoothly across space and that each component has zero cross-correlation functions with the other functions. Subsequent to PCA and selection of significant principal components, ESD can be used to extract the mapping signal, for better separation of mapping signals from global signals and movement artifacts (Stetter *et al.,* 2000).

3. Correlation Maps

In BOLD *f*MRI analysis, a common analysis is to determine the correlation of the measured signal with a predetermined hemodynamic response function (Bandettini *et al.,* 1993; Cohen, 1997). Although popular for BOLD *f*MRI analysis, this methodology is not commonly applied to intrinsic signal imaging. The major advantage of this technique over those presented above is that it can be used to generate statistical maps (based on the correlation coefficient), providing an estimate of the statistical reliability of the maps generated. These statistical maps, however, should be carefully considered since Pearson's test of correlation was designed to evaluate the correlation of independent samples. Consecutive time points in a physiological response are *not* independent; correlation analysis is therefore not ideal.

Mayhew and colleagues (1998) examined the correlation of intrinsic signals under red and green light illumination with three different hemodynamic models (with different lags). Not surprisingly, the maps revealed that responses to stimulation occurred with different lags at different spatial positions depending on wavelength. Therefore, in order to use correlation analysis effectively it is critical to know the timing of the response that is to be mapped and extracted. It can be extremely useful in separating out signals with time courses known to be different. Clearly, this analytic approach is limiting in that it requires assumptions to be made about the time course of intrinsic signals in advance. Although the time courses of intrinsic signals have been well characterized (see Section II.E), it should not be assumed that the time courses of intrinsic signals are uniform across different species and anesthetic states. Moreover, this technique cannot separate out signals of different etiologies with similar time courses. For example, if the mapping signal of interest has a time course similar to that of some global confounding signal, the two would be inseparable using this approach.

4. The Generalized Linear Model

The generalized linear model (GLM), like PCA, holds that any observed response is a linear sum of multiple individual underlying responses. In contrast to PCA but similar to correlation maps, when using GLM, the data are fitted to *predetermined* signal time courses instead of signals being extracted based on differences in variance (as is done with PCA). Briefly, GLM analysis can be represented mathematically as $X = G \cdot \beta + e$, where X is a vector representing the time course of a given pixel, G is the design matrix containing the series of predetermined response functions, β is a vector of coefficients representing the degree to which each response function contributes to the overall signal, and e is random noise. This equation is solved at each pixel using a least-squares approach.

Using GLM, one can determine how predetermined (or hypothetical) hemodynamic and metabolic responses may combine to contribute to the final observed intrinsic signal response at each pixel. Based on these calculations, maps can be generated which indicate to what degree the different predetermined response functions contribute to the signal at each pixel. Like correlation maps, GLM can also be used to generate maps of the statistical reliability of the results of the analysis. This method differs from correlation maps in that the time course of a pixel does not necessarily have to match a single predetermined function, but may be a linear sum of multiple predetermined functions.

Mayhew and colleagues (1998) demonstrated the application of GLM for analyzing intrinsic optical responses and discussed the limitations of this approach in detail. Briefly, they used three different response functions: one representing the hypothesized initial increase in deoxyhemoglobin peaking 2–3 s after stimulus onset (i.e., the first phase of the 600- to 630-nm response), one representing changes in total hemoglobin (peaking 3–4 s after stimulus onset), and one representing the second phase of the 600- to 630-nm response (peaking 8–10 s after stimulus onset). They further exploited the power of this technique by determining if adding other functions to the design matrix would reduce the residual signal after analyses. In particular, the effect of incorporating a response function for baseline vasomotion, or vascular oscillatory behavior, was assessed (see Section VI.C).

This approach has many of the same limitations as correlation maps, in that analysis must begin with a preconceived

notion of temporal response profiles. Residual maps demonstrate that if inappropriate functions are used, the residual signal retains a significant amount of spatial and temporal information, suggesting the inadequacy and limited applicability of this approach.

5. Analysis Using Weak Models

The major limitation of correlation maps and GLM is that the investigator must make assumptions about the time course of the response. Recently, Zheng and colleagues (2001) have suggested using "weak model" constraints or modifications to two of the above analyses (BSS and GLM). The so-called weak models make three assumptions: (1) The response begins after stimulation. The temporal profile of the response, however, is not specified. Rather, the models hold only that the time course is flat prior to stimulation and changes after stimulation. (2) The spatial distributions of noise and the mapping signal are different but constant over time. (3) The signal is a linear combination of all signal sources (similar to PCA and GLM). The details of these approaches are not provided here as they are explained in detail elsewhere (Zheng *et al.,* 2001). These techniques have been shown to be more effective at isolating mapping signals compared to other approaches. The difficulty with these approaches, however, arises from the need to record extended baselines (~8 s) prior to stimulation in order to model the response appropriately. Zheng and colleagues (2001) have shown that the method is still applicable with shorter prestimulus baselines (1 s), although not as effective.

B. Analysis of Spectral Data

By integrating a spectrophotometer into the optical imaging apparatus, investigators can simultaneously collect spectral and spatial information regarding the intrinsic signal response (Malonek and Grinvald, 1996; Mayhew *et al.,* 1999, 2000; Kohl *et al.,* 2000; Lindauer *et al.,* 2001). The analysis of the spectral data, however, remains controversial and the approach taken significantly alters the outcome and final interpretation of results.

All spectroscopic analysis methods are based on the Beer–Lambert Law,

$$\Delta A_\lambda = \varepsilon_{\text{chromophore},\lambda} \cdot \Delta[\text{chromophore}] \cdot l,$$

where ΔA_λ is the change in absorbance at a given wavelength, $\varepsilon_{\text{chromophore},\lambda}$ is the absorption coefficient of a given chromophore at a given wavelength, Δ[chromophore] represents the change in concentration of that chromophore, and l is a non-wavelength-dependent term which is required for proper dimensionality. Assuming several chromophores contribute to the changes in absorption at a given wavelength, this expression can be modified

$$\Delta A_\lambda = \varepsilon_{a,\lambda} \cdot \Delta[a] \cdot l + \varepsilon_{b,\lambda} \cdot \Delta[b] \cdot l + \varepsilon_{c,\lambda} \cdot \Delta[c] \cdot l.$$

Given three chromophores, absorbance changes must be measured using at least three different wavelengths so that this algebraic problem can be solved as a system of three equations. In many cases, more than three wavelengths are collected, and so a least-squares approach is used to fit the experimental data to the absorption spectra.

The basic Beer–Lambert relationship expressed above does not contain a wavelength-dependent path-length factor. Many groups argue that a path-length factor is necessary since different wavelengths of light have different scattering patterns and therefore travel different distances and have different path lengths (Mayhew *et al.,* 1999, 2000; Kohl *et al.,* 2000; Lindauer *et al.,* 2001). Considering this, the equations can be modified such that

$$\Delta A_\lambda = \text{DP}_\lambda(\varepsilon_{a,\lambda} \cdot \Delta[a] + \varepsilon_{b,\lambda} \cdot \Delta[b] + \varepsilon_{c,\lambda} \cdot \Delta[c]),$$

where DP_λ represents a wavelength-dependent path-length factor which depends not only on the wavelength of imaging but also on tissue properties (including assumptions of absolute concentrations of oxy-Hb and deoxy-Hb).

The major chromophores usually incorporated into spectroscopic analysis include oxyhemoglobin, deoxyhemoglobin, and cytochrome oxidase.

1. Linear Spectroscopic Analysis

The first spectroscopic study of intrinsic optical signal assumed that absorbance changes at a given wavelength were due to a linear sum of absorbance changes due to each chromophore (Malonek and Grinvald, 1996). In addition, a wavelength-independent factor, called LS, was included to represent a wavelength-independent light scattering component. This modification was based on previous optical imaging studies in blood-free slice preparations that showed that light scattering changes are independent of wavelength (Cohen and Keynes, 1971; Grinvald *et al.,* 1982).

Changes in absorbance were therefore estimated as

$$\Delta A_\lambda = \varepsilon_{a,\lambda} \cdot \Delta[a] + \varepsilon_{b,\lambda} \cdot \Delta[b] + \text{LS}.$$

A least-squares routine was used to fit the data. The authors state that using other wavelength-dependent models for the light scattering term did not affect the calculated chromophore time courses (Malonek and Grinvald, 1996).

Using this linear approach, Malonek and Grinvald demonstrated an initial increase in deoxyhemoglobin concentrations and a delayed increase in oxyhemoglobin concentrations (Malonek and Grinvald, 1996). Support for this approach has been provided by Shtoyerman and colleagues (2000), who showed that similar chromophore concentration changes and time courses are calculated regardless of wavelengths used for imaging and analysis. They suggest the robustness of the results across wavelengths validates linear spectrographic analysis. This approach, however, has been criticized because it is well known that tissue penetration as well as light scattering patterns is wavelength dependent.

Therefore, this approach may be an oversimplification an produce erroneous results. Kohl and colleagues (2000) posit, "Ignoring its wavelength dependence in the calculation of concentration changes has the same ef fect as calculating with wrong extinction spectra." This debate remains critical since the time course of chromophore changes depends critically on the analytic approach used (Mayhew *et al.,* 1999; Lindauer *et al.,* 2001).

2. Path-Length Scaling Spectroscopic Analysis

Nemoto and colleagues (1999) were the first group t include a path-length-dependent factor in the spectroscopic analysis. They include an additional path-length factor into the analysis (DP_λ above). The wavelength-dependent path length was assumed to be *constant* throughout the acquisition period and not to be af fected by functional changes in the hemoglobin concentration and oxygenation state under physiologic conditions (Nomura *et al.,* 1997). They still incorporated a wavelength-independent term that was presumed to represent light scattering changes [using the same rationale proposed by Malonek and Grinvald (1996) above]. Using this approach, Nemoto and colleagues also detected an early increase in deoxyhemoglobin concentrations followed by a delayed increase in oxyhemoglobin concentrations (Nemoto *et al.,* 1999). This approach may also be limited by the fact that DP_λ may change with functional activation since the tissue properties change significantly wit changes in blood flow and hemoglobin oxygenation

Both Mayhew and colleagues (1999, 2000) and Dirnagl and collaborators (Kohl *et al.,* 2000; Lindauer *et al.,* 2001) have proposed using a Monte Carlo simulation of light transport in tissue to determine DP_λ (see Mayhew *et al.,* 1999; Kohl *et al.,* 2000; Lindauer *et al.,* 2001; for methodological and theoretical details regarding Monte Carlo simulations). According to these groups, the DP_λ factor changes dynamically with the brain as the relative concentrations of deoxyhemoglobin, oxyhemoglobin, and cytochrome oxidase change with functional activation. These groups use the same general equation as Nemoto and colleagues (1999) except that DP_λ is dynamic. Interestingly, this modificatio eliminates the calculated initial increase in deoxyhemoglobin concentrations. Lindauer and colleagues (2001) therefore argue that there is no evidence for the early increase in deoxyhemoglobin concentrations. Mayhew and collaborators (1999), however, take the analysis one step further by applying GLM to remove the 0.1-Hz baseline vasomotion from the signal (see discussion of baseline vasomotion in section below). After applying this manipulation, they demonstrate that an early increase in deoxyhemoglobin concentrations can be identified (Fig. 8). Mayhew and col leagues have also shown that when blood pressure is controlled for and increased to physiological levels using

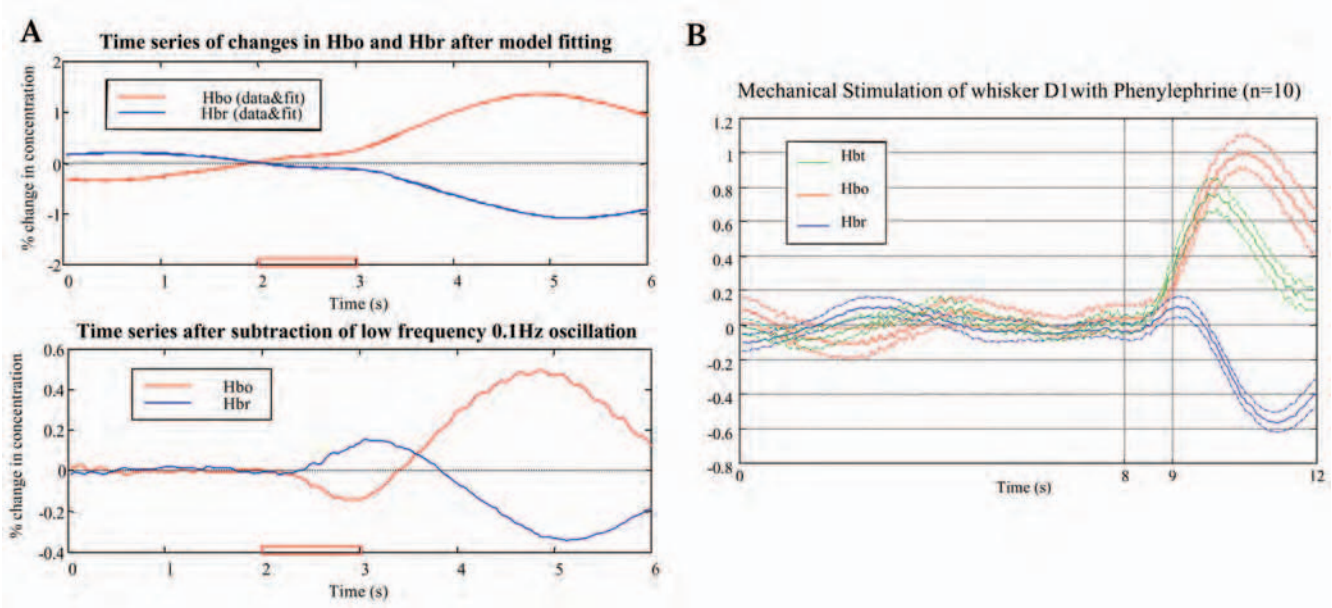

Figure 8 Spectroscopic analysis reveals initial increase in deoxyhemoglobin concentrations. (**A, top**) Initial spectroscopic analysis using path length scaling analysis reveals an decrease in deoxyhemoglobin concentrations concomitant with an increase in oxyhemoglobin concentrat ions in response to whisker stimulation over the rodent somatosensory cortex. (**A, bottom**) Subtraction of the 0.1-Hz underlying vasomotion signal, however , reveals that the initial increase in deoxyhemoglobin concentrations is present and was initially (top) not apparent due to the vasomotion signal complicating analysis. (**B**) Recent studies by Mayhew and colleagues (2000) suggest that the vasomotion signal can be minimized by increasing the systemic b lood pressure of the rodent using phenylephrine. Spectroscopic analysis using path length scaling without subtraction of a baseline oscillatory vasc ular signal (which has been suppressed by increasing blood pressure) reveals an initial increase in deoxyhemoglobin concentrations. The differences observed between the graphs on the left highlight the need for investigators to carefully consider any analysis technique used to interpret results. Adapted, with permission, from Mayhew *et al.* (1999, 2000).

phenylephrine, the contribution of the background vasomotion is minimized and the early increase in deoxyhemoglobin concentrations can be identified even withou applying GLM (Fig. 8). Although these groups ar gue that this approach better approximates true wavelength-specifi path lengths, these calculations are based on simulations and are not measured values. It has been proposed that true path lengths for different relative concentrations of oxyhemoglobin and deoxyhemoglobin can be calculated for each wavelength to better estimate the true changes in chromophore concentrations. This approach, however , has not yet been applied, so its efficacy is unclea .

As should be clear from this discussion, the approach taken to the analysis of the spectral data can significantl alter the conclusions of the investigation. Therefore, investigators should critically appraise any analytical or mathematical approach used to evaluate spectroscopic data. It is important to acknowledge the assumptions and limitations underlying each technique.

C. Baseline Vasomotion

Several groups are increasingly noting baseline oscillatory behavior in intrinsic signals (see Mayhew *et al.,* 1996, for example). The oscillations are most probably vascular in origin and represent baseline vasomotion or alternating relaxation and constriction of neurovasculature. These baseline oscillations are approximately 0.1 Hz, observed at all wavelengths (although more prominent in the red and green range), and may be several times the magnitude of activity-related intrinsic optical responses (Mayhew *et al.,* 1996). The presence of these lar ge baseline oscillations, if not accounted for , may therefore alter the interpretation or analysis of intrinsic maps.

Most groups deal with this oscillatory behavior by averaging several trials and thereby attempting to eliminate the regular background oscillations from the final map. This is possible since baseline oscillations are random over time but the functional response is locked to stimulus presentation. It is important, therefore, to collect a sufficient numbe of prestimulus images to make sure that the baseline oscillations are adequately suppressed by trial averaging. Although some argue that this approach does not adequately cancel the ef fect of these lar ge oscillatory patterns, many groups have been able to produce functional intrinsic signal maps using this approach (see for example Polley *et al.,* 1999a).

Another approach to removing these slow oscillations is to use the so-called "first-frame analysis." Since the tim course of these "vascular" oscillations (~10 s) is signifi cantly slower than the duration of a trial (in some cases ~3–4 s), the vascular signal can be assumed to be represented as a fixed pattern in all the frames acquired during th trial: if the first data frame is taken prior to any stimulation it will contain the spatial representation of the oscillatory signal, but no information about the pattern of the stimulus-evoked activity . Thus, to minimize slow noise, the firs frame can be subtracted from all subsequent frames before any additional analysis.

Mayhew and colleagues have implemented several algorithms (presented above) to deal with and try to extract these oscillations from the intrinsic signal maps, including GLM and analyses using weak models (Mayhew *et al.,* 1998; Zheng *et al.,* 2001). These approaches attempt to model the slow intrinsic oscillations and subsequently extract the signal prior to any subsequent analysis. Details are provided in Sections VI.A.4 and VI.A.5.

D. Color Coding of Functional Maps

Color coding of functional maps can be extremely helpful in relaying a lar ge quantity of information within a single functional map (Blasdel and Salama, 1986; Ts'o *et al.,* 1990; Bonhoef fer and Grinvald, 1991; Blasdel, 1992a,b). For instance, for comprehensive analysis of the organization of iso-orientation domains in visual cortex, a color-coded display in which the color at each pixel represents the angle of preferred grating orientation at each pixel is advantageous (Fig. 9B). Preferred orientations are determined by using vector sums of single-condition responses to different orientation gratings at each pixel. So-called "angle maps" can be produced to display only the angle of the resulting vector, with no information about the magnitude of the resulting vector (originally introduced by Blasdel and Salama, 1986). Alternatively, the magnitude of the resulting vector (which relates to the degree of orientation preference) can also be conveyed by using differences in color intensity. Note that a small-magnitude response can represent multiple situations. For example, a small-magnitude vector may represent either a poor response to a single orientation or strong but slightly unequal responses to gratings moving in opposite directions.

To overcome this ambiguity , one can calculate maps called "hue-lightness-saturation maps" (HLS maps) (Fig. 9B). This type of map simultaneously displays the three values of (1) preferred orientation, (2) overall response strength, and (3) tuning sharpness (T s'o *et al.,* 1990; Bonhoef fer and Grinvald, 1993a). As with angle maps, color codes for orientation preference. Also, like angle maps, the overall response magnitude at each pixel (i.e., the response of one particular site summed over all orientations) is represented by color intensity . The final parameter displayed in thes maps, which is dif ferent from angle maps, is color saturation, which reveals the quality of the orientation tuning (the worse the tuning the less saturated, i.e., the "whiter" the color). Consequently, if many different orientations activate a particular pixel (as was presented hypothetically at the end of the previous paragraph), the color of that pixel would be

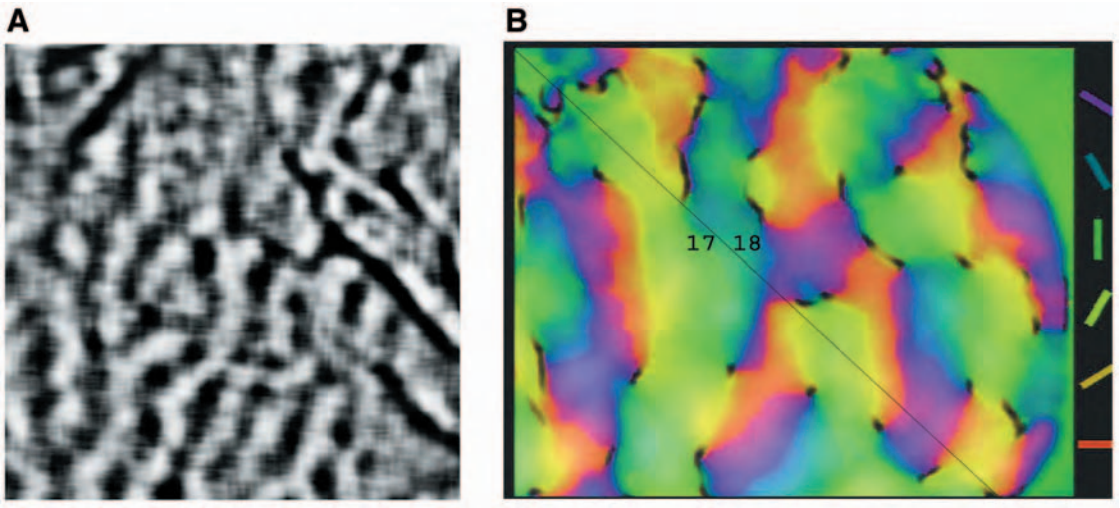

Figure 9 Optical intrinsic signal mapping of visual cortex. (**A**) Ocular dominance map, demonstrating distinct "strips" in a 1-cm^2 patch of cortex, activated by a stationary bar presented monocularly to the visual system of a rhesus monkey . (**B**) HLS map of orientation selectivity in areas 17 and 18 of the cat visual cortex. This image shows the preference of neurons to lines of dif ferent orientations, when presented to the retina. The legend on the right shows the relationship between the color of each pixel and orientation. The brightness of each pixel indicates the selectivity of each point in the map: dark indicates points in the map that are not part icularly selective to any orientation, while bright points signify points in the map that are tuned specifically to a given orientation. (A) was adapted, with permission, from Macknik and Haglund (1999). (B) was provided by S. L. Macknik and G. G. Blasdel (Harvard Medical School).

less saturated, or "whiter." By conveying more information about the underlying maps which were summed to produce the orientation maps, these HLS maps eliminate much of the ambiguity present in the angle maps.

VII. Chronic Optical Imaging

In addition to its superior spatial *and* temporal resolution, one of the strengths of optical imaging of intrinsic signals is that it is relatively noninvasive, in that the cortex is not touched or damaged by the imaging procedures. Consequently, subjects can easily endure long-term optical imaging, both within the span of the day and over a period of several weeks. In order to make optical imaging over a period of weeks or months successful, several methodological modifications may be necessar .

A. Imaging through the Intact Skull and/or Dura

Several groups have now demonstrated successful intrinsic signal imaging through both intact dura and thinned bone (Blood *et al.,* 1995; Polley *et al.,* 1999a). Frostig and colleagues (1990) showed, in cats, that orientation columns in the visual cortex identified by imaging through the dur were identical to ones obtained directly from the exposed cortex after removing the dura.

Different wavelengths will penetrate the thin bone and dura to dif ferent degrees and so imaging may not be possible through the intact dura and skull in all subjects. Originally, imaging through the thin bone preparations was done using only near -infrared light because these longer wavelengths are better able to penetrate tissue than shorter wavelengths. However , thin bone preparations have also successfully been used for imaging between 500 and 700 nm (see for example, Polley *et al.,* 1999a). The quality and extent of bone thinning will lar gely determine the likelihood of successful imaging. Success will depend on the degree to which the skull is thinned (in rodents, the bone should be thinned to approximately 250 μm so that the branches of the major cerebral arteries and veins can be visualized using green light illumination) and whether any epidural or subdural hematomas were induced by the thinning procedure (if so, such subjects should be excluded from studies). Polley and colleagues (1999a) elegantly used a thin bone preparation in rodents to study experience-dependent modification of intrinsic optical maps of whisker represen tations in the somatosensory cortex. Subjects were imaged at three different time points, each 4 weeks apart, while the whiskers and the environments were manipulated to determine their ef fects on whisker representations. This study was clearly made possible by using the thin bone preparation that enabled the investigators to image the same subjects over a period of months (Polley *et al.,* 1999a).
When using a thin bone or intact dura preparation it is necessary to provide prophylaxis against infection. Investigators should make sure that antibiotics and analgesics used in the care of research subjects do not have vasoactive properties that may otherwise introduce a confounding factor

in the interpretation of chronic optical imaging studies. For example, steroids and opioids are often recommended as analgesics. These drugs, however, may alter vascular responsiveness and so investigators should opt for other analgesics such as nonsteroidal anti-inflammatory drugs

B. Chronic Optical Imaging in the Awake Monkey

Experiments in awake monkeys of fer many advantages for the study of higher cognitive functions. Since such studies require very long preparatory periods and financia investment, which are devoted to training the animal, it is essential that the imaging should not be restricted to a single experiment and thus that chronic recordings are feasible.

The foremost problem with chronic recordings in primates is maintaining the cortical tissue in optimal condition for long periods of time. In order to achieve this and at the same time provide good optical access to the brain, Shtoyerman and colleagues (2000) examined the feasibility of implanting a transparent artificial dura made of silicon. After affixing chamber to the primate's skull with stainless steel screws, the skull was removed from the region circumscribed by the chamber . Once the cortex was not exerting any pressure on the dura (see Section III.C.1), the dura was opened and the cortex was *immediately* covered with the artificial dura (homemade) After the artificial dura was in place, the chamber was fill with an agarose and antibiotic solution. Agarose is necessary to prevent rapid regrowth of the natural dura. Finally , the chamber was sealed with a glass plate and a metal plate to protect the exposed cortex. Subjects were treated 7–14 days with antibiotics and regularly tested for infections. Regularly sampling the chamber for both bacterial and mycological infections is key since infections can spread quickly from within the chamber into the cortex.The authors report that the immediate covering of the cortex is crucial for prevention of infections and maintaining the cortex for long periods (Shtoyerman *et al.,* 2000). The advantages of this procedure are that the cortex remains visible for periods of greater than 1 year and the artificial dura is easily penetrable by electrode (which is key for matching intrinsic signal maps with electrophysiological maps).

C. Reproducibility of Optical Maps

Defining the reproducibility of maps over time is critica for chronic imaging studies, especially those which aim to define the e fect of an experimental manipulation (e.g., monocular deprivation or whisker plucking) on functional representations. In order to conclude that a particular treatment alters functional maps, one must first be confident th maps do not spontaneously change over time.

Having established a methodology for chronic imaging in primates, Shtoyerman and colleagues (2000) explored the stability and reproducibility of functional maps over a period of greater than 1 year . Ocular dominance columns followed over 1 year did not change significantly an appeared extremely reproducible. The variability of ocular dominance column maps over a period of 1 year was similar to the variability of ocular dominance column maps from a single imaging session or over a few consecutive days (Shtoyerman *et al.,* 2000) (Fig. 15).

The reproducibility of maps was also investigated in rodents by Masino and Frostig (1996). Unlike the results of Shtoyerman *et al.* (2000), they found that functional whisker representations in rodents may vary by as much as 48% over a period of months. Although the location of the whisker maps was consistent over months, they identified nonsys tematic changes in size, shape, and response magnitude of the intrinsic signal map (Masino and Frostig, 1996). Despite the intrinsic variability in functional representations, the rodent model can still be used to investigate the ef fect of a manipulation on functional maps by demonstrating that a manipulation causes an even *greater* variability in functional maps. Polley and colleagues (1999a), in fact, showed that whisker plucking can change functional whisker representations in rodents by greater than 100%, which clearly cannot be attributed to intrinsic fluctuations in functiona maps alone. Moreover , they showed that functional maps consistently expanded or contracted depending on the manipulation (Polley *et al.,* 1999a).

Many factors other than intrinsic cortical map changes may contribute to chronic variability in functional mapping signals. Most importantly , anesthetic depth will greatly influence the extent of intrinsic signals. Therefore, investigators should have a consistent method of inducing and assessing anesthetic depth to ensure that differences in maps are not due to anesthesia. Slight changes in the quality of the stimulus presented may also greatly influence the intrinsi signal map. With respect to visual stimuli, stimulus contrast, brightness, and speed can all be expected to impact the amplitude and possibly the extent of intrinsic signal maps. In rodent experiments using the barrel cortex, it is important to ensure that the degree of whisker stimulation (e.g., 15° vs 30°) and the distance of the whisker perturbator from the base of the whisker are consistent across experiments. It is critical that all parameters except for the experimental manipulation itself be kept constant in order to be able to ascribe changes in functional representation to the manipulation rather than other confounding factors.

The advantage of chronic imaging is the ability to image changes in functional representation, either developmental (Bonhoeffer, 1995) or plasticity related (Dinse *et al.,* 1997b; Antonini *et al.,* 1999; Polley *et al.,* 1999a; Pouratian *et al.,* 1999; Nguyen *et al.,* 2000). In some cases, these experience-dependent changes may become a confounding factor . It is important to consider what ef fect, if any, the chronic implantation of a chamber and the incision of the scalp may have on

the behavior of the animal and therefore experience-dependent cortical representations. In some cases, it may be difficult t isolate the relative ef fects of the optical imaging preparation and the experimental manipulation on the functional map.

VIII. Optical Imaging of the Human Neocortex

Intrinsic signal imaging of the human neocortex is particularly attractive as an intraoperative mapping modality because it can rapidly assess the functional activity of a large area of exposed cortex with very high spatial resolution (micrometers). The high spatial resolution of optical imaging can be quite clinically useful. By mapping the functional or ganization of the exposed cortex, resection of pathological tissue can be maximized and iatrogenic damage to healthy cortex can be minimized. Studies using optical imaging in humans, however , have been limited because of their technical difficulty (Haglun *et al.,* 1993; Toga *et al.,* 1995a; Cannestra *et al.,* 1996, 1998a,b, 2000, 2001; Pouratian *et al.,* 2000a).

Haglund and colleagues were the first to observe optica signals in humans, reporting activity-related changes in cortical light reflectance during cortical stimulation, epilepti form afterdischar ges, and cognitive tasks (Haglund *et al.,* 1992). Lar ge optical signals were found in the sensory cortex during tongue movement and in Broca' s and Wernicke's language areas during naming exercises. They also reported that surrounding afterdischar ge activity , optical changes were of the opposite sign, possibly representing inhibitory surround. This was a landmark paper as it demonstrated the use of optical methods in humans, which up until this point had been employed only in monkeys, cats, and rodents. Since then, there have been reports describing the evolution of optical signals in the human cortex (T oga *et al.,* 1995a), the mapping of primary sensory and motor cortices (Cannestra *et al.,* 1998a), and the delineation of language cortices within (Cannestra *et al.,* 2000) and across languages (Pouratian *et al.,* 2000a) and comparing intraoperative intrinsic signals with preoperative BOLD *f*MRI signals (Cannestra *et al.,* 2001; Pouratian *et al.,* 2001).

A. Imaging during Neurosurgery

A major concern for intraoperative optical imaging studies is that the imaging system be compatible with the traditional operating room environment since the primary concern must always be the welfare and health of the subject (Fig. 10). Intraoperative optical imaging, fortunately , can be done with very little modification of the traditional operatin room environment. The imaging device (e.g., CCD) can be mounted directly onto the operating microscope. The scope and mounted camera, under a sterile drape, can then be

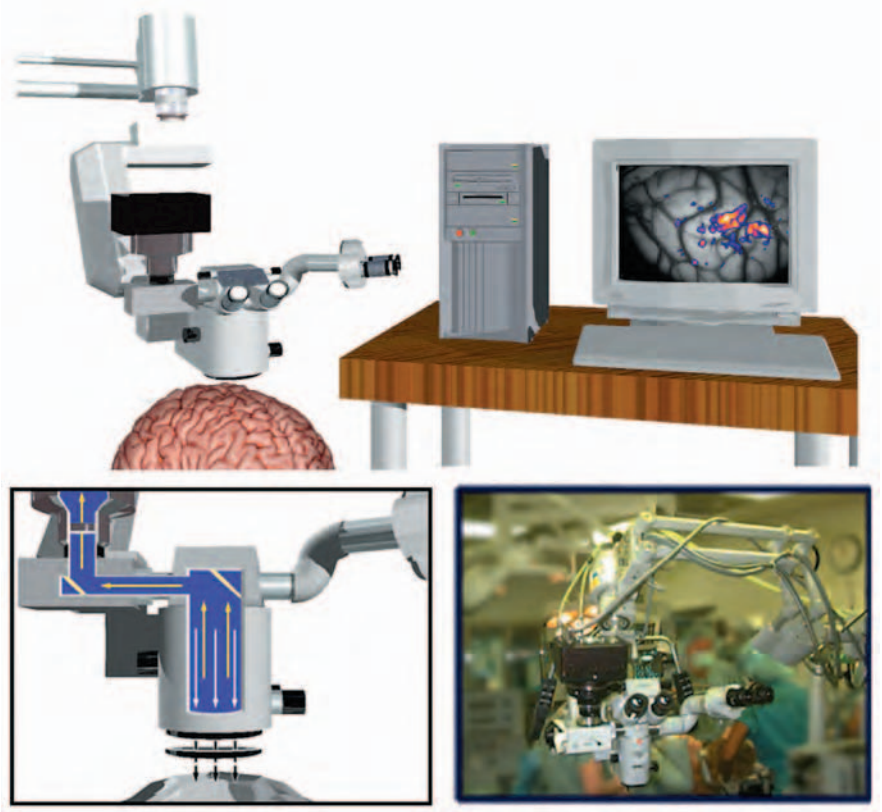

Figure 10 Schematic of intraoperative setup for optical imaging of intrinsic signals. The basic setup for optical imaging in the intraoperative environment is very similar to that seen in Fig. 5. The major modification is that th CCD camera (or other detector) must be mounted onto the operating microscope (top and bottom right). Illumination is provided through the operating microscope optics and the reflecte light is directed back through the microscope optics and toward the mounted CCD (bottom left). **Bottom right:** Photograph of the CCD camera used by Toga and collaborators mounted onto the operating microscope immediately prior to optical imaging in the operating room.

moved into the sterile field over the cortical exposure Sterilized circular polarizing and heat filters are placed unde the main objective of the operating microscope to reduce glare artifacts from the cortical surface. Voltage-stabilized white light illumination is provided by the operating microscope light source, through a fiber optic illuminato. Reflecte light is filtered through a band-pass transmission filter befo being captured by the camera. In general, the temporal resolution of imaging ranges between 200 and 500 ms per frame (which is sufficient to image the slowly evolving perfusion related response) with image exposure times between 50 and 200 ms. The image exposure time should be kept short in order to minimize intraimage brain movement.

The movement of the cortex due to cardiac and respiratory motion complicates intrinsic signal imaging intraoperatively. Imaging during awake procedures (in which the patient is performing cognitive tasks) is an even greater challenge because the subject's respiration rate is not under the direct control of the anesthesiologists.

1. Strategies for Reducing Movement Artifacts

Strategies for reducing cortical movement have previously been discussed in Section III.C. Relevant approaches for intraoperative imaging are briefly discussed here. Severa strategies have emer ged to minimize the ef fect of cortical movement during imaging, including imaging through a sterile glass plate which lies atop the cortex (Section III.C.3) (Haglund *et al.,* 1992), synchronizing image acquisition with respiration and heart rate (Section III.C.4) (T oga *et al.,* 1995a), and using postacquisition image registration (Section III.C.5) (Haglund *et al.,* 1992; Cannestra *et al.,* 2000; Pouratian *et al.,* 2000a). While each significantly improve the SNR of intrinsic signal image analysis, each also has some drawbacks that should be considered. The first report o intrinsic signals in humans used a glass plate to immobilize the cortex. However, it is unclear how this physical restraint of the cortex affects the physiology which underlies the intrinsic signal etiology. Synchronizing data acquisition with respiration and heart rate ensures that the brain is in the same position during each image acquisition. However , this strategy can limit temporal resolution and may be technically challenging since it requires interfacing with intraoperative anesthesiology monitoring equipment. Finally , postacquisition image registration alleviates the need to interface with operating room equipment and has no temporal resolution limitations, but the movement of the cortex during acquisition may introduce movement-related cortical reflectance change that are independent of activity, even after image registration. For more detailed discussion, see Section III.C.

2. Clinical Utility of Intrinsic Signal Maps

Other than the technical challenges discussed, the major limitation of intraoperative optical imaging as a clinical tool is that optical imaging does not directly detect neuronal activity. Instead, optical signals arise from physiological processes (perfusion-related and metabolic) that are coupled to, yet whose temporal/spatial profiles are somewhat distinc from, neuronal activity. Although several groups have characterized the relationship between intrinsic signals and electrophysiological activity, a precise understanding of this relationship will be necessary in order to base clinical decisions on intrinsic signal maps. In a survey of 10 human subjects, Pouratian *et al.* found that 98% of sites deemed active by electrocortical stimulation mapping (ESM) demonstrated optical changes at 610 nm (Pouratian *et al.,* 2000c) (Fig. 11). [ESM is the current gold standard of intraoperative cortical

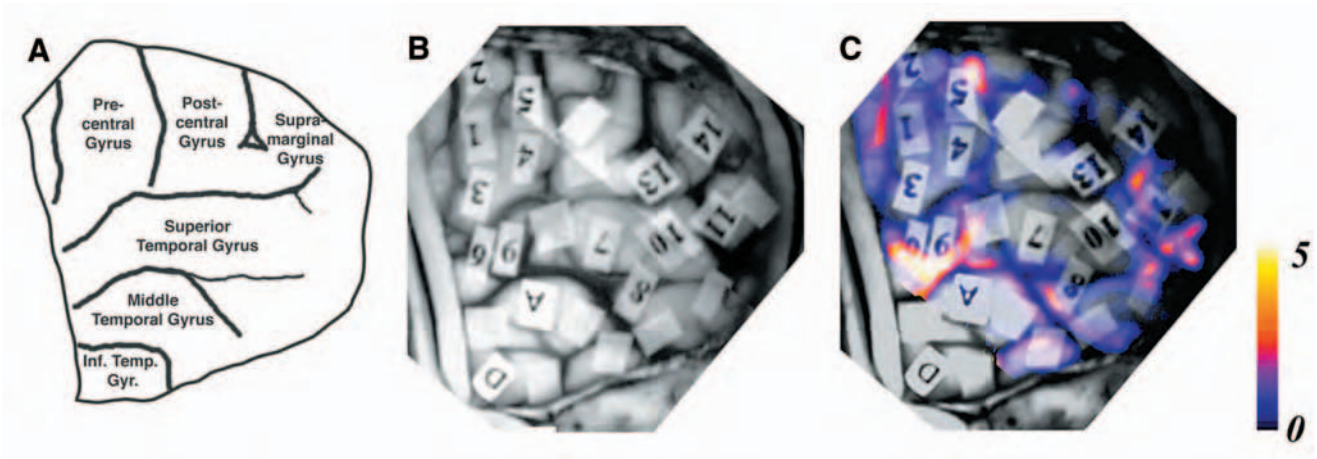

Figure 11 Correlation of optical signals with electrocortical stimulation maps intraoperatively . (**A**) Schematic indicating the gyral morphology displayed in (B) and (C). (**B**) Electrocortical stimulation map (ESM) showing areas essential for language processing tagged with numbers, areas not essentia l for language processing with blank tags, and areas which when stimulated induced afterdischar ge activity. (**C**) Optical map (positive 610-nm signal) show very high spatial correlation with ESM map shown in (B). Note that all areas which were deemed active by ESM in (B) have optica l activity within millimeters of the numbered tags and those areas with blank tags do not show adjacent optical activity . Color bar represents perce ntage reflectance change Adapted, with permission, from Pouratian *et al.* (2000a).

mapping: a direct current is applied to the cortical surface via bipolar electrodes (4 to 20 mA for 2–7 s). Stimulation results in a movement if over motor cortex, a perception (over sensory or limbic areas), or task disruption in awake language testing.] In addition, ~25% of areas deemed *inactive* by ESM were also optically active, indicating that intrinsic signal maps extend beyond the regions indicated by ESM. This phenomenon of "spread" has also been observed in the rodent somatosensory cortex in response to whisker stimulation (Godde *et al.,* 1995; Chen-Bee and Frostig, 1996; Masino and Frostig, 1996). In humans, the spread may be due, in part, to the fact that optical imaging detects both essential and secondary (i.e., active but not necessary for completion of task) cortices while ESM detects only essential areas. Alternatively, this spread may represent an inexact colocalization of optical signals and electrophysiological activity due to imprecise physiological coupling of neuronal activity, metabolism, and perfusion. The significance of th spread of optical signals must be clarified before intrinsi signal maps can be used for clinical decision-making.

B. Optical Imaging through the Intact Human Skull—NIRS

Several studies have demonstrated that imaging in animals can be performed through the intact (thinned skull) (Frostig *et al.,* 1990; Blood *et al.,* 1995; Masino and Frostig, 1996). In these studies, the skull was thinned to a few hundred micrometers. Is optical imaging through the intact human skull, measuring 515 mm, at all realistic? Using longer wavelengths of light (near infrared) that penetrate the skull much more efficiently than visible light, several groups have been able t produce functional maps of the human cortex through the intact human skull. This method, known as near -infrared spectroscopy, can be considered a variant of intrinsic optical imaging since it also measures metabolism and perfusion-related changes in light absorbance. Imaging through the intact skull, however , introduces and necessitates significan methodological and analytical modification of intrinsic signa imaging techniques. Consequently , NIRS is discussed in detail in its own chapter (Chapter 6, this volume).

C. Applications

Intraoperative optical imaging of fers the opportunity to answer questions about basic neurophysiology (Cannestra *et al.,* 1996, 1998b) and characterization of brain or ganization and relationships (Cannestra *et al.,* 1998a, 2000, 2001; Pouratian *et al.,* 2000a) and to develop a clinical tool that can help guide clinicians through procedures. Clinically , mapping the cortex prior to procedures can help delineate functional boundaries by which resections can proceed, ensuring that as much pathologic tissue as possible is resected and healthy tissue remains intact. Another potential application of intrinsic imaging in human neurosurgery is in the visualization of epileptic foci (if they are on the surface of the brain) with a precision much better than currently achieved with electrical recording (approximately 1 cm).

Although this chapter focuses on intrinsic signal imaging and only intrinsic signal changes have been reported in humans, optical signals can also be measured using dyes that are restricted to physiological compartments, such as intravascular dyes (Frostig *et al.,* 1990; Narayan *et al.,* 1995), and dyes that are sensitive to physiological events, such as oxygen-dependent phosphorescence quenching dyes (Vanzetta and Grinvald, 1999). Optical signals which are specific to pathological tissue, such as tumors, can also b detected by using tracers specific to tissue properties or eve metabolic rates (Daghighian *et al.,* 1994), which may also improve neurosur gical planning. To date, the toxicity of such dyes has made this approach prohibitive in humans.

IX. Combining Optical Imaging with Other Techniques

Intermodality comparisons are useful because each imaging technique offers different information about the cortical or ganization, anatomy , and physiology of the cortex of interest. Specificall , intrinsic signal imaging can be combined with tracer injections for investigating anatomical and functional relationships. Alternatively, intrinsic signal imaging can be combined with other perfusion-related brain mapping modalities to characterize the etiology of perfusion-related neuroimaging signals, since each technique of fers slightly different information about perfusion responses and holds different assumptions.

A. Targeting Tracer Injection into Selected Functional Domains

Tracers and markers are often injected into cortex to determine the anatomic connectivity between one cortical area with another . It is unclear whether the markers are injected into a single functional domain or into several neighboring regions with dif ferent functional properties (e.g., the border between two cortical areas with diferent orientation preferences). Maps obtained with optical imaging can be very helpful for systematically tar geting tracer injections into discrete functional domains. By combining optical imaging with tracer injection techniques, both functional and anatomical data can be obtained from a single subject, enabling investigators to define functional-anatomical rela tionships with much higher precision.

The most critical step in combining *in vivo* optical imaging with histological observations is to precisely match the optically derived maps with the histological sections. This can be accomplished by matching the pattern of

superficial blood vessels recorded *in vivo* using the optical imaging apparatus with reconstructions of the vascular patterns observed in histological sections. Alternatively, fiducial lesions can be recorded in the optical image an later identified and matched with the same lesions in the his tological samples. In order to get good correspondence between the optically acquired maps and the histology , it is very important that the cortical tissue is not flattened or dis torted in any other way before the histology is performed.

Optical imaging has been combined with histological investigation in the visual cortex of macaque monkey as well as in area 18 in the cat (Malach *et al.,* 1993; Kisvarday *et al.,* 1994). In one such study , an anterograde tracer , biocytin, was injected into monocular domains, binocular domains, and cortical areas corresponding to dif ferent orientations, as defined by functional intrinsic optical signa mapping. By using optical-map-directed injections, the authors were able to demonstrate that intrinsic anatomical connections tended to link monocular regions with same-eye ocular dominance columns (skipping columns corresponding to the other eye), binocular regions projected to other binocular regions but not to monocular regions, and cortical areas subserving a specific orientation preferenc connected with other areas with a similar orientation preference (Malach *et al.,* 1993). It becomes clear that studies of this sort can lead to a better understanding of the relationship between anatomy and function in the cerebral cortex at both the single-cell and the macroscopic level.

B. Combining Optical Imaging with Electrical Recordings or Stimulation

The chamber described in Section III.C.1 can be modified to be compatible with electrical recordings o stimulation. This chamber (originally described in *Brain Mapping: The Methods,* first edition, Chapter 3) consists o a chamber with a square coverglass that is much larger than the chamber diameter. The chamber is sealed by pressing the coverglass against an O ring. The special coverglass is fitte with a rubber gasket, flexible enough to be penetrated by hypodermic needle. Both the cover glass (held by a thin metal frame) and the syringe (attached to a hydraulic manipulator used to penetrate the rubber gasket on the coverslip) are attached to an *xy* manipulator and can thereby be moved relative to the base of the cranial window . Once the syringe is in the vicinity of the recording site of interest, an electrode that resides within the needle is pushed out of the needle and advanced into the cortex, using the hydraulic manipulator .

This device is very useful for the electrical confirmation o optically obtained functional maps as well as for tar geted microelectrode recordings. Shmuel and Grinvald (1996) used it to perform both perpendicular and nearly tangential penetrations studying the relationships between unit responses and optically imaged functional domains for orientation and direction. The same device is theoretically applicable for microstimulation during optical recording experiments.

Evoked potentials and electroencephalographs (EEG) can also be recorded simultaneously with intrinsic signal imaging without the modified cranial chambe . Using a thinned bone preparation, a burr hole can be drilled over the cortex of interest and an electrode can be advanced through it (Chen *et al.,* 2000; O'Farrell *et al.,* 2000). This method is feasible only for recording of evoked potentials (EPs) or continuous EEG of populations of neurons. EPs are often considered the most appropriate measurement of electrophysiological activity because, like intrinsic signal imaging, EPs measure net cortical responses over broad regions rather than activity of individual neurons (Fig. 12). Although single-unit recordings may reveal more detailed information about the activity of individual neurons, these recordings require craniotomy and administration of intravenous mannitol to reduce cerebral swelling, potentially interfering with chronic imaging experiments and optical signals arising from cellular swelling, respectively.

Intrinsic signal imaging of direct cortical stimulation has been done in both nonhuman primates (Haglund *et al.,* 1993) and humans (Haglund *et al.,* 1992). Haglund and colleagues found that while subthreshold stimulation did not produce any optical changes, the spatial extent and intensity of intrinsic signal response to suprathreshold stimulation depended on the duration and magnitude of bipolar cortical stimulation (Fig. 13). Further, they found that intrinsic signal changes did not activate nearby ocular dominance columns or orientation patches; stimulation-induced intrinsic signal changes were localized. Similar results were found in humans, in which graded responses to stimulation intensity were observed.

C. Combining Optical Imaging and fMRI

BOLD *f*MRI has become one of the most commonly used perfusion-based brain mapping modalities (Ogawa *et al.,* 1992). Although most believe the BOLD signal is due to cerebral blood flow (CBF) increases in excess of increase in the cerebral metabolic rate of oxygen, resulting in decreased capillary and venous deoxyhemoglobin concentrations (see Chapter 13 of this volume for more details), the exact etiology of the BOLD signal continues to be debated (Boxerman *et al.,* 1995; Menon *et al.,* 1995; Hess *et al.,* 2000; Kim *et al.,* 2000). Characterization of the etiology of BOLD is critical for the accurate interpretation and analysis of BOLD *f*MRI brain mapping studies.

Studies comparing BOLD with optical intrinsic signals are particularly advantageous for characterizing BOLD signals because the etiology of optical signals has been well scrutinized (Frostig *et al.,* 1990; Narayan *et al.,* 1995; Malonek and Grinvald, 1996; Nemoto *et al.,* 1999). Although many cite optical imaging studies to support the etiology of the BOLD signal, only a few intrasubject comparisons of optical intrinsic signals and BOLD *f*MRI exist (Hess *et al.,* 2000; Pouratian

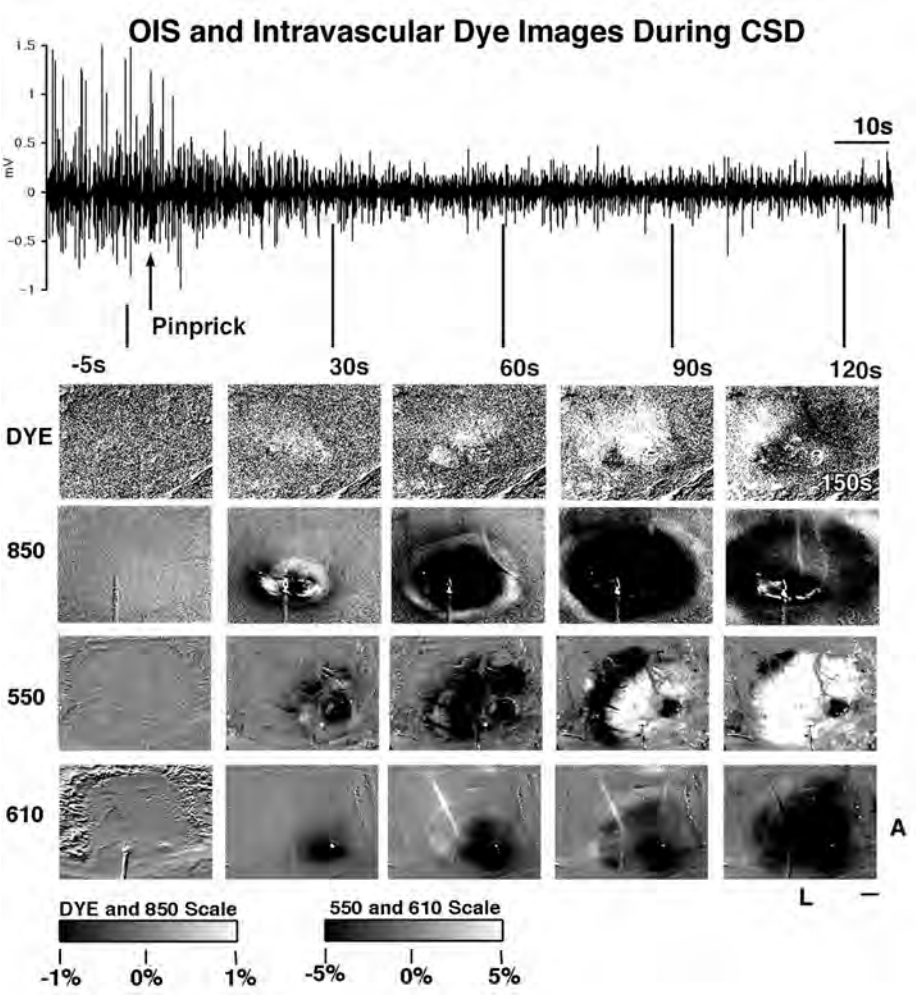

Figure 12 Triphasic optical intrinsic signal response to cortical pinprick-induced cortical spreading depression. **Top:** EEG demonstrating suppression of spontaneous cortical activity within 20–30 s of pinprick. **Bottom:** Intrinsic signal responses at different wavelengths and intravascular dye imaging. At least three distinct phases can be identified at all three wavelengths of intrinsi signal imaging. Intravascular dye imaging, on the other hand, indicates only two phases coincident with the second and third phase of the intrinsic signal responses, suggesting that these two phases are due to changes in blood volume. The first phase, on the othe hand, is hypothesized to be due to light scattering changes. Interestingly, at 610 nm, different polarity signals are observed arising from the parenchyma and vasculature, suggesting that different physiological processes occur in these different compartments. This differentiation once again highlights the advantage of the high spatial resolution of optical imaging. Figure provided by Alyssa Ba.

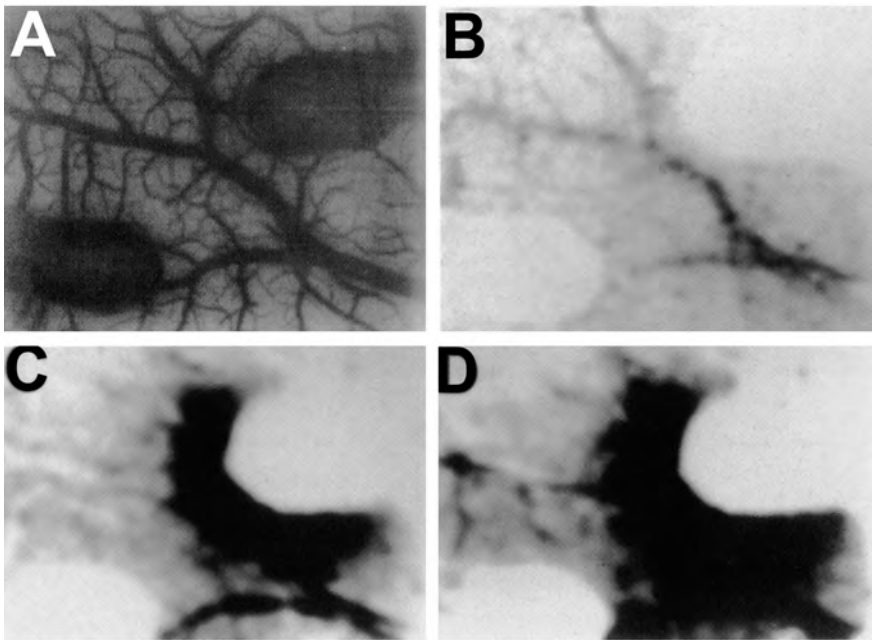

Figure 13 Optical imaging of bipolar cortical stimulation. (**A**) Raw image of primate cortex. The two darkened circles on the top right and bottom left indicate placement of the bipolar electrode. (**B**) Subthreshold stimulation of the cortex. (**C**) 1 mA stimulation of the cortex. (**D**) 1.5 mA stimulation of the cortex. Darkened areas in (C) and (D) indicate activity-related changes. Note that activity-related changes are limited to the area surrounding the electrodes. This study, however, does not preclude the possibility that ESM may cause activation of distant cortices. Adapted with permission from Haglund *et al.* (1993).

et al., 2000a; Cannestra *et al.,* 2001). Considering that many optical imaging studies draw conclusions and discuss the implication of such studies on functional magnetic resonance imaging (see for example Malonek and Grinvald, 1996; Vanzetta and Grinvald, 1999; Mayhew *et al.,* 2000), characterization of the relationship between the signals from these two modalities is critical.

Comparing *f*MRI signals, which are tomographic, with optical signals, which are surface signals, presents a challenge. In order to compare mapping signals from multiple modalities within a single subject, the dif ferent modalities must be warped into a common space (Fig. 14). The common space used is the three-dimensional (3D) cortical model (i.e., cortical extraction) of each subject' s brain (generated from high-resolution T1-weighted MR scans, see middle of Fig. 14 for example). Before extracting cortical surfaces from the high-resolution T1-weighted MR scan, each scan is skull and cerebellum stripped and corrected for radiofrequency nonuniformity (Sled *et al.,* 1998). A 3D active surface algorithm is used to generate an external cortical surface mesh for each subject (MacDonald *et al.,* 1994). In order to align the *f*MRI activations with this cortical model, one must determine the transformation necessary to align high-resolution structural scans (which are coplanar with the *f*MRI scans of interest) with the T1-weighted MR scans used to create the cortical model. This transformation should be a rigid-body (i.e., six parameter—three rotations and three translations) transformation since two structural scans of the same subject are being aligned. The resulting transformation is then applied to the original *f*MRI data to line up the functional data with the 3D cortical model (see Pouratian *et al.,* 2001, and Cannestra *et al.,* 2001, for examples of this approach). Optical intrinsic signal (OIS) maps are projected onto the cortical model by matching sulcal landmarks on the cortical model with identical sulcal landmarks on the raw optical images. The accuracy of these projections is demonstrated in Fig. 15 (middle). It is clear from Fig. 15 that sulci in the optical images are continuous with sulci on cortical extractions, confirming the succes of these projections.

The Ojemann group has adopted a similar methodology (Corina *et al.,* 2000). However, instead of relying on sulcal landmarks for registration, they use the position of the cortical blood vessels. Preoperatively , an MR angiogram (an MRI scan sequence which highlights surface vasculature) is performed and superimposed onto the subject' s cortical extraction. After reflection of the dura and exposure of th brain surface, the arteries and branch points that have been superimposed onto the cortical extraction are identified o the cortical surface and subsequently used to register intraoperative maps with preoperative scans.

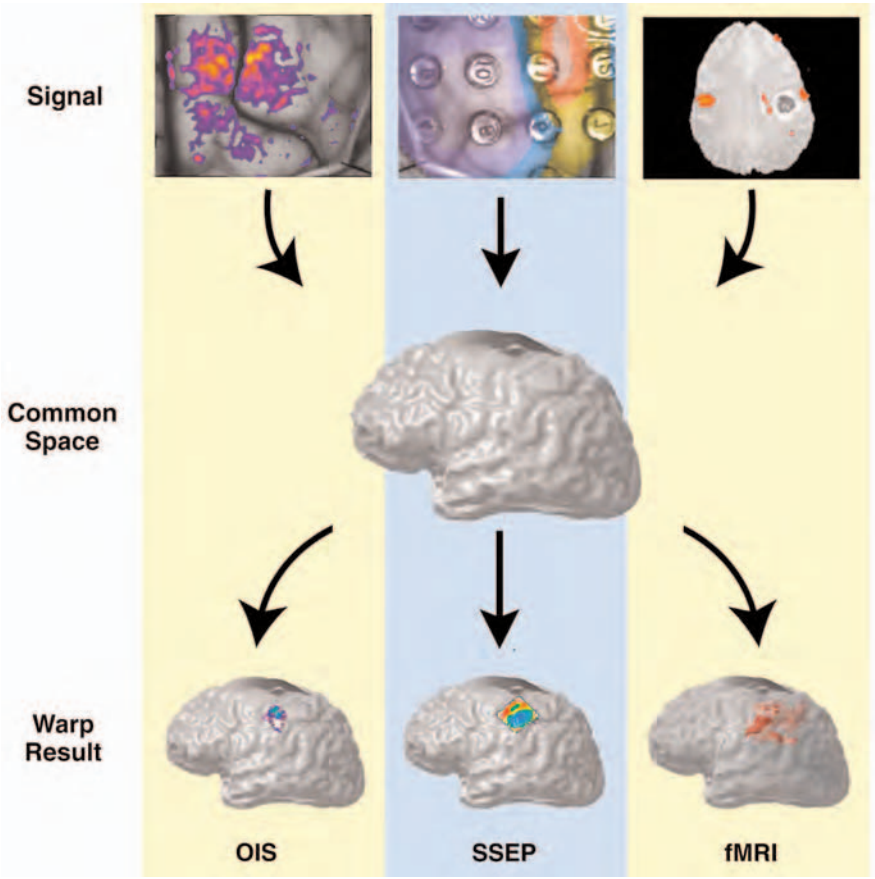

Figure 14 Intermodality comparisons. In order to compare mapping signals across modalities, the different modalities being compared must be warped into a common space. The common space is the cortical extraction of each subject's brain. Depending on the modality, different warping strategies are employed to warp the different mapping signal into a common space. While optical imaging is a surface imaging technique and requires projection of the data onto the cortical surface, *f*MRI is a tomographic technique and is warped into the common space using rigid body transformations to align the *f*MRI volume with the high-resolution MRI used to extract the cortical surface. The darkened area at the top of each cortical extraction demarcates tumor localization.

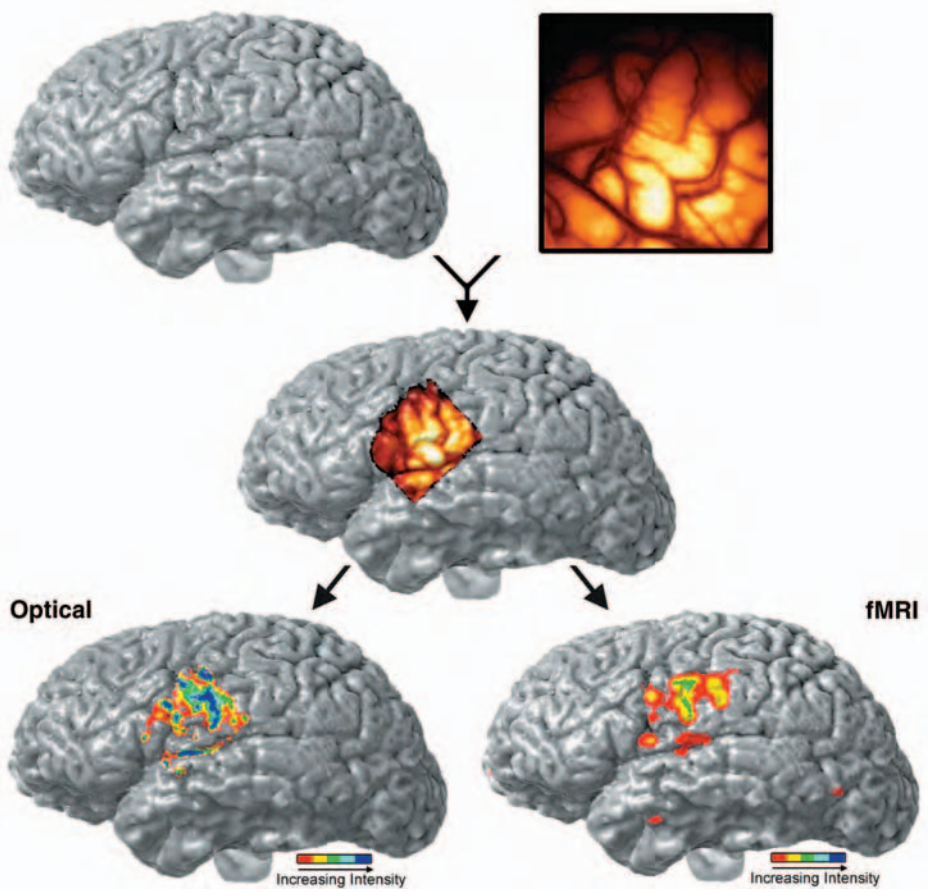

Figure 15 Strategy for comparing intrinsic signal imaging (a surface-based mapping technique) with functional magnetic resonance imaging (a tomographic technique). A 3D cortical surface extraction is used as the common space for comparing multiple modalities (top left, see Fig. 14). A photograph of the cortical surface imaged for intrinsic signal imaging (top right) is warped onto this surface by matching sulcal landmarks on the photograph and the 3D surface extraction. The accuracy of this warp is confirmed by th fact that the sulci in the optical image (projected photograph) are continuous with sulci on cortical extraction (middle). The warping parameters used to project the photograph onto the cortical surface are then applied to the intrinsic signal map to project the functional signal onto the cortical surface (bottom left). Other modalities, such as *f*MRI, can also be projected into the "common space," or the 3D surface extraction (bottom right), in order to compare across modalities.

Recently, Hess *et al*. (2000) imaged both BOLD signals and OIS in rodents, demonstrating that positive BOLD signals can occur even if deoxyhemoglobin levels are persistently elevated (as determined by decreased reflectance a 605 nm). It is unclear, however, whether such results can be generalized to human subjects, whose brains are gyrencephalic (vs lissencephalic in rodents) and whose vascular architecture dif fers significantly from rodents (Bä , 1981; Duvernoy *et al.,* 1981; Dirnagl *et al.,* 1991; Reichenbach *et al.,* 1997). In contrast to these findings, Cannestra an colleagues have demonstrated a spatial/temporal mismatch between the early negative 610-nm response [which Hess *et al*. (2000) and others attribute to increases in deoxyhemoglobin] and the BOLD signal in response to brief (2 s) somatosensory stimulation (Cannestra *et al.,* 2001). While the BOLD signal is centered on sulci, the negative 610-nm response is centered on gyri (Fig. 16). Furthermore, when the negative 610-nm OIS activation was used as an objective region of interest for analysis of BOLD signals, an initial dip was identified in the BOLD signal (Cannestr *et al.,* 2001). In a case study comparing *f*MRI and OIS activations, Pouratian and collaborators (2000a) found that the *positive* 610-nm response and the BOLD signal demonstrated much greater spatial correlation (than the negative 610-nm response and the BOLD signals). Despite the greater spatial correlation, the positive 610-nm response still demonstrated greater gyral activations than BOLD signals (Pouratian *et al.,* 2000a) (Fig. 16).

Recent technological advancements have led to the development of a low-cost combined optical imaging and functional MRI (3 T) system for animals (Paley *et al.,* 2001). The system allows concurrent MR imaging, optical spectroscopy , and interventional capabilities, for both physiological monitoring of the rodent and experimental manipulation. With the

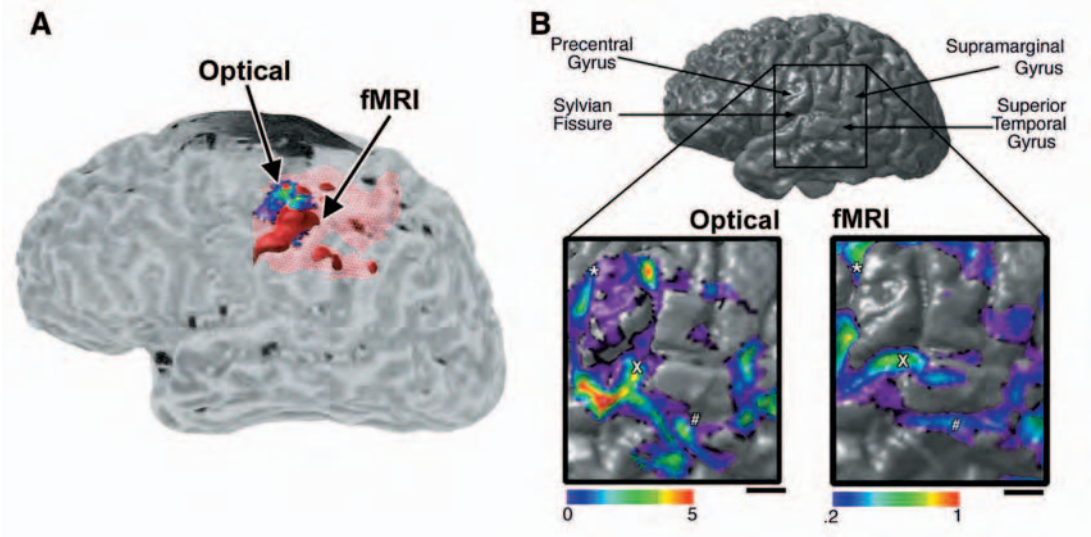

Figure 16 Comparison of 610-nm optical signals and BOLD *f*MRI. (**A**) Responses to brief (2 s) somatosensory stimuli (110-Hz finger vibration) were imaged using both optical imaging of intrinsic signals and BOLD*f*MRI. The initial decreased reflectance at 610 nm (labeled "Optical") was neither spatially nor temporally (data not shown) correlated with the BOL *f*MRI signal (labeled "*f*MRI"). While the *f*MRI signal centered on the sulcus and extended deep within the sulcus (where the venous vasculature is located), the negative 610-nm response centered on gyri and better matched somatosensory evoked potential maps (data now shown). Adapted, with permission of Oxford University Press, from Cannestra *et al.* (2001). (**B**) The positive 610-nm response, or late increased 610-nm reflectance, is more spatially and temporally correlated with th BOLD signal. In a case study comparing *f*MRI and OIS activations, we found that the *positive* 610-nm response and the BOLD signal demonstrated much higher spatial correlation (compare bottom left optical signal with bottom right *f*MRI signal). Despite the higher spatial correlation, the positive 610-nm response still demonstrated greater gyral activations than BOLD signals. Adapted, with permission, from Pouratian *et al.* (2000a).

advent of interventional MR imaging devices for neurosurgery, intraoperative optical imaging can also be integrated with intraoperative MR (iMR) for better comparison of mapping signals within a single subject. The advantage of having concurrent intraoperative optical imaging and MRI is that both modalities can be used to image the brain after craniotomy and dural reflection so that the brain is imaged in th same space and (possibly) time. The iMR environment imposes imaging restrictions above and beyond that of the normal operating room environment in that investigators must be cautious of high magnetic field physically a fecting the imaging device and interfering with the imaging system (and distorting image capture), which was not designed to be MR compatible. Nonetheless, Toga and colleagues have confirmed the feasibility of intraoperative optical imaging i the intraoperative MR environment (unpublished data).

D. Combining Optical Imaging and Micro-PET

Micro-PET offers the opportunity to image functional changes in the rodent brain with millimeter resolution (Kornblum *et al.,* 2000). A comparison of optical imaging and micro-PET data has yet to be published but with recent technological advancements, it is feasible and may of fer a greater understanding of the etiology of optical signals and better elucidate the nature of perfusion-related responses. The specific advantage of micro-PE is that known tracers are used (e.g., [^{18}F]fluorodeoxyglucose) so that the etiolog of the functional changes observed by micro-PET are unambiguous. Similar intermodality comparisons were done several years ago between *f*MRI and PET , serving to help clarify the etiology and significance of the *f*MRI signal (Ramsey *et al.,* 1996).

The challenges faced in comparing intrinsic signals and micro-PET are similar to those faced in comparing intrinsic signals with *f*MRI. Namely , while micro-PET is a tomographic technique, intrinsic signals are surface signals. Consequently, a common space must be identified in whic to compare the signals. By analogy, it seems that the appropriate space would be the three-dimensional model of the subject's brain. Similar to the other techniques, fiducia markers must be used to align the maps appropriately after imaging. Unfortunately , micro-PET does not of fer any anatomical information by which to perform image registration. Alternatively, radioactive sources can be placed during micro-PET imaging and identified on the optical image fo subsequent registration.

X. Applications

Based on the specific advantages which optical imagin of intrinsic signals offers, including ease of implementation,

high spatial and temporal resolution, relatively noninvasive imaging, the opportunity to image a single subject chronically, and the ability to determine the time course of underlying functional chromophore changes, four areas of application to which optical imaging has been applied have emerged. These include characterizing the functional architecture of sensory cortices, investigating patterns of functional perfusion and neurovascular physiology , imaging development and plasticity, and characterizing the dynamic profile of disease processes

A. Characterization of Visual and Somatosensory Cortices

The high spatial resolution of optical imaging has made it an ideal modality for characterizing the fine functiona architecture of sensory (both visual and somatosensory) cortices. Studies by Bonhoef fer and Grinvald (1991, 1993) perhaps best highlight the utility of this modality for characterizing the functional architecture of the visual cortex in cats. By imaging visual cortex responses to gratings of different orientations, they established "pinwheels" as an important structural element underlying the or ganization of orientation domains in the visual cortex (Bonhoef fer and Grinvald, 1991, 1993a) (Fig. 9B). Similarly, optical imaging of intrinsic signals has been used to demonstrate ocular dominance domains in the primary visual cortex of macaque monkeys (T s'o *et al.,* 1990) (Fig. 9A). Methodological improvements made it possible to investigate more subtle features of cortical organization. For example, Ts'o and colleagues recently reporting using optical imaging in conjunction with single-unit electrophysiology and cytochrome oxidase (CO) histology to characterize the functional organization within the CO stripes of visual area V2 of primates with greater detail. They report previously unrecognized subcompartments within individual CO stripes that are specific for colo , orientation, and retinal disparity (T s'o *et al.,* 2001). The organization of V2 is reminiscent of V1, for which Victor and colleagues used optical imaging of intrinsic signals to identify orientation, spatial frequency , and color (Victor *et al.,* 1994).

Macknik and Haglund (1999) have also used optical imaging of intrinsic signals to characterize the primate visual cortex. Unlike some other optical imaging studies that seek only to characterize the functional architecture of the cortex, this study went on to ask: What is the stimulus for visual system activation, the physical visual scene or the perception of the visual scene? (Macknik and Haglund, 1999) That is, in the case of a visual illusion in which a physical stimulus is not perceived, does the visual system still respond to that physical stimulus? These optical imaging studies demonstrate that, for the visual illusions investigated, the visual system does not in fact respond to the entire physical visual stimulus, but rather the visual perception (Macknik and Haglund, 1999). These types of studies begin to demonstrate the versatility and the diverse array of questions that can be answered using optical imaging of intrinsic signals.

Optical imaging has similarly been applied in human subjects to characterize somatosensory and language cortices. Cannestra and colleagues stimulated the face, thumb, and index and middle fingers to obtain maps of cortical acti vation for each. While peak responses were distinct for each activation paradigm, nonpeak signals were more dispersed and overlapped (Cannestra *et al.,* 1998a). This is consistent with a report by Godde and colleagues who, using rodents, reported large and overlapping cortical representations with distinct foci in response to stimulation of dif ferent digits (Godde *et al.,* 1995). The organization of language cortices in humans has also been characterized both within (Cannestra *et al.,* 2000) and across languages (Pouratian *et al.,* 2000a). While Pouratian and colleagues showed that different languages in a bilingual subject can produce both overlapping and distinct areas of activation, Cannestra and collaborators showed that spatial and temporal activation patterns of both Broca' s and Wernicke's area is (language) task dependent (e.g., a visual object naming task activates Broca's area dif ferent from an auditory responsive naming task) (Fig. 17).

B. Characterization of Functional Perfusion and Neurovascular Physiology

Intrinsic optical signals have multiple sources, including perfusion- and metabolism-related etiologies, making it a suitable modality for characterizing functional perfusion and neurovascular physiology. It is an especially powerful tool for answering these types of questions because of its superior spatial and temporal resolution. Optical imaging studies have been critical for describing the time course of functional perfusion-related changes, including changes in blood volume (Frostig *et al.,* 1990; Narayan *et al.,* 1995) and hemoglobin concentration changes (Frostig *et al.,* 1990; Malonek and Grinvald, 1996; Nemoto *et al.,* 1999; Mayhew *et al.,* 2000, 2001). Moreover , intrinsic signal imaging was used to describe baseline vasomotion and to compare the magnitude of these oscillatory changes with functional perfusion-related changes (Mayhew *et al.,* 1996). In addition to characterizing the time course of these functional signals, optical imaging has been used to determine the parameters which influenc the magnitude of functional signals, including the absolute number of stimuli as well as the frequency of stimulation (Blood *et al.,* 1995; Polley *et al.,* 1999b). Several studies also have used optical imaging to determine how functional signals are affected by either temporally or spatially adjacent stimuli (Blood and Toga, 1998; Cannestra *et al.,* 1998b) (Fig. 18). Blood and colleagues demonstrated that simultaneous activation of nearby cortices can af fect the magnitude of the functional signals emanating from the regions of interest (Blood and Toga, 1998) (Fig. 18A). Cannestra and colleagues

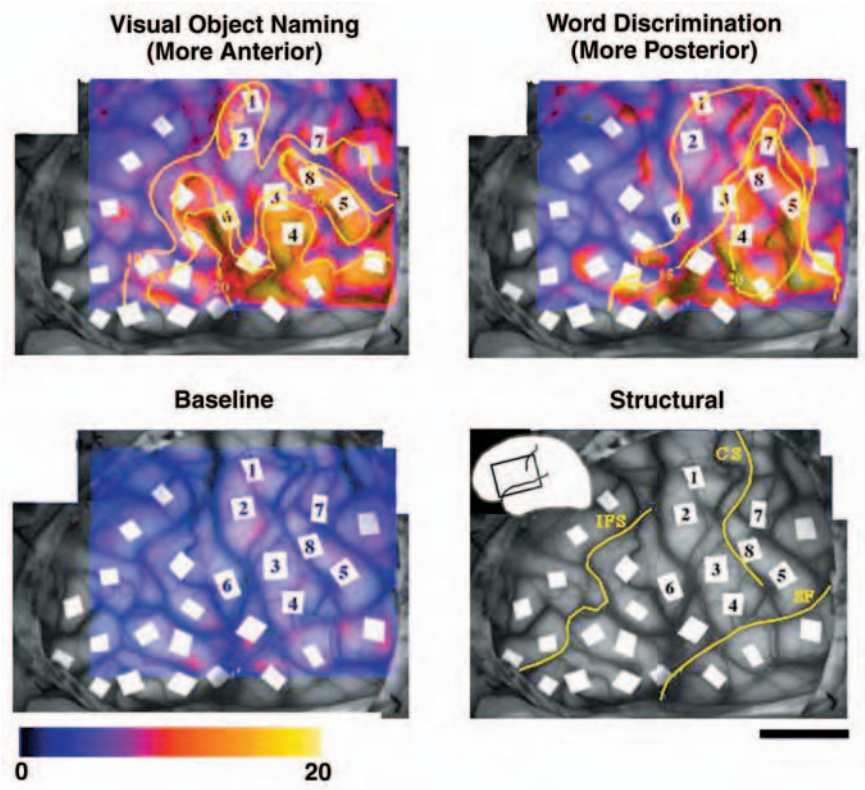

Figure 17 Optical imaging of Broca's area during different language tasks reveals different patterns of activation. Each language task requires dif fering degrees of semantic, syntactic, and lexical processing. It was hypothesized, therefore, that dif ferent language tasks (e.g., visual object naming vs word discrimination) would activate both Broca's and Wernicke's area differently. Activation patterns for two dif ferent language tasks are shown, visual object naming and word discrimination. While the first task activated more anterior regions of Brocas area, the latter task activated more posterior regions. In the study by Cannestra and colleagues (2000), the investigators were able to use optical imaging of intrinsic signals to define subdivisions of both Broca s and Wernicke's area and to describe different patterns of temporal activations within each region. **Bottom left:** Baseline image showing no optical activity. **Bottom right:** Identification of gyri of interest and position of exposur relative to a schematic brain diagram. Color bar denotes reflectance decrease at 610 nm $\times 10^{-4}$. Scale bar is 1 cm. Adapted, with permission, from Cannestra *et al.* (2000).

reported "neurovascular refractory periods," showing that functional responses are diminished in magnitude if they are preceded by another temporally close response (in the face of identical electrophysiological responses) (Cannestra *et al.,* 1998b) (Fig. 18B).

With the advent of spectroscopic intrinsic signal imaging, many studies have been published which aim to characterize the time course of functional changes in blood volume, different hemoglobin moieties, and light scattering (Malonek and Grinvald, 1996; Nemoto *et al.,* 1999; Kohl *et al.,* 2000; Mayhew *et al.,* 2000, 2001; Shtoyerman *et al.,* 2000; Lindauer *et al.,* 2001). These studies dif fer in their spectroscopic analysis techniques. In general, however, most studies suggest an early increase in deoxyhemoglobin concentrations upon cortical activation, followed by a delayed increase in total blood volume and increase in oxyhemoglobin concentrations [exceptions include Kohl *et al.* (2000) and Lindauer *et al.* (2001), which do not observe the initial increase in deoxyhemoglobin concentrations]. Clearly , the temporal profile of functional changes is still questioned and muc work remains to be done to overcome the ambiguities and questions.

Recently, optical imaging has been combined with other imaging modalities in order to better describe functional perfusion-related changes and understand the etiology of the different brain mapping signals. Three recent reports have compared optical imaging with *f*MRI (see Section IX.C) (Hess *et al.,* 2000; Pouratian *et al.,* 2000a; Cannestra *et al.,* 2001) (Fig. 16). These types of studies are critical since each modality holds dif ferent assumptions and limitations, and intermodality comparisons may be one of the best ways of overcoming the limitations of each individual technique.

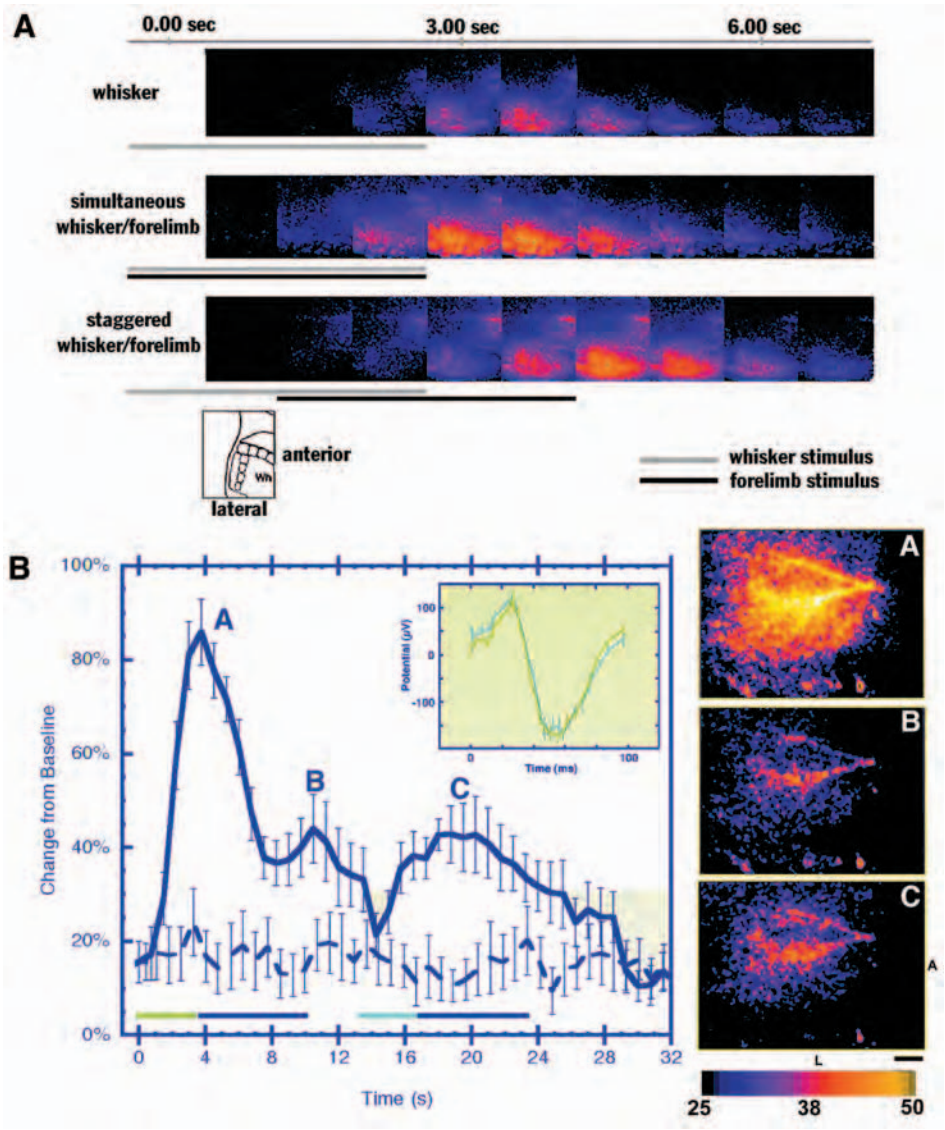

Figure 18 Modulation of optical responses to whisker stimulation by spatially (A) and temporally (B) adjacent stimuli. Optical imaging has been used extensively to characterize factors that modulate functional perfusion-related responses. (**A**) Top: 850-nm optical response to 3 s whisker stimulation. Middle: Optical response to simultaneous whisker and forelimb stimulation. By simultaneous stimulation of the forelimb, the perfusion-related response over the whisker somatosensory cortex is potentiated. Bottom: Optical response to whisker stimulus followed by forelimb stimulation (staggered condition). The response over the whisker somatosensory cortex is delayed and potentiated. Adapted, with permission, from Blood and Toga 1998. (**B**) Hemodynamic refractory periods. The time course of the optical response to two consecutive whisker stimulations (2 s each) with a 3-s interstimulus interval. The response to the second stimulus is nearly half that of the response to the first stimulus even though the evoked potentials (shown in the top right window) ar unchanged for the two stimuli. Horizontal bars at bottom indicate stimulus timing. Dashed line represents baseline optical activity. Error bars are standard errors of the mean. Time courses were calculated using principal component analysis. Adapted, with permission, from Cannestra *et al.* (1998).

C. Imaging Development and Plasticity

More recently, several groups have taken advantage of the ability to use optical imaging for chronic imaging to characterize both developmental and plasticity-related changes in functional architecture and perfusion-related signals. The development of orientation domains has been characterized in ferret visual cortex, from the time that they are first observe (p32) to the time at which they are fully developed (p43) (Chapman *et al.,* 1996). The authors demonstrate that during this time (which is the peak of the critical period) the structure of the maps is remarkably stable (Chapman *et al.,* 1996). A

similar analysis of the development of kitten primary visual cortex has been reported (Bonhoef fer, 1995). Pouratian and collaborators characterized developmental changes in intrinsic signals in the rodent "barrel" cortex, showing that while some intrinsic signals change throughout the developmental period (i.e., 850 nm), intrinsic signals at other wavelengths remain relatively stable and unchanged throughout development (i.e., 550 and 610 nm) (Pouratian *et al.,* 2000b).

Recently, optical imaging has been applied to imaging plasticity-related changes in functional signals (Prakash *et al.,* 1996; Dinse *et al.,* 1997a; Antonini *et al.,* 1999; Polley *et al.,* 1999a). While Prakash and collaborators demonstrated *rapid* representational changes in barrel cortex response after addition of either brain-derived neurotrophic factor or nerve growth factor , other groups have used optical imaging to demonstrate more long-term changes in functional representations secondary to physical manipulations of the subject (Dinse *et al.,* 1997a; Antonini *et al.,* 1999; Polley *et al.,* 1999a). The ability to image chronically was key to the success of such studies. Polley and colleagues, for example, showed that long-term whisker removal and differential housing of rodents can alter intrinsic signal responses in the barrel cortex dif ferently in two distinct ways (Polley *et al.,* 1999a). While a single whisker's functional representation underwent expansion following innocuous removal of all neighboring whiskers, a contraction could also be induced, using the same manipulation, if the animal was given a brief opportunity to use its whiskers for active exploration of a dif ferent environment (Polley *et al.,* 1999a). Pouratian and collaborators have similarly investigated the ef fect of innocuous whisker removal on functional responses to stimulation of the spared whisker (Fig. 19). Optical responses at 850 nm were not potentiated relative to age-matched control until 2 weeks after initial whisker plucking, despite reports that electrophysiological and autoradiographic changes may occur within minutes to days (Kossut, 1998; Kelly *et al.,* 1999). Clearly, the chronic imaging ability of optical imaging combined with its superior spatial resolution makes this modality amenable to many more questions of plasticity-related changes in cortical architecture.

D. Imaging Disease

Optical imaging of intrinsic signals has recently been applied to imaging disease. Haglund and colleagues (1992) first reported imaging epileptiform afterdischa ges following direct cortical stimulation of the human neocortex. They reported that activation patterns were dependent on the intensity and duration of the afterdischar ge activity and often found a pattern of alternating increased and decreased reflection, which they hypothesized to represent a centra area of activation surrounded by areas of cortical inhibition or decreased activity . More recently , Chen and colleagues

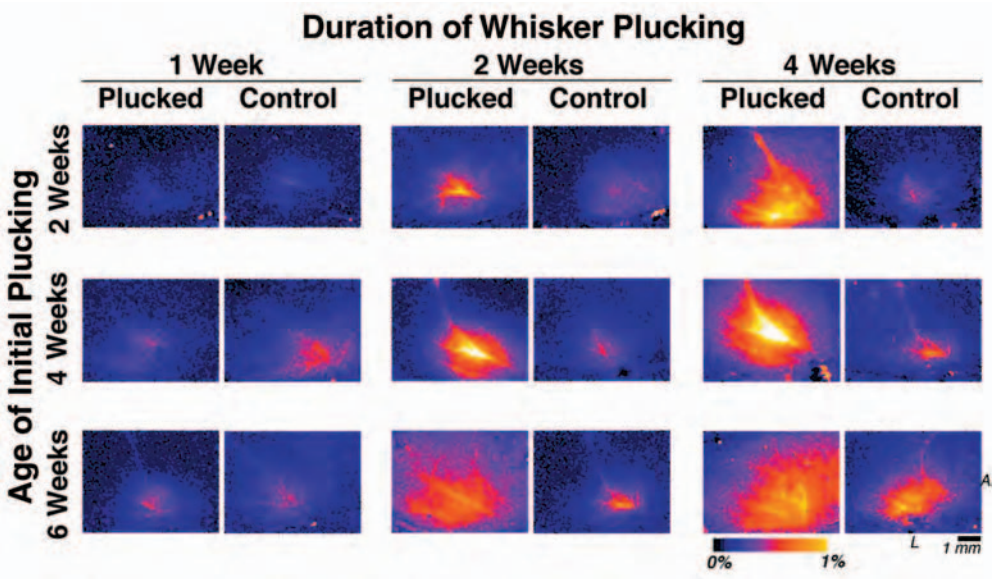

Figure 19 Plasticity-related changes in optical images. The effect of removing all but one whisker on functional optical responses was investigated in the rodent somatosensory cortex. Whisker removal induced more expansive and intense optical responses to spared whisker stimulation relative to age-matched controls. Images in columns labeled "Plucked" are representative responses from each experimental group while images in columns labeled "Control" are representative responses from age-matched controls. Images in the first column demonstrate that increases were no observed after 1 week of whisker plucking. When duration of whisker plucking was increased to 2 and 4 weeks (as represented by the second and third columns), optical responses were consistently lar ger and more intense in each group relative to age-matched controls. Color bar represents percentage reflectance decrease. A, anterior; L, lateral.

reported imaging seizure propagation in the rodent neocortex, induced by topical penicillin application (Chen *et al.,* 2000). Seizure-related cortical reflectance changes correlated well with EEG epileptiform discharges and often preceded initial EEG spikes, suggesting that OIS may provide sensitive cues for seizure detection. This may have important clinical implications. Many have hypothesized that optical imaging may be used intraoperatively to image epileptic foci and to delineate functional borders prior to neurosurgical intervention. These studies suggest that this may in fact be possible.

Optical imaging has also been used to study cortical spreading depression (CSD) (Yoon *et al.,* 1996; O'Farrell *et al.,* 2000). CSD is an important disease model for migraine (Lauritzen, 1994). Yoon and colleagues first described CSD *in vivo,* reporting the propagation of a nonuniform wavefront (Yoon *et al.,* 1996). In order to characterize CSD further, O'Farrell and collaborators imaged the CSD response to cortical pinprick for a longer duration and compared the intrinsic signal response to intravascular dye imaging results. They identified a triphasic response to CSD, with an initial highly uniform wavefront, which was not matched by intravascular dye signals, and two subsequent intrinsic signal phases (of alternating polarity), which were matched by intravascular dye signals (O'Farrell *et al.,* 2000) (Fig. 12).

These studies only begin to show the exciting application potential of optical imaging for imaging and characterizing functional disease progression in the neocortex. No doubt, this application will become increasingly important as optical imaging continues to be integrated into the clinical setting.

XI. Comparison of Intrinsic Optical Imaging with Other Imaging Techniques

A. fMRI and PET

*f*MRI and PET rely on signal sources similar to those of intrinsic optical imaging (Fox and Raichle, 1986; Ogawa *et al.,* 1990; Belliveau *et al.,* 1991). In some cases, they yield similar results, whereas in other cases they are complementary. As explained in Section II.B, the early increase in deoxyhemoglobin concentrations is far more localized to the site of electrical neuronal activity than blood flow and blood volume changes, which spread considerably beyond the electrically active cortex. Thus, it is not surprising that the resolution that can be attained in optical imaging when imaging between 600 and 630 nm (which is approximately 100 μm) is more than an order of magnitude better than that achieved with *f*MRI or PET, which normally image blood flow and volume changes (Cannestra *et al.,* 2001). Studies suggested that if *f*MRI could focus on the initial deoxygenation of the blood, higher resolution and more specific functional maps could be created (Frahm *et al.,* 1994; Cannestra *et al.,* 2001). Consistent with these hypotheses, Kim and colleagues recently used the initial increase in deoxygenation, or "initial dip," in the BOLD *f*MRI signal to map orientation columns with much higher spatial resolution than is traditionally available using *f*MRI (Kim *et al.,* 2000). However, the validity of initial dip imaging remains extremely controversial, with some groups doubting its validity (Kohl *et al.,* 2000; Lindauer *et al.,* 2001) and others adamantly supporting its existence and utility for high-resolution functional mapping (Vanzetta and Grinvald, 1999; Kim *et al.,* 2000).

Technical differences in *f*MRI, PET, and optical imaging instrumentation are also responsible for differences in spatial and temporal resolution. It is commonly accepted that optical imaging offers the best combination of both spatial and temporal resolution of brain function. Other factors, however, such as the possibility to measure structures deep within the brain and the absolute noninvasiveness, at least of *f*MRI, cannot be overestimated.

B. NIRS

NIRS, as mentioned earlier, may be considered a variant of intrinsic signal imaging. NIRS signals share a similar etiology with intrinsic signal etiology: perfusion- and metabolism-related changes (Villringer *et al.,* 1993; Obrig *et al.,* 2000). Similar to optical imaging, NIRS detects changes in the attenuation of light with functional activation and, using spectral decomposition techniques, estimates concentration changes of the different hemoglobin moieties. Although NIRS offers highly specific signals in terms of defining the etiology of the signal, it suffers from poor spatial resolution. Increasing the number of optodes has improved the spatial resolution of the technique. However, significant interpolation must still be used to create two dimensional images of functional activation changes. For a more detailed look into the advantages and disadvantages of NIRS, see Chapter 6, this volume.

C. Laser Doppler Flowmetry (LDF)

LDF exploits the Doppler phenomenon to detect changes in flow. Unlike optical intrinsic signal imaging, which can image and detect functional changes over several millimeters of exposed cortex simultaneous with relatively high spatial resolution (~25 μm), LDF offers very poor spatial resolution with extremely high temporal resolution (milliseconds). The LDF probe must be placed over a certain area of interest and used to detect blood flow changes under that probe but offers no spatial resolution. Mayhew and colleagues (1998) pointed out that within the area imaged by LDF, there can be several different time courses and response patterns which LDF would not be able to discern. Therefore, the spatial resolution offered by LDF may not be

adequate to capture the subtleties of the cascade of perfusion-related responses occurring within adjacent compartments in the cortex (i.e., capillaries vs venules). The increased temporal resolution of LDF is generally not very useful since the time course of perfusion-related changes in the brain is on the order of seconds.

The advantage of LDF over intrinsic signal imaging is that the nature of the signal is well understood. The signal is unambiguously due to changes in flow patterns within th volume of tissue being sampled. Furthermore, LDF probes can be adjusted to measure flow from di ferent depths of tissue. Optical imaging depth of imaging can also be adjusted by raising or lowering the plane of focus. However, LDF still offers the opportunity to monitor flow changes occurring a greater depths than is available by intrinsic signal imaging.

Scanning laser Doppler flowmetry (SLDF) o fers two-dimensional images of flow patterns. Although traditionally used for retinal imaging, recently this technology has been used to monitor flow changes on the surface of the roden brain following functional activation (Nielsen *et al.,* 2000). This offers an exciting means of monitoring flow change over a large spatial extent with relatively good spatial resolution. Unlike traditional LDF, however, depth flow record ings are not possible. The cost of increased spatial resolution is severely impaired temporal resolution: The temporal resolution of SLDF (on the order of several seconds) is limited and so dynamic imaging of blood flow changes with func tional activation may not be possible.

D. Dye Imaging

One of the principal shortcomings of intrinsic imaging is its limited temporal resolution. Voltage-sensitive dyes are in this respect at least three orders of magnitude better . A fin temporal resolution is, of course, required for a detailed understanding of the flow of information and its processin at dif ferent cortical sites. This fine temporal resolution is however, also the reason for some of the technical diffi culties associated with voltage-sensitive dyes. It is, for instance, much easier to obtain a good SNR if signals are slow: a measurement of small slow signals with a rise time of a second rather than a millisecond will, for instance, yield a 33-fold improvement in SNR due to the square root relationship between the number of samples and the SNR. Moreover, the excellent temporal resolution with the current voltage-sensitive dyes is achieved at the cost of a limited spatial resolution. The spatial resolution with the current voltage-sensitive dyes is, however, not ultimately limited by the number of pixels of the photodetector or by the available computer and instrumentation capabilities, but rather by obtainable signal size and concomitant photodynamic damage. Without a significant improvement in the quality o currently available dyes, a 64×64-pixel array is close to the usable limit.

In addition to voltage-sensitive dyes, intravascular dyes (Texas red dextran, MW = 70,000; Frostig *et al.,* 1990; Narayan *et al.,* 1995), oxygen-sensitive phosphorescence quenching dyes (V anzetta and Grinvald, 1999; Lindauer *et al.,* 2001), and molecule-specific dyes (e.g., DAF-2, nitric oxide-sensitive dye) are available for imaging specifi processes. These dyes all suf fer from the same limitation as voltage-sensitive dyes, namely, the SNR using these dyes is significantly less than with intrinsic signal imaging and the can induce photodynamic damage. The advantage of using such dyes is that the investigator knows unambiguously the etiology of the signal being imaged, whereas with optical imaging and optical spectroscopy the exact nature of the signal being observed is not entirely clear.

In addition to the photodynamic damage associated with the use of any dye upon prolonged or intense illumination, the use of dyes has other difficulties, such as bleaching limited depth of penetration into the cortex, and possible pharmacological side effects. While the extent of pharmacological side ef fects on cortical function has not been carefully evaluated, it is already clear that stained cortical cells still maintain their principal response properties.

XII. Conclusions and Outlook

Optical imaging based on intrinsic signals is unique among functional neuroimaging techniques in that it of fers both high spatial (on the order of micrometers) and high temporal (on the order of milliseconds to seconds) resolution *simultaneously*. Moreover, no other functional neuroimaging technique of fers comparable spatial resolution, allowing visualization of the fine structure of individua functional domains within cortical areas. Additionally, high spatial resolution maps can be acquired over relatively large cortical areas. The resolution of optical imaging makes it ideal for a variety of experimental investigations, including studying the functional or ganization of and functional relationships within the brain, characterizing neurovascular physiology, and examining pathophysiological changes due to certain disease processes.

Optical imaging of *intrinsic signals* is a particularly attractive methodology because of its relatively noninvasive nature. Although imaging intrinsic signals is invasive in the sense that the skull has to be thinned or opened in order to gain optical access to the brain, the brain itself is left completely untouched: no physical cortical contact is required, no dyes (which may be phototoxic) are necessary, and animal sacrifice is not necessary for acquiring results In addition to providing data about the brain in its native state, the noninvasive nature of optical imaging makes this modality ideal for chronic investigations, such as development and plasticity, which may last up to several weeks or months.

One of the more exciting and challenging applications of optical imaging of intrinsic signals is studying the human cortex. This not only allows us to characterize the physiology and functional architecture of the human brain, but may also be clinically useful as an intraoperative functional brain mapping tool for neurosurgical guidance.

Recent advances in detector technology and microscope optics have increased the sensitivity, speed, and applications of optical imaging. Recent advances in spectroscopic techniques, for example, have made it possible to make highly specific determinations of changes in hemoglobin concen trations. No doubt, technological advances will continue to revolutionize this modality. We anticipate that by explicitly stating some methodological considerations involved with optical imaging and by introducing investigators to the different approaches used to analyze optical imaging data, we have increased interest in this modality and demonstrated its versatility.

Acknowledgments

The overall structure of this chapter has been adapted from a chapter by Tobias Bonhoeffer and Amiram Grinvald that appeared in the first editio of *Brain Mapping: The Methods*. Moreover, some of the content has been adapted from the original chapter. The authors are indebted to these authors for their original contribution. The authors also thank members of the UCLA Laboratory of Neuro Imaging for contributing figures to thi chapter, including Andrew Cannestra, Michael Guiou, Sanjiv Narayan, Alyssa O'Farrell Ba, and Sameer Sheth. The authors also thank Sameer Sheth for his critical review of the manuscript. N.P is supported, in part, by the Medical Scientist Training Program (GM08042) and a National Research Service Award (MH12773-01). Additional support was provided by research grants to A.W.T. (NIMH MH/NS52083).

References

Ances, B. M., Greenber g, J. H., and Detre, J. A. (2000). Ef fects of variations in interstimulus interval on activation-flow coupling response an somatosensory evoked potentials with forepaw stimulation in the rat. *J. Cereb. Blood Flow Metab.* **20,** 290–297.

Antonini, A., Fagiolini, M., and Stryker, M. P. (1999). Anatomical correlates of functional plasticity in mouse visual cortex.*J Neurosci.* **19,** 4388–4406.

Bandettini, P. A., Jesmanowicz, A., Wong, E. C., and Hyde, J. S. (1993). Processing strategies for time-course data sets in functional MRI of the human brain. *Magn. Reson. Med.* **30,** 161–173.

Bär, T. (1981). Distribution of radially penetrating arteries and veins in the neocortex of rat. In *Cereb. Microcirc. Metab.* pp. 1–8 (J.C. Navarro and E. Fritschka *eds.*) Raven Press, New York.

Belliveau, J. W., Cohen, M. S., Weisskoff, R. M., Buchbinder , B. R., and Rosen, B. R. (1991). Functional studies of the human brain using high-speed magnetic resonance imaging. *J. Neuroimaging* **1,** 36–41.

Berwick, J., Johnston, D., Zheng, Y., Coffey, P., Mayhew, J., and Whiteley, S. J. O. (2000). Spectroscopic analysis of the action of 7-nitroindazole. *Soc. Neurosci. Abstr.* **26,** 1737.

Blasdel, G. G. (1992a). Differential imaging of ocula dominance and orientation selectivity in monkey striate cortex. *J. Neurosci.* **12,** 3115–3138.

Blasdel, G. G. (1992b). Orientation selectivity , preference, and continuity in monkey striate cortex. *J. Neurosci.* **12,** 3139–3161.

Blasdel, G. G., and Salama, G. (1986). Voltage-sensitive dyes reveal a modular organization in monkey striate cortex. *Nature* **321,** 579–585.

Blood, A. J., Narayan, S. M., and Toga, A. W. (1995). Stimulus parameters influence characteristics of optical intrinsic signal responses i somatosensory cortex. *J. Cereb. Blood Flow Metab.* **15,** 1109–1121.

Blood, A. J., and Toga, A. W. (1998). Optical intrinsic signal imaging responses are modulated in rodent somatosensory cortex during simultaneous whisker and forelimb stimulation. *J. Cereb. Blood Flow Metab.* **18,** 968–977.

Bonhoeffer, T. (1995). Optical imaging of intrinsic signals as a tool to visualize the functional architecture of adult and developing visual cortex. *Arzneimittelforschung* **45,** 351–356.

Bonhoeffer, T., and Grinvald, A. (1991). Iso-orientation domains in cat visual cortex are arranged in pinwheel-like patterns. *Nature* **353,** 429–431.

Bonhoeffer, T., and Grinvald, A. (1993a). The layout of iso-orientation domains in area 18 of cat visual cortex: Optical imaging reveals a pinwheel-like organization. *J. Neurosci.* **13,** 4157–4180.

Bonhoeffer, T., and Grinvald, A. (1993b). Optical imaging of the functional architecture in cat visual cortex: The layout of direction and orientation domains. *Adv. Exp. Med. Biol.* **333,** 57–69.

Bonhoeffer, T., and Grinvald, A. (1996). Optical imaging based on intrinsic signals: The methodology. *In* "Brain Mapping: The Methods" (A. W. Toga and J. C. Mazziotta, eds.). Academic Press, San Diego.

Boxerman, J. L., Bandettini, P. A., Kwong, K. K., Baker, J. R., Davis, T. L., Rosen, B. R., and Weisskoff, R. M. (1995). The intravascular contribution to *f*MRI signal change: Monte Carlo modeling and dif fusion-weighted studies in vivo. *Magn. Reson. Med.* **34,** 4–10.

Buchweitz, E., and Weiss, H. R. (1986). Effect of withdrawal from chronic naltrexone on regional cerebral oxygen consumption in the cat. *Brain Res.* **397**, 308–314.

Cannestra, A. F., Black, K. L., Martin, N. A., Cloughesy, T., Burton, J. S., Rubinstein, E., Woods, R. P., and Toga, A. W. (1998a). Topographical and temporal specificity of human intraoperative optical intrinsi signals. *NeuroReport* **9,** 2557–2563.

Cannestra, A. F., Blood, A. J., Black, K. L., and Toga, A. W. (1996). The evolution of optical signals in human and rodent cortex. *NeuroImage* **3,** 202–208.

Cannestra, A. F ., Bookheimer , S. Y., Pouratian, N., O'Farrell, A. M., Sicotte, N. M., Martin, N. A., Becker, D., Rubino, G., and Toga, A. W. (2000). Temporal and topographical characterization of language cortices using intraoperative optical intrinsic signals. *NeuroImage* **12,** 41–54.

Cannestra, A. F., Pouratian, N., Bookheimer , S. Y., Martin, N. A., Becker, D., and Toga, A. W. (2001). Temporal spatial dif ferences observed by functional MRI and human intraoperative optical imaging. *Cereb. Cortex* **11,** 773–782.

Cannestra, A. F., Pouratian, N., Shomer , M. H., and Toga, A. W. (1998b). Refractory periods observed by intrinsic signal and fluorescent dy imaging. *J. Neurophysiol.* **80,** 1522–1532.

Chapin, J. K., and Lin, C. S. (1984). Mapping the body representation in the SI cortex of anesthetized and awake rats. *J. Comp. Neurol.* **229,** 199–213.

Chapman, B., Stryker , M. P., and Bonhoef fer, T. (1996). Development of orientation preference maps in ferret primary visual cortex. *J. Neurosci.* **16,** 6443–6453.

Chen, J. W. Y., O'Farrell, A. M., and Toga, A. W. (2000). Optical intrinsic signal imaging in a rodent seizure model. *Neurology* **55,** 312–315.

Chen-Bee, C. H., and Frostig, R. D. (1996). Variability and interhemispheric asymmetry of single-whisker functional representations in rat barrel cortex. *J. Neurophysiol.* **76,** 884–894.

Chen-Bee, C. H., Kwon, M. C., Masino, S. A., and Frostig, R. D. (1996). Areal extent quantification of functional representations using intrinsi signal optical imaging. *J. Neurosci. Methods* **68,** 27–37.

Chen-Bee, C. H., Polley, D. B., Brett-Green, B., Prakash, N., Kwon, M. C., and Frostig, R. D. (2000). Visualizing and quantifying evoked cortical activity assessed with intrinsic signal imaging. *J. Neurosci. Methods* **97,** 157–173.

Cohen, L., and Keynes, R. D. (1971). Changes in light scattering associated with the action potential in crab nerves. *J. Physiol. (London)* **212,** 259–275.

Cohen, M. S. (1997). Parametric analysis of *f*MRI data using linear systems methods. *NeuroImage* **6,** 93–103.

Corina, D. P., Poliakov, A., Steury, K., Martin, R., Mulligan, K., Maravilla, K., Brinkly, J. F., and Ojemann, G. A. (2000). Correspondences between language cortex identified by cortical stimulation mapping and *f*MRI. *NeuroImage* **11,** S295.

Cox, S. B., Woolsey, T. A., and Rovainen, C. M. (1993). Localized dynamic changes in cortical blood flow with whisker stimulation corresponds t matched vascular and neuronal architecture of rat barrels. *J. Cereb. Blood Flow Metab.* **13,** 899–913.

Daghighian, F., Mazziotta, J. C., Hoffman, E. J., Shenderov, P., Eshaghian, B., Siegel, S., and Phelps, M. E. (1994). Intraoperative beta probe: A device for detecting tissue labeled with positron or electron emitting isotopes during surgery. *Med. Phys.* **21,** 153–157.

Dinse, H. R., Godde, B., Hilger , T., Haupt, S. S., Spengler , F., and Zepka, R. (1997a). Short-term functional plasticity of cortical and thalamic sensory representations and its implication for information processing. *Adv. Neurol.* **73,** 159–178.

Dinse, H. R., Reuter , G., Cords, S. M., Godde, B., Hilger , T., and Lenarz, T. (1997b). Optical imaging of cat auditory cortical or ganization after electrical stimulation of a multichannel cochlear implant: Dif ferential effects of acute and chronic stimulation. *Am. J. Otol.* **18,** S17–18.

Dirnagl, U., Villringer, A., Gebhardt, R., Haberl, R. L., Schmiedek, P., and Einhäupl, K. M. (1991). Three-dimensional reconstruction of the rat brain cortical microcirculation in vivo. *J. Cereb. Blood Flow Metab.* **11,** 353–360.

Durham, D., and Woolsey, T. A. (1977). Barrels and columnar cortical organization: Evidence from 2-deoxyglucose (2-DG) experiments. *Brain Res.* **137,** 168–174.

Duvernoy, H. M., Delon, S., and Vannson, J. L. (1981). Cortical blood vessels of the human brain. *Brain Res. Bull.* **7,** 519–579.

Ferrari, M., Wilson, D. A., Hanley , D. F ., and Traystman, R. J. (1992). Effects of graded hypotension on cerebral blood flo , blood volume, and mean transit time in dogs. *Am. J. Physiol.* **262,** H1908–1914.

Fox, P. T., and Raichle, M. E. (1986). Focal physiological uncoupling of cerebral blood flow and oxidative metabolism during somatosensory stimula tion in human subjects. *Proc. Natl. Acad. Sci. USA* **83,** 1140–1144.

Fox, P . T., Raichle, M. E., Mintun, M. A., and Dence, C. (1988). Nonoxidative glucose consumption during focal physiologic neural activity. *Science* **241,** 462–464.

Frahm, J., Merboldt, K. D., Hanicke, W., Kleinschmidt, A., and Boecker, H. (1994). Brain or vein—Oxygenation or flow? On signal physiology i functional MRI of human brain activation. *NMR Biomed.* **7,** 45–53.

Frostig, R. D., Lieke, E. E., Ts'o, D. Y., and Grinvald, A. (1990). Cortical functional architecture and local coupling between neuronal activity and the microcirculation revealed by in vivo high-resolution optical imaging of intrinsic signals. *Proc. Natl. Acad. Sci. USA* **87,** 6082–6086.

Gabbay, M., Brennan, C., Kaplan, E., and Sirovich, L. (2000). A principal components-based method for the detection of neuronal activity maps: Application to optical imaging. *NeuroImage* **11,** 313–325.

Geladi, P., Iasksson, H., Lindqvist, L., Wold, S., and Esbensen, K. (1989). Principal component analysis of multivariate images. *Chem. Intell. Lab. Syst.* **5,** 209–220.

Godde, B., Hilger , T., von Seelen, W., Berkefeld, T., and Dinse, H. R. (1995). Optical imaging of rat somatosensory cortex reveals representational overlap as topographic principle. *NeuroReport* **7,** 24–28.

Grinvald, A. (1992). Optical imaging of architecture and function in the living brain sheds new light on cortical mechanisms underlying visual perception. *Brain Topogr.* **5,** 71–75.

Grinvald, A., Frostig, R. D., Siegel, R. M., and Bartfeld, E. (1991). High-resolution optical imaging of functional brain architecture in the awake monkey. *Proc. Natl. Acad. Sci. USA* **88,** 11559–11563.

Grinvald, A., Lieke, E., Frostig, R. D., Gilbert, C. D., and Wiesel, T. N. (1986). Functional architecture of cortex revealed by optical imaging of intrinsic signals. *Nature* **324,** 361–364.

Grinvald, A., Manker, A., and Segal, M. (1982). Visualization of the spread of electrical activity in rat hippocampal slices by voltage-sensitive optical probes. *J. Physiol. (London)* **333,** 269–291.

Gross, D., Loew, L. M., and Webb, W. W. (1986). Optical imaging of cell membrane potential changes induced by applied electric fields. *Biophys. J.* **50,** 339–348.

Haglund, M. M., Ojemann, G. A., and Blasdel, G. G. (1993). Optical imaging of bipolar cortical stimulation. *J. Neurosurg.* **78,** 785–793.

Haglund, M. M., Ojemann, G. A., and Hochman, D. W. (1992). Optical imaging of epileptiform and functional activity in human cerebral cortex. *Nature* **358,** 668–671.

Hess, A., Stiller, D., Kaulisch, T., Heil, P ., and Scheich, H. (2000). New insights into the hemodynamic blood oxygenation level-dependent response through combination of functional magnetic resonance imaging and optical recording in gerbil barrel cortex. *J. Neurosci.* **20,** 3328–3338.

Hill, D. K., and Keynes, R. D. (1949). Opacity changes in stimulated nerve. *J. Physiol. (London)* **108,** 278–281.

Hodge, C. J., Jr ., Stevens, R. T., Newman, H., Merola, J., and Chu, C. (1997). Identification of functioning cortex using cortical optica imaging. *Neurosurgery* **41,** 1137–1144; discussion 1144–1145.

Hu, X., Le, T. H., and Ugurbil, K. (1997). Evaluation of the early response in *f*MRI in individual subjects using short stimulus duration. *Magn. Reson. Med.* **37,** 877–884.

Kauer, J. S. (1988). Real-time imaging of evoked activity in local circuits of the salamander olfactory bulb. *Nature* **331**, 166–168.

Kelly, M. K., Carvell, G. E., Kodger , J. M., and Simons, D. J. (1999). Sensory loss by selected whisker removal produces immediate disinhibition in the somatosensory cortex of behaving rats. *J. Neurosci.* **19,** 9117–9125.

Kim, D. S., Duong, T. Q., and Kim, S. G. (2000). High-resolution mapping of iso-orientation columns by *f*MRI. *Nat. Neurosci.* **3,** 164–169.

Kisvarday, Z. F ., Kim, D. S., Eysel, U. T., and Bonhoef fer, T. (1994). Relationship between lateral inhibitory connections and the topography of the orientation map in cat visual cortex. *Eur. J. Neurosci.* **6,** 1619–1632.

Kohl, M., Lindauer , U., Royl, G., Kuhl, M., Gold, L., Villringer, A., and Dirnagl, U. (2000). Physical model for the spectroscopic analysis of cortical intrinsic optical signals. *Phys. Med. Biol.* **45,** 3749–3764.

Kornblum, H. I., Araujo, D. M., Annala, A. J., Tatsukawa, K. J., Phelps, M. E., and Cherry, S. R. (2000). In vivo imaging of neuronal activation and plasticity in the rat brain by high resolution positron emission tomography (microPET). *Nat. Biotechnol.* **18,** 655–660.

Kossut, M. (1988). Modifications of the single cortical vibrissal column *Acta Neurobiol. Exp. (Warsz)* **48,** 83–115.

Kossut, M. (1998). Experience-dependent changes in function and anatomy of adult barrel cortex. *Exp. Brain Res.* **123,** 110–116.

Kwong, K. K., Belliveau, J. W., Chesler, D. A., Goldberg, I. E., Weisskoff, R. M., Poncelet, B. P ., Kennedy, D. N., Hoppel, B. E., Cohen, M. S., Turner, R., *et al.* (1992). Dynamic magnetic resonance imaging of human brain activity during primary sensory stimulation. *Proc. Natl. Acad. Sci. USA* **89,** 5675–5679.

Lauritzen, M. (1994). Pathophysiology of the migraine aura. The spreading depression theory. *Brain* **117,** 199–210.

Lee, P. A., Sylvia, A. L., and Piantadosi, C. A. (1988). Effect of fluorocar bon-for-blood exchange on regional cerebral blood flow in rats. *Am. J. Physiol.* **254,** H719–H726.

LeManna, J. C., Sick, T. J., Pirarsky , S. M., and Rosenthal, M. (1987). Detection of an oxidizable fraction of cytochrome oxidase in intact rat brain. *Am. Physiol. Soc.* **253,** C477–C483.

Lindauer, U., Royl, G., Leithner , C., Kuhl, M., Gold, L., Gethmann, J., Kohl-Bareis, M., Villringer, A., and Dirnagl, U. (2001). No evidence for

early decrease in blood oxygenation in rat whisker cortex in response to functional activation. *NeuroImage* **13,** 988–1001.

Lindauer, U., Villringer, A., and Dirnagl, U. (1993). Characterization of CBF response to somatosensory stimulation: Model and influence o anesthetics. *Am. J. Physiol.* **264,** H1223–1228.

Logothetis, N. K., Guggenber ger, H., Peled, S., and Pauls, J. (1999). Functional imaging of the monkey brain. *Nat. Neurosci.* **2,** 555–562.

Lou, H. C., Edvinsson, L., and MacKenzie, E. T. (1987). The concept of coupling blood flow to brain function: Revision required? *Ann. Neurol.* **22,** 289–297.

MacDonald, D., Avis, D., and Evans, A. C. (1994). Multiple surface identification and matching in magnetic resonance imaging. *Proc. SPIE* **2359,** 160–169.

Macknik, S. L., and Haglund, M. M. (1999). Optical images of visible and invisible percepts in the primary visual cortex of primates. *Proc. Natl. Acad. Sci. USA* **96,** 15208–15210.

Malach, R., Amir, Y., Harel, M., and Grinvald, A. (1993). Relationship between intrinsic connections and functional architecture revealed by optical imaging and in vivo tar geted biocytin injections in primate striate cortex. *Proc. Natl. Acad. Sci. USA* **90,** 10469–10473.

Malonek, D., and Grinvald, A. (1996). Interactions between electrical activity and cortical microcirculation revealed by imaging spectroscopy: Implications for functional brain mapping. *Science* **272,** 551–554.

Masino, S. A., and Frostig, R. D. (1996). Quantitative long-term imaging of the functional representation of a whisker in rat barrel cortex. *Proc. Natl. Acad. Sci. USA* **93,** 4942–4947.

Masino, S. A., Kwon, M. C., Dory , Y., and Frostig, R. D. (1993). Characterization of functional or ganization within rat barrel cortex using intrinsic signal optical imaging through a thinned skull. *Proc. Natl. Acad. Sci. USA* **90,** 9998–10002.

Mayhew, J., Hu, D., Zheng, Y., Askew, S., Hou, Y., Berwick, J., Coffey, P. J., and Brown, N. (1998). An evaluation of linear model analysis techniques for processing images of microcirculation activity . *NeuroImage* **7,** 49–71.

Mayhew, J., Johnston, D., Berwick, J., Jones, M., Coffey, P., and Zheng, Y. (2000). Spectroscopic analysis of neural activity in brain: Increased oxygen consumption following activation of barrel cortex. *NeuroImage* **12,** 664–675.

Mayhew, J., Johnston, D., Martindale, J., Jones, M., Berwick, J., and Zheng, Y. (2001). Increased oxygen consumption following activation of brain: Theoretical footnotes using spectroscopic data from barrel cortex. *NeuroImage* **13,** 975–987.

Mayhew, J., Zheng, Y., Hou, Y., Vuksanovic, B., Berwick, J., Askew, S., and Cof fey, P. (1999). Spectroscopic analysis of changes in remitted illumination: The response to increased neural activity in brain. *NeuroImage* **10,** 304–326.

Mayhew, J. E., Askew, S., Zheng, Y., Porrill, J., Westby, G. W., Redgrave, P., Rector, D. M., and Harper, R. M. (1996). Cerebral vasomotion:A 0.1-Hz oscillation in reflected light imaging of neural activit . *NeuroImage* **4,** 183–193.

Mazziotta, J. C., Toga, A. W., and Frackowiak, R. S. J., eds. (2000). "Brain Mapping: The Disorders." Academic Press, San Diego.

Menon, R. S., Ogawa, S., Hu, X., Strupp, J. P ., Anderson, P., and Ugurbil, K. (1995). BOLD based functional MRI at 4 tesla includes a capillary bed contribution: Echo-planar imaging correlates with previous optical imaging using intrinsic signals. *Magn. Reson. Med.* **33,** 453–459.

Narayan, S. M., Esfahani, P ., Blood, A. J., Sikkens, L., and Toga, A. W. (1995). Functional increases in cerebral blood volume over somatosensory cortex. *J. Cereb. Blood Flow Metab.* **15,** 754–765.

Narayan, S. M., Santori, E. M., and Toga, A. W. (1994). Mapping functional activity in rodent cortex using optical intrinsic signals. *Cereb. Cortex* **4,** 195–204.

Nemoto, M., Nomura, Y., Sato, C., Tamura, M., Houkin, K., Koyanagi, I., and Abe, H. (1999). Analysis of optical signals evoked by peripheral nerve stimulation in rat somatosensory cortex: Dynamic changes in hemoglobin concentration and oxygenation. *J. Cereb. Blood Flow Metab.* **19,** 246–259.

Ngai, A. C., Ko, K. R., Morii, S., and Winn, H. R. (1988). Effect of sciatic nerve stimulation on pial arterioles in rats. *Am. J. Physiol.* **254,** H133–139.

Nguyen, T. T., Yamamoto, T., Stevens, R. T., and Hodge, C. J., Jr . (2000). Reorganization of adult rat barrel cortex intrinsic signals following kainic acid induced central lesion. *Neurosci. Lett.* **288,** 5–8.

Nielsen, A. N., Fabricius, M., and Lauritzen, M. (2000). Scanning laser - Doppler flowmetry of rat cerebral circulation during cortical spreadin depression. *J. Vasc. Res.* **37,** 513–522.

Nomura, Y., Fujii, F ., Sato, C., Nemoto, M., and Tamura, M. (2000). Exchange transfusion with fluorocarbon for studying synapticall evoked optical signal in rat cortex. *Brain Res. Protocols* **5,** 10–15.

Nomura, Y., Hazeki, O., and Tamura, M. (1997). Relationship between time-resolved and non-time-resolved Beer–Lambert Law in turbid media. *Phys. Med. Biol.* **42,** 1009–1022.

Obrig, H., Wenzel, R., Kohl, M., Horst, S., Wobst, P ., Steinbrink, J., Thomas, F., and Villringer, A. (2000). Near-infrared spectroscopy: Does it function in functional activation studies of the adult brain? *Int. J. Psychophysiol.* **35,** 125–142.

O'Farrell, A. M., Rex, D. E., Muthialu, A., Pouratian, N., Wong, G. K., Cannestra, A. F ., Chen, J. W. Y., and Toga, A. W. (2000). Characterization of optical intrinsic signals and blood volume during cortical spreading depression. *NeuroReport* **11,** 2121–2125.

Ogawa, S., Lee, T. M., Kay, A. R., and Tank, D. W. (1990). Brain magnetic resonance imaging with contrast dependent on blood oxygenation.*Proc. Natl. Acad. Sci. USA* **87,** 9868–9872.

Ogawa, S., Tank, D. W., Menon, R., Ellermann, J. M., Kim, S. G., Merkle, H., and Ugurbil, K. (1992). Intrinsic signal changes accompanying sensory stimulation: Functional brain mapping with magnetic resonance imaging. *Proc. Natl. Acad. Sci. USA* **89,** 5951–5955.

Orbach, H. S., and Cohen, L. B. (1983). Optical monitoring of activity from many areas of the in vitro and in vivo salamander olfactory bulb: A new method for studying functional or ganization in the vertebrate central nervous system. *J. Neurosci.* **3,** 2251–2262.

Paley, M., Mayhew , J. E., Martindale, A. J., McGinley , J., Berwick, J., Coffey, P., Redgrave, P ., Furness, P ., Port, M., Ham, A., Zheng, Y., Jones, M., Whitby, E., van Beek, E. J., Wilkinson, I. D., Darwent, G., and Griffiths, . D. (2001). Design and initial evaluation of a low-cost 3-tesla research system for combined optical and functional MR imaging with interventional capability . *J. Magn. Reson. Imaging* **13,** 87–92.

Polley, D. B., Chen-Bee, C. H., and Frostig, R. D. (1999a). Two directions of plasticity in the sensory-deprived adult cortex. *Neuron* **24,** 623–637.

Polley, D. B., Chen-Bee, C. H., and Frostig, R. D. (1999b). Varying the degree of single-whisker stimulation dif ferentially af fects phases of intrinsic signals in rat barrel cortex. *J. Neurophysiol.* **81,** 692–701.

Pouratian, N., Bookheimer, S. Y., O'Farrell, A. M., Sicotte, N. L., Cannestra, A. F., Becker, D., and Toga, A. W. (2000a). Optical imaging of bilingual cortical representations: Case report. *J. Neurosurg.* **93,** 686–691.

Pouratian, N., Kamrava, A., Nettar, K. D., O'Farrell, A. M., and Toga, A. W. (2000b). Developmental changes in perfusion-related responses in rodent somatosensory cortex. *Soc. Neurosci. Abstr.* **26,** 133.

Pouratian, N., Kamrava, A., O'Farrell, A. M., and Toga, A. W. (1999). Plasticity induced changes in functional perfusion.*NeuroImage* **9,** S288.

Pouratian, N., Martin, N. A., Cannestra, A. F., Becker, D., Bookheimer, S. Y., Sicotte, N. M., and Toga, A. W. (2000c). Intraoperative sensorimotor and language mapping using optical intrinsic signal imaging: Comparison with electrophysiologic techniques and *f*MRI in 40 patients. *In* "2000 American Association of Neurological Sur geons Annual Meeting," San Francisco, California.

Pouratian, N., Sicotte, N. L., Rex, D. E., Cannestra, A. F., Martin, N. A., Becker, D., and Toga, A. W. (2001). Spatial/temporal correlation of optical intrinsic signals and BOLD. *Magn. Reson. Med.* **47**, 760–776.

Prakash, N., Cohen-Cory, S., and Frostig, R. D. (1996). Rapid and opposite effects of BDNF and NGF on the functional or ganization of the adult cortex in vivo. *Nature* **381,** 702–706.

Ramsey, N. F., Kirkby, B. S., Van Gelderen, P., Berman, K. F., Duyn, J. H., Frank, J. A., Mattay, V. S., Van Horn, J. D., Esposito, G., Moonen, C. T., and Weinberger, D. R. (1996). Functional mapping of human sensorimotor cortex with 3D BOLD *f*MRI correlates highly with $H_2(15)O$ PET RCBF. *J. Cereb. Blood Flow Metab.* **16,** 755–764.

Ratzlaff, E. H., and Grinvald, A. (1991). A tandem-lens epifluorescenc macroscope: Hundred-fold brightness advantage for wide-field imaging *J. Neurosci. Methods* **36,** 127–137.

Reichenbach, J., Venkatesan, R., Schillinger, D., Kido, D., and Haacke, E. (1997). Small vessels in the human brain: MR venography with deoxyhemoglobin as an intrinsic contrast agent. *Radiology* **204,** 272–277.

Roy, C. W., and Sherrington, C. S. (1890). On the regulation of the blood-supply of the brain. *J. Physiol. (London)* **11,** 85–108.

Schuette, W. H., Whitehouse, W. C., Lewis, D. V., O'Connor, M., and Van Buren, J. M. (1974). A television fluorometer for monitoring oxidativ metabolism in intact tissue. *Med. Instrum.* **8,** 331–333.

Shmuel, A., and Grinvald, A. (1996). Functional organization for direction of motion and its relationship to orientation maps in cat area 18. *J. Neurosci.* **16,** 6945–6964.

Shmuel, A., and Grinvald, A. (2000). Coexistence of linear zones and pinwheels within orientation maps in cat visual cortex. *Proc. Natl. Acad. Sci. USA* **97,** 5568–5573.

Shtoyerman, E., Arieli, A., Slovin, H., Vanzetta, I., and Grinvald, A. (2000). Long-term optical imaging and spectroscopy reveal mechanisms underlying the intrinsic signal and stability of cortical maps in V1 of behaving monkeys. *J. Neurosci.* **20,** 8111–8121.

Simons, D. J. (1978). Response properties of vibrissa units in rat SI somatosensory neocortex. *J. Neurophysiol.* **41,** 798–820.

Sled, J. G., Zijdenbos, A. P., and Evans, A. C. (1998). A nonparametric method for automatic correction of intensity nonuniformity in MRI data. *IEEE Trans. Med. Imaging* **17,** 87–97.

Sokoloff, L., Reivich, M., Kennedy, C., Des Rosiers, M. H., Patlak, C. S., Pettigrew, K. D., Sakurada, O., and Shinohara, M. (1977). The [^{14}C]deoxyglucose method for the measurement of local cerebral glucose utilization: Theory, procedure, and normal values in the conscious and anesthetized albino rat. *J. Neurochem.* **28,** 897–916.

Stepnoski, R. A., LaPorta, A., Raccuia-Behling, F., Blonder, G. E., Slusher, R. E., and Kleinfeld, D. (1991). Noninvasive detection of changes in membrane potential in cultured neurons by light scattering. *Proc. Natl. Acad. Sci. USA* **88,** 9382–9386.

Stetter, M., Schiessl, I., Otto, T., Sengpiel, F., Hubener, M., Bonhoeffer, T., and Obermayer, K. (2000). Principal component analysis and blind separation of sources for optical imaging of intrinsic signals. *NeuroImage* **11,** 482–490.

Toga, A. W., Cannestra, A. F., and Black, K. L. (1995a). The temporal/spatial evolution of optical signals in human cortex. *Cereb. Cortex* **5,** 561–565.

Toga, A. W., Santori, E. M., Hazani, R., and Ambach, K. (1995b). A 3D digital map of rat brain. *Brain Res. Bull.* **38,** 77–85.

Ts'o, D. Y., Frostig, R. D., Lieke, E. E., and Grinvald,A. (1990). Functional organization of primate visual cortex revealed by high resolution optical imaging. *Science* **249,** 417–420.

Ts'o, D. Y., Roe, A. W., and Gilbert, C. D. (2001). A hierarchy of the functional organization for color, form and disparity in primate visual area V2. *Vision Res.* **41,** 1333–1349.

Vanzetta, I., and Grinvald, A. (1999). Increased cortical oxidative metabolism due to sensory stimulation: Implications for functional brain imaging. *Science* **286,** 1555–1558.

Victor, J. D., Purpura, K., Katz, E., and Mao, B. (1994). Population encoding of spatial frequency, orientation, and color in macaque V1. *J. Neurophysiol.* **72,** 2151–2166.

Villringer, A., and Dirnagl, U. (1995). Coupling of brain activity and cerebral blood flow: Basis of functional neuroimaging. *Cerebrovasc. Brain Metab. Rev.* **7,** 240–276.

Villringer, A., Planck, J., Hock, C., Schleinkofer, L., and Dirnagl, U. (1993). Near infrared spectroscopy (NIRS): A new tool to study hemodynamic changes during activation of brain function in human adults. *Neurosci. Lett.* **154,** 101–104.

Woods, R. P., Cherry, S. R., and Mazziotta, J. C. (1992). Rapid automated algorithm for aligning and reslicing PET images. *J. Comput. Assisted Tomogr.* **16,** 620–633.

Woolsey, T. A., and Van der Loos, H. (1970). The structural organization of layer IV in the somatosensory region (SI) of mouse cerebral cortex. The description of a cortical field composed of discrete cytoarchitectoni units. *Brain Res.* **17,** 205–242.

Yacoub, E., Le, T. H., Ugurbil, K., and Hu, X. (1999). Further evaluation of the initial negative response in functional magnetic resonance imaging. *Magn. Reson. Med.* **41,** 436–441.

Yap, J. T., Chen, C. T., Cooper, M., and Treffert, J. D. (1994). Knowledge-based factor analysis of multidimensional nuclear medicine image sequences. *Proc. SPIE* **2168,** 289–297.

Yoon, R. S., Tsang, P. W., Lenz, F. A., and Kwan, H. C. (1996). Characterization of cortical spreading depression by imaging of intrinsic optical signals. *NeuroReport* **7,** 2671–2674.

Zdrojkowski, R. J., and Pisharoty, N. R. (1970). Optical transmission and reflection by blood. *IEEE Trans. Biomed. Eng.* **17,** 122–128.

Zheng, Y., Johnston, D., Berwick, J., and Mayhew, J. (2001). Signal source separation in the analysis of neural activity in brain. *NeuroImage* **13,** 447–458.